UNIVERSITÉ DU QUÉBEC À MONTRÉAL

STUDY OF THE VEINS, ALTERATIONS AND MINERALIZATION OF THE COMTOIS GOLD DEPOSIT, ABITIBI SUBPROVINCE, QUEBEC,CANADA

THESIS SUBMITTED IN
PARTIAL FULLFILMENT OF THE
REQUIREMENTS FOR THE MASTERS
DEGREE IN EARTH SCIENCES

BY
FRANCIS DUPRÉ

MAY 2010

UNIVERSITÉ DU QUÉBEC À MONTRÉAL

ÉTUDE DES VEINES, DES ALTÉRATIONS ET DE LA MINÉRALISATION DU GÎTE AURIFÈRE DE COMTOIS, SOUS-PROVINCE DE L'ABITIBI, QUÉBEC, CANADA

MÉMOIRE
PRÉSENTÉ
COMME EXIGENCE PARTIELLE
DE LA MAÎTRISE EN SCIENCES DE LA TERRE

PAR
FRANCIS DUPRÉ

MAI 2010

REMERCIEMENTS

Je tiens à remercier en premier lieu Michel Jébrak, directeur de cette recherche, ainsi que Stéphane Faure, codirecteur, pour l'intérêt qu'ils ont manifesté jusqu'au terme de ce projet. Je remercie particulièrement Anne Slivitzky de Maude Lake Exploration et tous les membres du Consorem pour l'opportunité et le financement nécessaire pour la réalisation de cette étude. Je tiens également à remercier Yvon Trudeau, Pierre Riopelle et l'équipe technique de Maude Lake Exploration pour leur appui, encouragement et expertise sur le terrain.

La portion analytique de cette étude a bénéficié de l'aide de plusieurs agents de recherche de l'UQAM. Je remercie Michel Preda pour la diffraction aux rayons X, Raymond Mineau pour la microscopie à balayage électronique et Michèle Lanthier pour la réalisation de l'affiche et des cartes.

Finalement, je tiens à remercier mes parents qui m'ont inculqué la soif d'apprentissage, ma conjointe Carine Rabbath, qui m'a encouragé dans la poursuite de mes études et mes enfants, Caroline et Olivier, qui m'ont inspiré à terminer mes études.

TABLE OF CONTENTS

LIST OF FIGURES

Figure Page

LIST OF TABLES

RÉSUMÉ

Le gîte de Comtois est situé dans le complexe volcanique archéen du Nord de la sous province de l'Abitibi. Les roches volcaniques hôtes sont de compositions mafiques, intermédiaires et felsiques. La séquence volcanique est verticalisée. Elle montre des textures massives et clastiques. Comtois se caractérise par ses nombreux dykes, des veines et des altérations hydrothermales. Cette étude vise à découvrir un lien entre la minéralogie des veines, les altérations hydrothermales et la minéralisation aurifère afin d'identifier le type de modèle génétique.

L'étude des veines a permis d'établir quatre types sur la base de leur paragenènes et leur orientation. Les veines de type I sont composées de quartz gris d'orientation variable. Les veines de type II sont composées d'actinote + quartz ± épidote ± pyrite orientée 60°N et 100°N. Les veines de type III sont composées de pyrite ± chalcopyrite orientée 120°N. Les veines de type IV sont composées de quartz laiteux orienté 70°N.

Les roches volcaniques ont subi plusieurs altérations hydrothermales. La cordiérite et andalousite sont trouvées de façon envahissante partout dans la zone d'étude. L'épidote et l'albite sont associées aux veines de type II. Une enveloppe d'altération à quartz est localement observée avec les veines de type III.

La minéralisation en or est associée aux veines de types III dans l'enveloppe d'altération siliceuse. L'or se trouve en grain d'électrum dans la pyrite et ses fractures. Le ratio Au :Ag se situe entre 9:1 et 1:2. Des grains de BiTe sont aussi présents dans le même contexte.

Le contexte géologique, les altérations hydrothermales et la composition des grains d'électrum sont consistants avec un modèle génétique de type sulfures massifs volcanogène.

Mots-Clés : Altération, Cordiérite, Andalousite, Veines, Sulfures Massifs

ABSTRACT

The Comtois deposit is located in the Achaean Volcanic Complex in the Abitibi Sub province. Mafic, intermediate and felsic volcanic rocks host the deposit. The verticalised volcanic sequence of mafic and intermediate volcanics is observed in massive and clastic textures. This deposit characterises itself by the variety of dykes, veins and hydrothermal alterations. This study aim to discover links between the vein mineralogy, the hydrothermal alterations and the gold mineralisation in order to identify a possible genetic model type.

Study of the veins has established four types of veins according to their mineralogy and their orientations. Type I are grey quartz veins of various orientations. Type II are actinolite+quartz±epidote±pyrite veins oriented 60°N and 100°N. Type III are pyrite±chalcopyrite veins oriented 120°N. Type IV are milky quartz veins oriented 70°N.

The volcanic rocks have sustained many hydrothermal alterations. Cordierite and andalusite are pervasively found throughout the study area. Epidote and albite are associated to the type II veins. A quartz alteration envelope is frequently associated to the type III veins.

The gold mineralisation is associated to the type III veins with a silicic alteration envelope. The gold is present as electrum grains in pyrite grains and fractures. The Au:Ag ratio of the electrum ranges from 9:1 to 1:2. BiTe grains are also observed in the same context.

The geological setting, hydrothermal alterations and the electrum composition are consistent with a VMS type genetic model.

Keywords: Alteration, cordierite, andalusite, veins, VMS

CHAPTER I

STUDY OF THE VEINS, ALTERATIONS AND MINERALIZATION OF THE COMTOIS GOLD DEPOSIT, ABITIBI SUBPROVINCE, QUEBEC, CANADA

1.1 Introduction

The Comtois deposit is located within the Northern Volcanic Zone (NVZ) of the Archean Abitibi sub-province, Quebec, Canada. The NVZ hosts a large number of gold and polymetallic mines such as the Matagami (Piché et al. 1990) and Grevet massive sulfide deposits, the Eagle-Telbel shear zone gold deposit (Wyman et al. 1986) and the Sleeping Giant quartz vein gold deposit (Gaboury and Daigneault 1999). Even with the large amount of past discoveries, the region still holds a great potential for new discoveries.

The Comtois gold deposit is located 15km northwest of Lebel-sur-Quevillon and is still at the exploration stage. Mr. Brian Osborne discovered the auriferous zone. Cameco Gold did preliminary exploration work between 1994 and 1997. Maude Lake Exploration acquired the property in 1997 and has since established indicated resources of 705 000 t @ 9.05 g/t Au with surface drilling.

The property is located at the northern periphery of the Beehler granitic intrusion. The deposit is hosted in mafic to felsic volcanic rocks. The volcanic sequence is verticalized and trends E-W. This sequence is crosscut by many mafic, porphyry, aplitic and gabbroic dykes. The Comtois has an unusual style of mineralization and alteration when compared to the other deposits in the area. The

volcanic setting, geometry and gold mineralization suggests a VMS type deposit but lacks the typical chloritic alteration usually associated to a VMS alteration pipe. Its close proximity to a granitic intrusion indicates the possibility of a skarn type deposit. Finally, the planar morphology of the gold-bearing zone and local dextral displacements suggest a possible shear zone type deposit.

This study aims to discover links between the vein mineralogy, the hydrothermal alterations and the gold mineralization in order to identify a possible deposit type.

1.2 Regional Geology

The NVZ is subdivided into two segments based on differing volcano-sedimentary successions and stratigraphic relationships (Fig.1.1; Chown et al. 1992). The southern portion is composed of monocyclic volcanic sequence whereas the northern segment is characterized by a polycyclic volcanic sequence. The Comtois deposit is located in the Monocyclic Volcanic Segment. This segment is dominated by massive, pillowed and brecciated basalts of tholeiitic composition in an extensive 1 to 3 km thick subaqueous basalt plain (Mueller et al.1989; Pilote 1989; Picard and Piboule 1986; Ludden et al. 1984). Massive and brecciated rhyolitic to rhyodacitic lava flows are dispersed throughout the Northern Volcanic Zone in edifices varying from 0.2 to 5 km thick (Potvin 1991; Piché et al. 1990; Gagnon 1981). These lava flows range in age from 2730 to 2720 Ma (Daigneault et al. 2003). All edifices show a dominant sub aqueous volcanic constructional phase. The majority of felsic edifices are sub oceanic and many of the smaller felsic extrusions are covered with pillowed basalt flows (Bloomer et al. 1989).

Sedimentary assemblages occur as thin discontinuous east-trending belts over 100km in length. These are primarily Bouma-cycled turbidities intercalated with volcanogenic conglomerates, banded iron-formation, shale and chert (Hocq 1983;

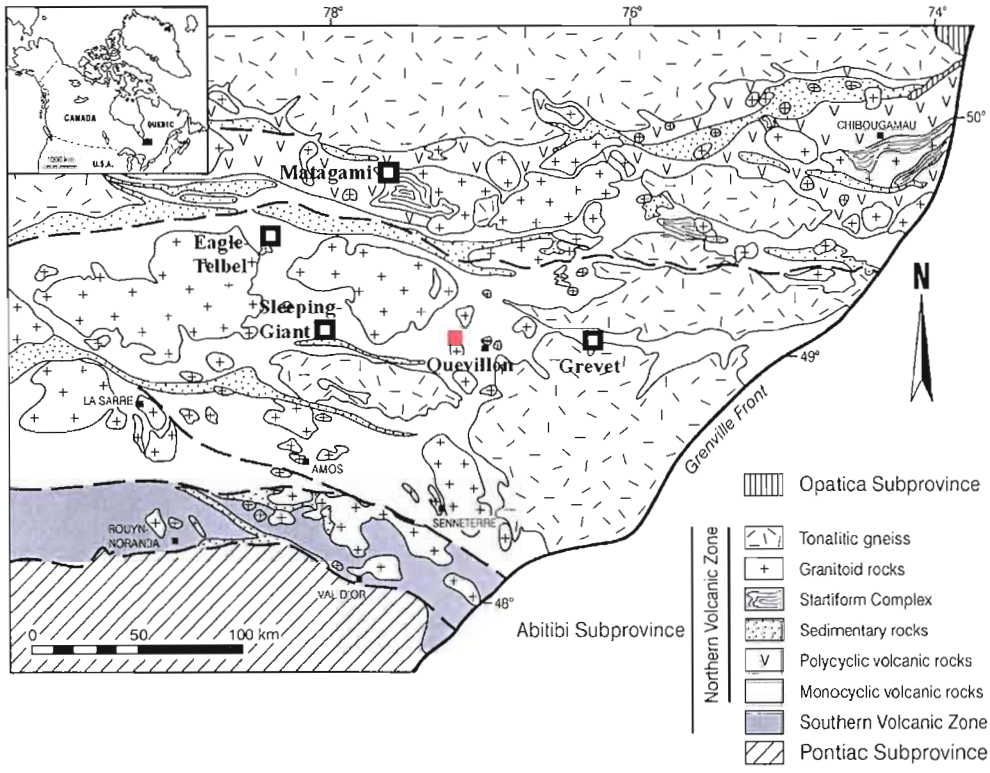

Fig.1.1: Generalized geological map of Abitibi's Northern Volcanic Zone as defined by Chown et Al. (1992). The study area is found within the red region, north of Quevillon. Other major gold and polymetallic mines outlined.

Lauzière et al. 1989; Dussault 1990). Minor pyroclastic deposits, basalt flows, sills and dykes reveals a continued volcanic activity within these basins.

Various episodes of plutonic activity occur in the NVZ. A group of batholiths that are categorized as synvolcanic (Chown et al. 1992). These plutons have been deformed and metamorphosed by regional constraints. The second group of plutons are related to the main deformational events. They are classified as syntectonic (Peterson et al. 1989). A smaller group of post-tectonic intrusions are associated with the final deformational phase (Chown et al. 1992).

A series of deformational events (D1-D6) is consistent with a major continuous compressional event rather than several orogenic phases (Chown et al.1992; Daigneault et al. 2003). NNW-SSE shortening was first obtained by sub-vertical east-trending folds. Continued compression deformation produced east-trending fault zones and contact strain aureoles around synvolcanic intrusion. This major compressional event took place within a 25 Ma interval beginning at 2710 Ma (Daigneault et al. 2003).

1.3 Local Geology

The local geology of the Comtois deposit (fig. 1.2) is composed of mafic to felsic volcanic rocks (fig. 1.3). These mafic-intermediate volcanic rocks have basaltic to andesitic composition. The felsic rocks have a dacitic to a rhyolitic composition. The mafic-intermediate monocyclic volcanic rocks demonstrate fine grained massive to epiclastic textures (fig. 1.4A+B). The felsic volcanic rocks are a fine-grained rhyodacite found within a 100m wide WNW trending corridor. The volcanic rocks have undergone various episodes of hydrothermal alteration.

The deposit is crosscut by a variety of dykes and a coarse grained granitic intrusion of km scale to the south. There are mafic, potassic porphyry, aplitic and gabbroic dykes. The dykes have a particular chronology determined by crosscutting relationships. The oldest dykes are fine-grained and mafic in

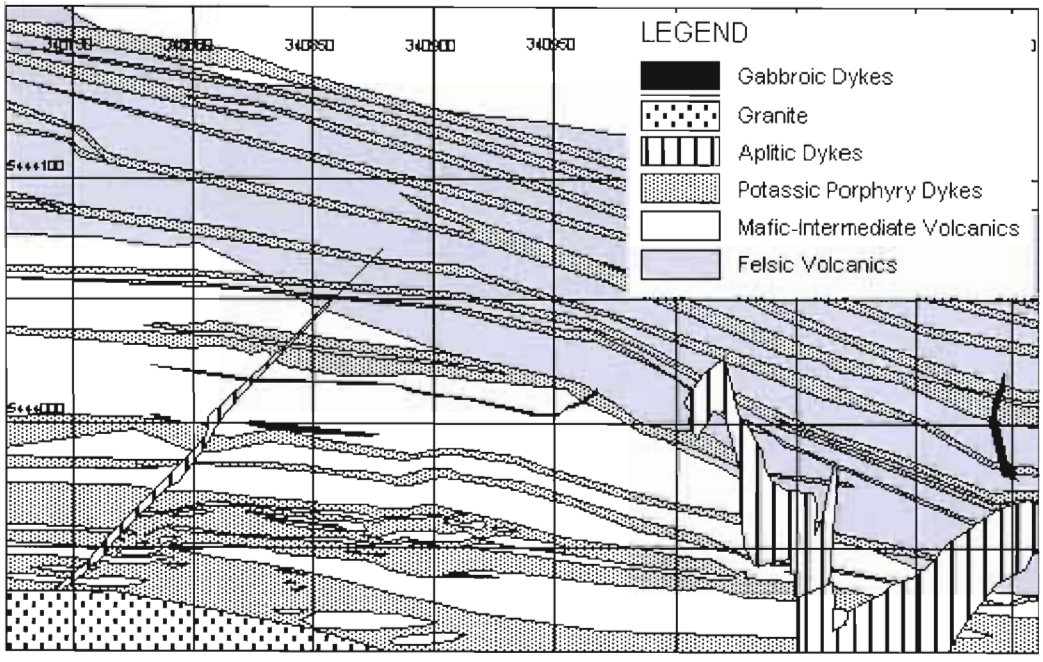

Fig. 1.2: Local geology of the study area within the Comtois property.

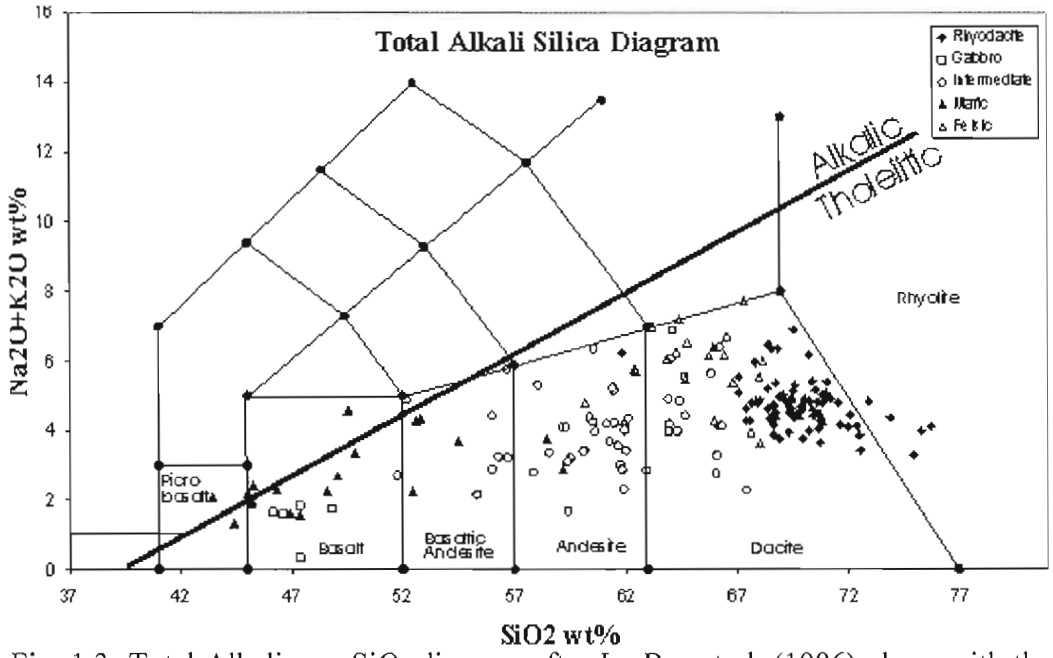

Fig. 1.3: Total Alkalis vs. SiO_2 diagram after Le Bas et al. (1986) along with the Hawaiian boundary between tholeiitic and alkaline lavas after MacDonald and Katsura (1964). This shows the rocks to be tholeiitic basalts, andesites and dacites. Note: the classifications of the lithologies in the legend are the classifications given on the field.

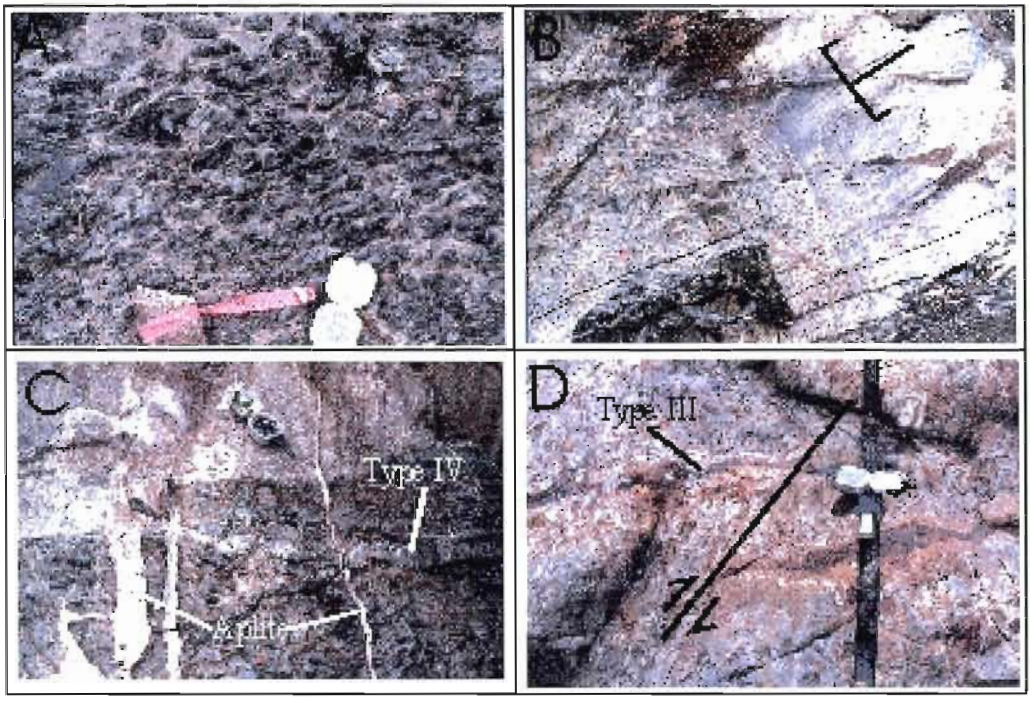

Fig. 1.4: Field photographs: A) The epiclastic texture of the mafic volcanic rocks; B) Stratigraphy of the mafic volcanic rocks shown by a contact between a massive and a epiclastic texture (polarity towards the North); C) Crosscutting relationships between the mafic volcanic rocks, milky quartz veins, potassic porphyry dykes and aplitic dykes; D) Mineralised pyrite vein with a dextral displacement

composition. The mafic dykes are interpreted as synvolcanic due to quartz ladder veines commonly associated and an extremely porous dissolution texture of the mafic dykes. The second type of dykes is the potassic porphyry dyke. These dykes are the most abundant dykes and represent 10% of the studied surface. At least two generations of potassic feldspar porphyry dykes are distinguished. One generation is biotite bearing whereas others have no biotite. The porphyry dykes range from 50 to 150 cm in width. The porphyry dykes increase in quantity and become jointive towards the south. They are post-tectonic, being unfoliated, and parallel to the regional schistosity. The third type of dykes is a very fine-grained rose-colored aplitic dyke ranging from 1 to 30 mm in width. The final types of dykes observed are medium to coarse-grained gabbroic ranging from 5 to 200 cm in width.

The granitic intrusion, located to the south, is very coarsely grained. There is no foliation observed within the granitic rocks, which is an indication that it is post tectonic. The granitic intrusion produced a thermal metamorphic aureole recorded in the volcanic rocks. The biotite and actinolite mineral assemblage of the volcanic rocks is indicative of an amphibolite metamorphic facies. Retrograde metamorphism of biotite produced the only chlorite observed within the study area.

There is only one schistosity observed within the study area. It is penetrative, subvertical and trends E-W (fig. 1.5) and it is parallel to the volcanic sequence. There is no fold observed. The clasts observed in the volcanic rocks are elongated in a cigar shape with a subvertical long axis. The long axis: short axis ratio is estimated at 5:1. There are many NE-SW brittle faults that display centimetric to metric dextral displacements (fig. 1.4D). Hydraulic brecciation is observed locally to the southeast of the property. However, the magnitude of the total displacement produced by the brittle faults is undetermined. Chronologically, the brittle faults crosscut all geological units and represent the last deformational event at the Comtois deposit (fig. 1.6).

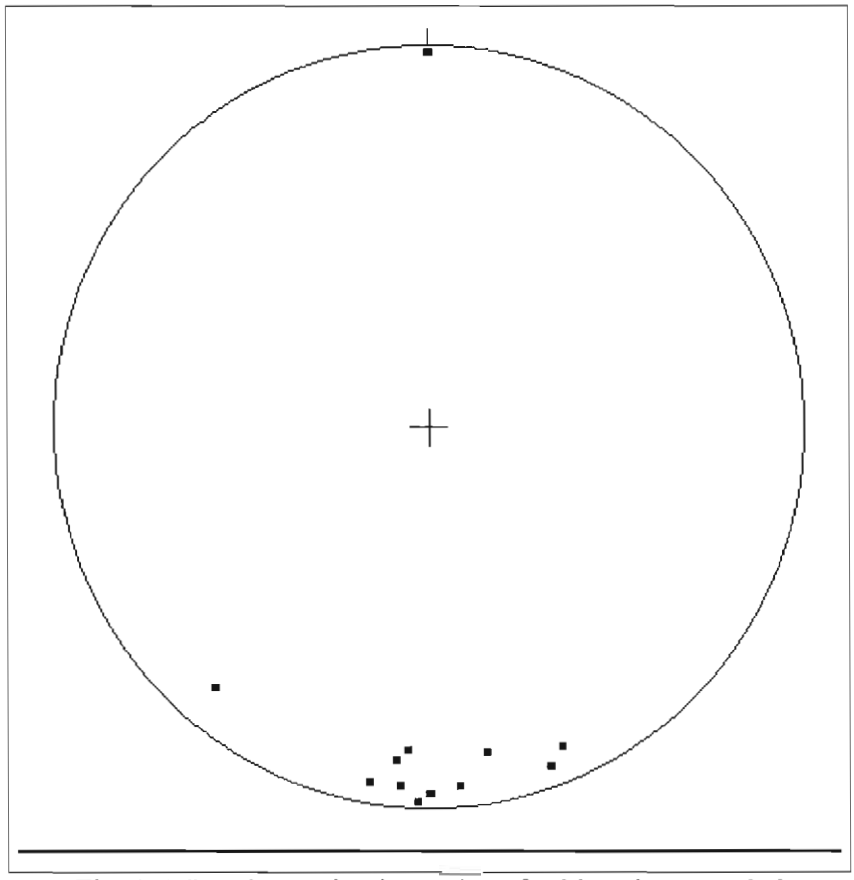

Fig. 1.5: Interior projection poles of schistosity recorded in volcanic rocks (n=14)

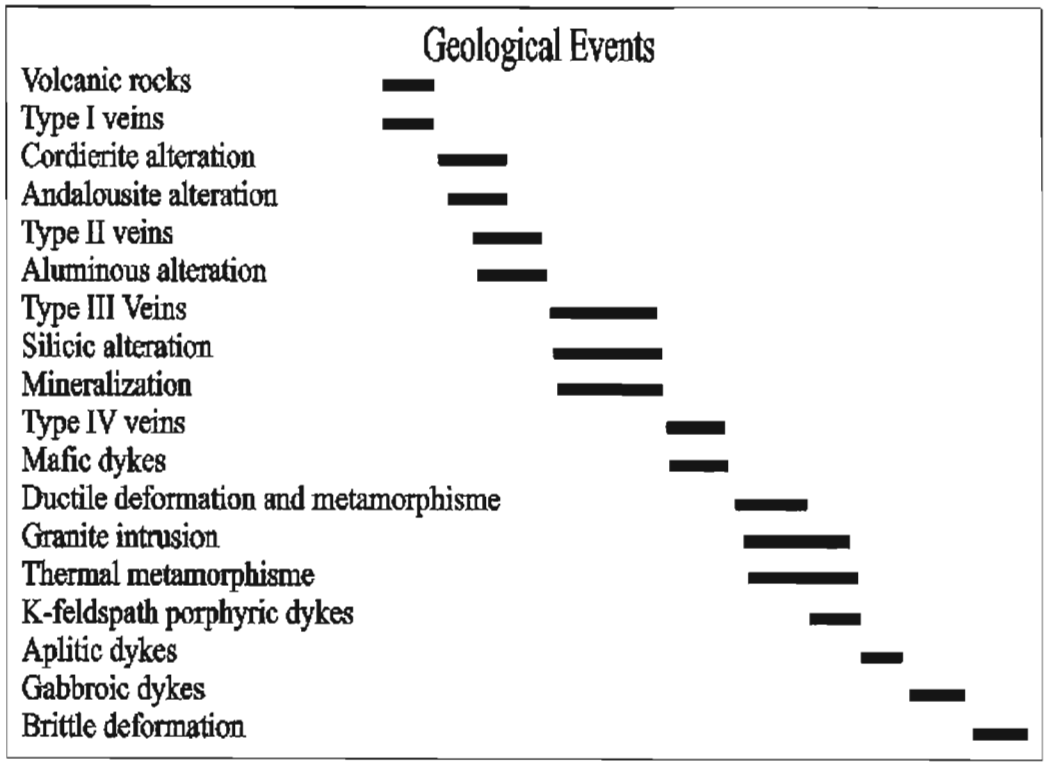

Fig. 1.6: Relative chronology of geological events based on field crosscutting relationships

1.4 Ore Geology

There are four types of veins found within the study area. Among these types of veins, two are associated with significant hydrothermal alterations. However, only one type of vein is gold-bearing.

1.4.1 Veins

The Comtois deposit has four types of veins found within the volcanic rocks:

Type I: Quartz veins

Type II: Actinolite + quartz ± epidote ± pyrite veins

Type III: Pyrite +quartz ± chalcopyrite veins

Type IV: Milky quartz veins

The type I veins are composed of 1-2mm thick quartz veins. They are the oldest veins, being crosscut by all other vein types. There is no associated alteration in the host rock. They are found both in mafic and felsic volcanic rocks as stockwerks. However, the rose diagrams with emphasis on length differ for each lithology (fig. 1.7A+B). This demonstrates the impact of different rheologies on the propagation of the type I veins. The type I veins found in the mafic rocks propagate in almost all directions, however the N – S veins are more continuous. The type I veins found in the felsic rocks is more continuous when oriented E-W.

The type II veins (fig. 1.8A-B-C) are primarily composed of actinolite-quartz veins occasionally accompanied with epidote and pyrite. Locally, a vein with the same morphology as the type II veins was observed with a corundum-sericite mineral assemblage. They are distributed throughout the study area. They are preferentially oriented 60°N and 100°N (fig. 1.7C) with a sub vertical dip. The type II veins seem to have been introduced into a ductile environment. They lack

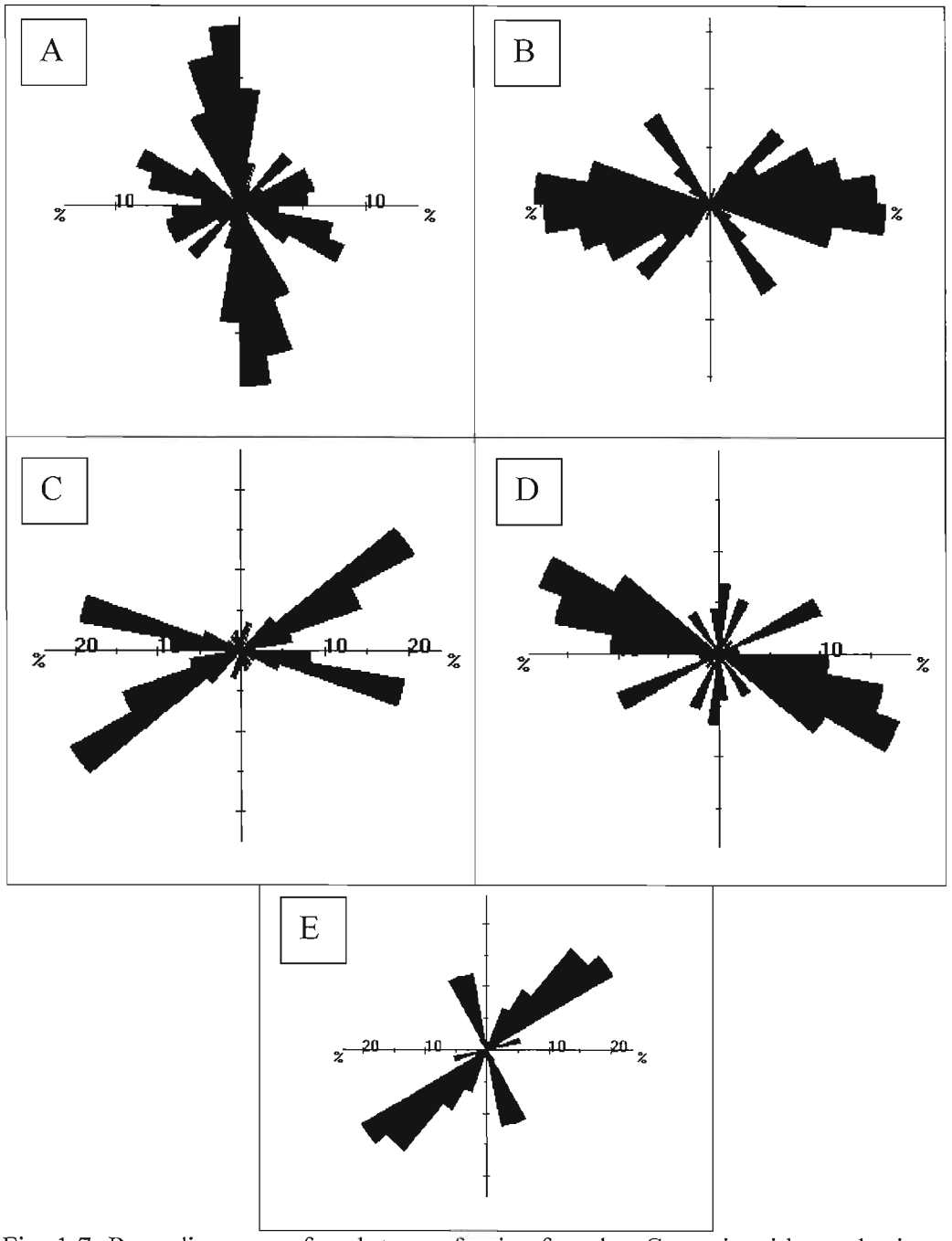

Fig. 1.7: Rose diagrams of each type of veins found at Comtois with emphasis on length. A) Type I veins in mafic volcanic rocks; B) Type I veins in felsic volcanic rocks; C) Type II veins; D) Type III veins; E) Type IV veins

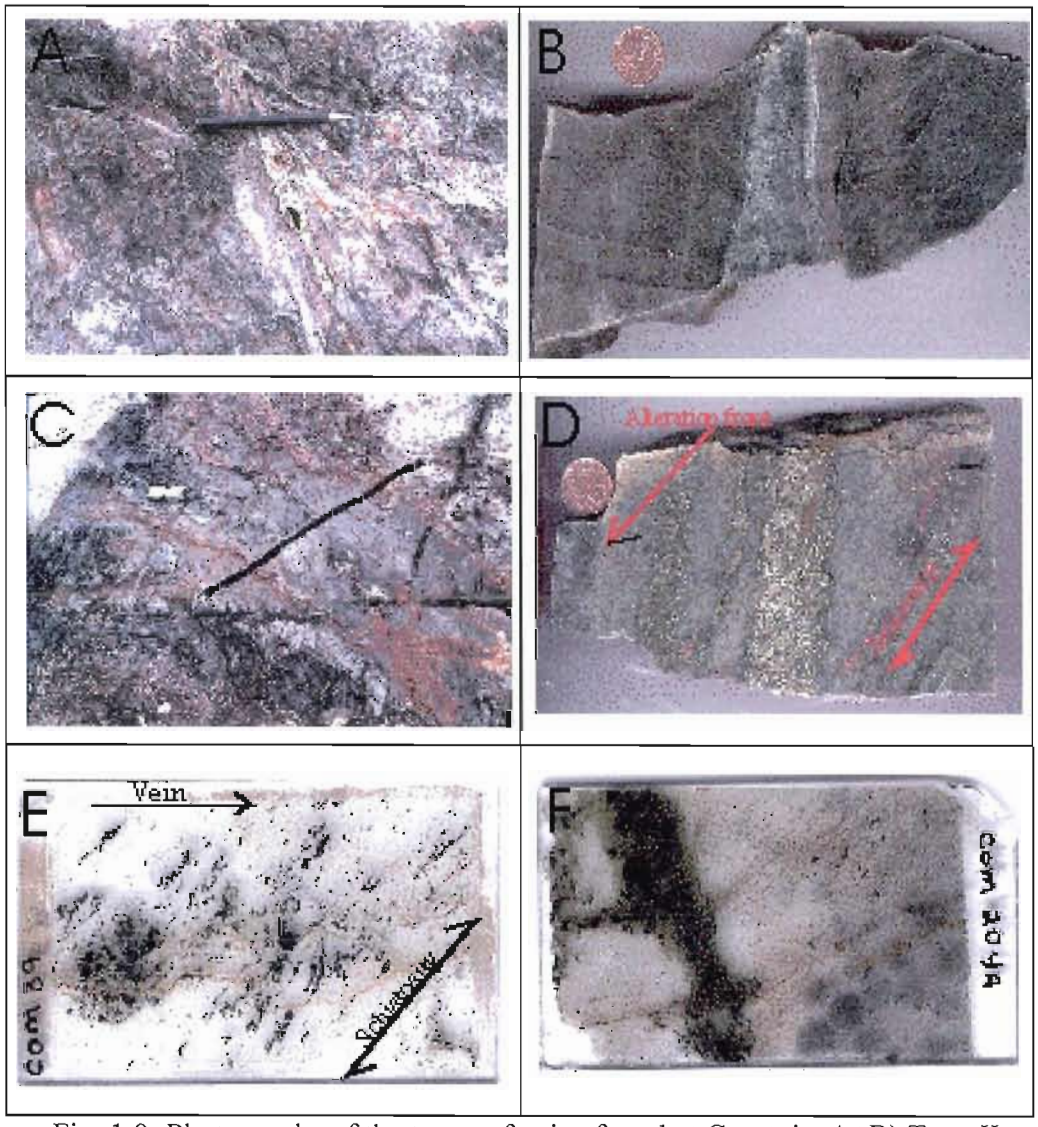

Fig. 1.8: Photographs of the types of veins found at Comtois. A+B) Type II veins; C) Type II veins with pyrite; D) Type III vein (note the silicification front ends at the penny); E) Thin section of a pyrite vein, encased in rhyodacite, remobilised in schistosity (the vein is horizontal and the schistosity is at a 40° angle in relation); F) Thin section of a pyrite vein in a mafic volcanic rock with halos of cordierite crystals. Note the obliteration of the cordierite by the type III vein.

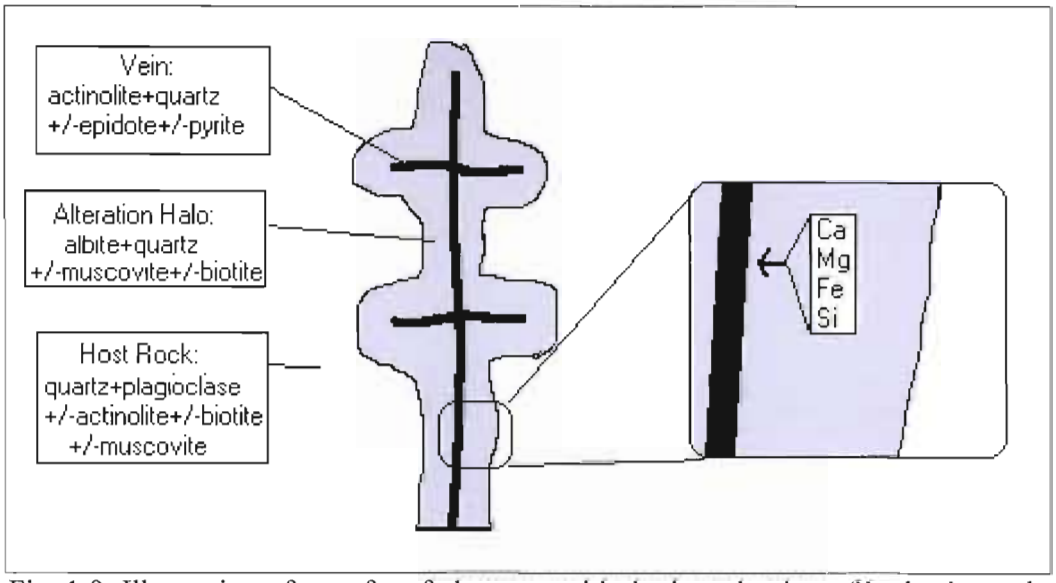

Fig. 1.9: Illustration of transfer of elements with the introduction of hydrothermal fluids to produce type II veins

the linear morphology usually exhibited by veins in a brittle environment. They propagated in a sinuous fashion and display a pinch and swell variation in thickness of 0-3cm.

The epidote bearing type II veins have a particular spatial distribution. They are uniquely found in the mafic-intermediate volcanic rocks of the western portion of the study area. Mineralization in the form of pyrite occurs in the type II veins (fig. 1.8C), however they are not gold-bearing. The type II veins have a particular alteration halo composed of albite (Fig.1.9).

The type III veins (fig.1.8D-E-F) are composed of pyrite +quartz ± chalcopyrite (±pyrrhotite ±sphalerite ±galena ±gold) veins. They are planar and vary in thickness from 0-3cm. They have a distinct orientation of ± 300°N (Fig. 1.7D) with a sub vertical dip. The pyrite veins are found in both the felsic and mafic volcanic rocks. The pyrite and chalcopyrite minerals show a particular paragenesis within the veins. The chalcopyrite is usually found at the rims of the pyrite veins (fig. 1.10A-B). The sulphides of the type III veins have been partially remobilised into the schistosity (fig 8D-E). They also occasionally show a silicic and sericitic alteration halo (fig. 8D).

The type IV veins (fig. 1.4C) are composed of only milky quartz and are oriented 70°N (Fig. 1.7E). They exhibit no alteration and no mineralization.

Chronologically, the type I are the oldest veins to appear within the study area. The type II and III are associated with the major hydrothermal alterations observed within the study area. However, no clear crosscutting evidence is observed to establish a chronology between the type II and III veins. The type IV are the latest veins. They have no hydrothermal alteration halo and they crosscut all hydrothermal alteration associated to the other veins.

1.4.2 Alterations

The volcanic rocks of the study area have sustained a large amount of hydrothermal alteration (fig. 1.11). The alteration zones were analysed by x-ray

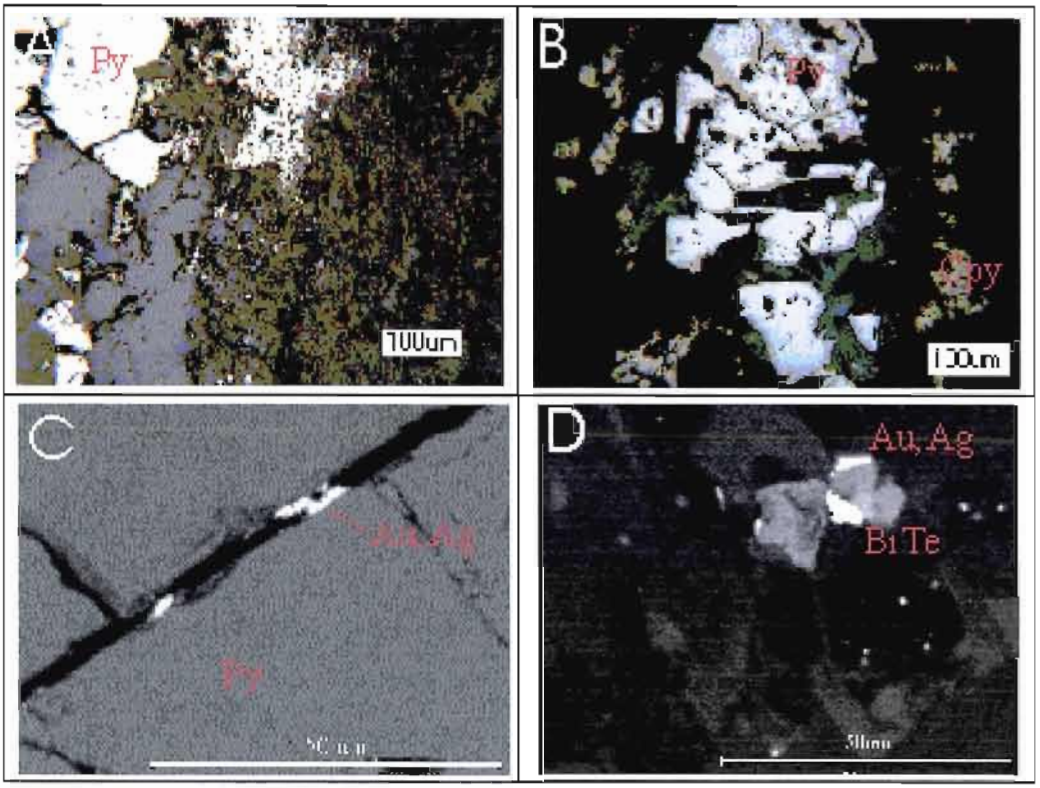

Fig. 1.10: Microscope photographs of type III veins. A+B) Paragenesis of type III veins show that chalcopyrite (cpy), when present, is located on the borders of the pyrite (py) and quartz. Observed with reflected light under optical microscope. C) Electrum grains (Au,Ag) in the pyrite fractures of type III veins observed under electron microscope. D) Electrum grain and bismuth telluride(BiTe) grain found with quartz in type III vein, observed under electron microscope.

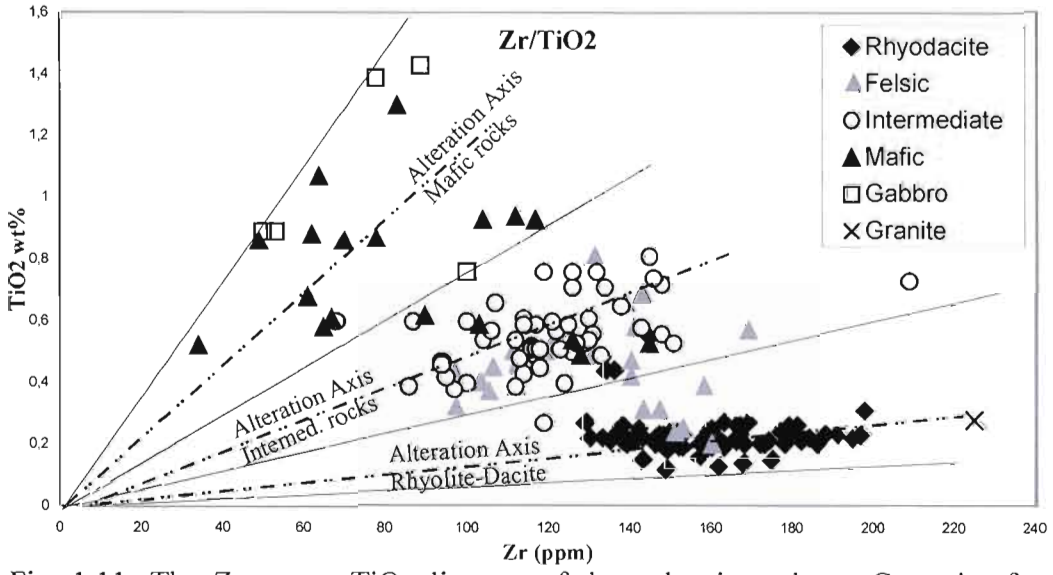

Fig. 1.11: The Zr versus TiO_2 diagram of the volcanic rocks at Comtois after (Barrett et al. 2001). Note that for each rock type the Zr-TiO_2 composition varies along an axis that represents the degree of alteration. No unaltered rocks were identified to determine the exact degree of alteration.

diffraction (appendix A) in addition to microscopic observations. This was done to determine the quantitative mineralogy of the alteration zones.

Cordierite is pervasively present in the mafic-intermediate volcanic rocks (fig.1.8F; 1.12A). The spotted texture of cordierite, termed dalmatianite (Riverin and Hodgson 1980), is observed macroscopically in hand samples and thin section. The spots range from 1-6mm in diameter. Microscopically, cordierite is difficult to observe due to an intense sericitic replacement, leaving only remnant halos of the cordierite crystals.

Andalusite is present in the volcanic rocks occasionally observed as large sugar-like grains. It is microscopically observed with sericite (fig. 1.12B). Corundum is observed in a vein that closely resembles a pebble dyke. This vein is composed of sericite – corundum and crosscuts an actinolite bearing volcanic rock with biotite at the contact (fig. 1.12 C-D). No quartz is observed in the assemblage.

Epidote is present within the western half of the study area. It is found within type II veins in a fine grained texture with quartz. Locally, large grained epidote is found as1-4cm patches with diffuse borders in mafic volcanic rocks.

Albite is commonly found in an alteration envelope associated to the type II veins (fig. 1.8C; 1.10). This envelope extends from 1-20cm around the veins. The albite alteration is more pervasive towards the center of the mapped area. The alteration envelopes eventually become jointive and cover the whole area, leaving no unaltered volcanic rocks at the heart of the study area.

The type III veins have a pervasive sericitic alteration. The sericite is oriented parallel to the schistosity. Biotite is found at the vein-host rock contact. The biotite is medium grained and oriented parallel to the adjacent pyrite veins. Occasionally, a quartz alteration halo envelopes the type III veins superimposing the sericitic alteration. Biotite is not observed at the vein-host rock contact when a silicic alteration halo is present.

.

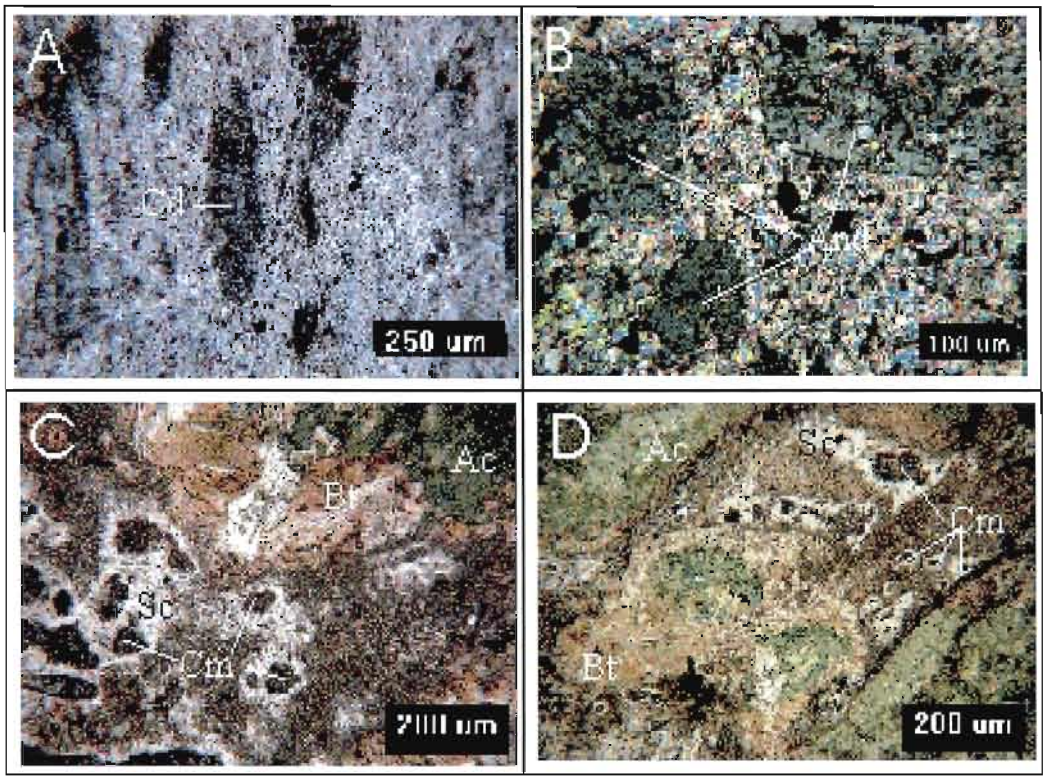

Fig. 1.12: Alteration mineralogy A) Cordierite (Cd) crystal halos; B) Andalusite (And) crystals in a sericitic matrix; C) and D) Vein composed of corundum (Cm) and sericite (Sc) crosscutting an actinolite (Ac) bearing volcanic rock with biotite (Bt) at the contacts

1.4.3 Mineralization

The main ore body has a calculated resource of 700 000t at 9.5g/t Au and is located to the east of the mapped area (fig.1.2) at a depth of 20 to 200m. This resource is divided into two enriched subvertical E-W trending planar zones. Based on drill holes, Zone A is located 50m to the SSE of Zone B. The background within the study area is anomalous for gold. The average Au value obtained for the volcanic rocks of the property is 200ppb, which is four times greater than usually expected. Only the samples that contain type III veins contain important gold grade. However, not all type III veins are gold bearing. The type III veins that are mineralized with important gold grades have an associated silicic alteration envelop (fig. 1.8D) that superimposes the more pervasive sericitic and albitic alterations. There are seven observed type III veins with a silicic alteration envelope. There is one found within the felsic volcanic rocks with a value of 17.8g/t. The 6 other type III veins found in mafic volcanic rocks with an associated silicic alteration envelope yield values between 6.2g/t and 62.5g/t.

The gold is found locked within the pyrite grains and within the fractures between pyrite grains (fig. 1.10C) in the form of electrum. The electrum has an Au: Ag ratio varying from 9:1 to 1:2 (fig.1.13 + 1.14). However, some core samples of the mineralised zones contain native gold with Au:Ag ratios > 50:1 while other samples contain grains of argentite. The BiTe grains are also observed in the same environments as the gold grains (Fig. 1.10D).

1.5 Discussion

The northern portion of the Abitibi region contains several types of deposits. There are massive sulphide deposits, shear hosted gold deposits and quartz vein deposits. However, the Comtois deposit's unusual styles of mineralization and alterations have made classification difficult. It is located 100-150m north of a granitic intrusion, which suggests a possible skarn type deposit. The E-W trending planar morphology of the anomalous gold envelop suggests a possible shear zone

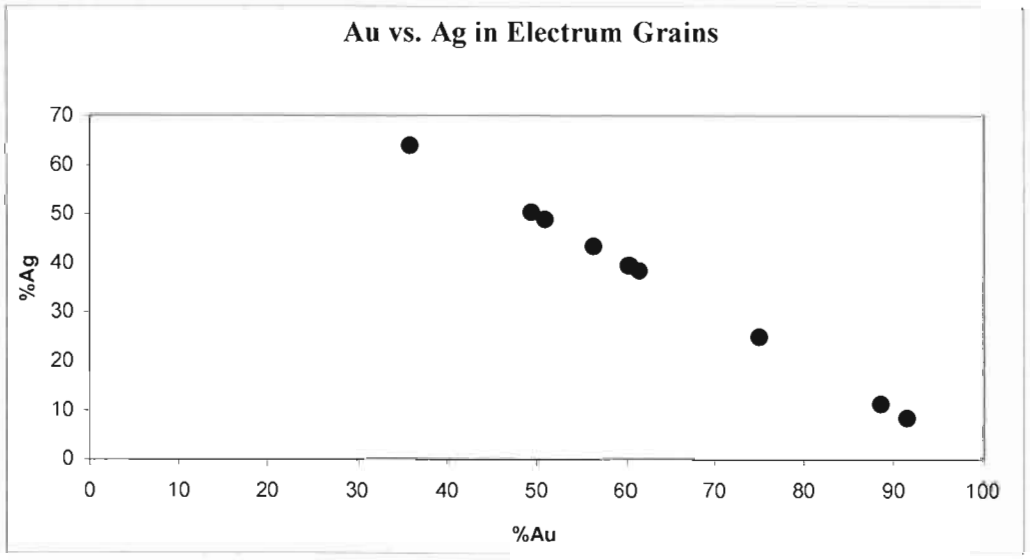

Fig. 1.13: Analysis of electrum grains by electron microscope

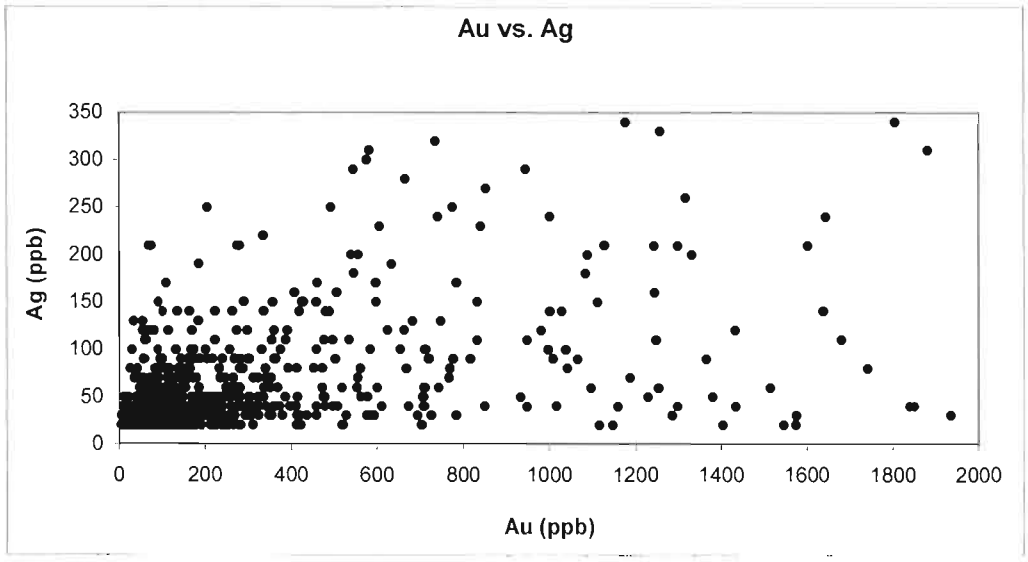

Fig. 1.14: Analysis of 730 portions of core samples of the Comtois deposit by ICPAS, Chimitec.

type deposit. However, it's geological setting, geometry, hydrothermal alterations and the nature of the gold mineralization suggests a VMS type deposit.

The veins and hydrothermal alterations distinguish the Comtois deposit. Cordierite and andalusite is pervasively dispersed throughout the study area. There are two types of veins that produced extensive hydrothermal alterations. Unmineralized actinolite veins produced a pervasive albitic alteration. The only gold bearing veins are pyrite +quartz +chalcopyrite veins with a sericitic and silicic alteration envelop. The gold in the pyrite is locked in the pyrite grains and it's fractures. The composition of the gold grains is 9:1 to 1:2 Au:Ag. There are also many dykes found at Comtois. However, they crosscut all veins and their associated hydrothermal alterations.

Auriferous skarns typically have a mineralization enriched in As, Bi and Te (Dawson, 1996). The Comtois deposit does contain small amounts of Bi and Te but no As enrichment is observed. Also the relative chronology of the deposit shows that the complete system of potassic porphyry dykes, which root into the granitic intrusion, crosscuts the mineralised veins and their associated hydrothermal alterations.

The shear zone related deposits are typically characterised by banded quartz associated to a shear zone in carbonitized volcanic rocks (Knopf 1929; Robert 1996). The shear hosted gold deposits usually have a typical Au:Ag ratio varying between 5:1 and 9:1 (Robert 1996). No banded quartz was observed. Also the schistosity crosscuts the gold bearing veins and the associated hydrothermal alterations, therefore indicating that deformation postdate the main phase of mineralization. Analysis of gold grains under an electron microscope and analysis of core samples at Comtois show that the average Au:Ag ratio varies from 9:1 to 1:2 (fig. 1.13) with some rare grains of argentite. The Comtois deposit hosts much more Ag than usually found in shear zone deposits.

The volcanic geological context at Comtois is favourable for development of a massive sulphide deposit. The volcanic rocks have undergone a large amount of

hydrothermal alteration (fig. 1.11). This is observed as the volcanic chemistry varies along an alteration axis illustrating it's mass gain or loss (Barrett et al. 2001).

Cordierite, andalusite, albite, sericite and epidote are the main hydrothermal alteration minerals found at Comtois. Cordierite is found in the mafic to intermediate volcanic rocks. It is characteristically a highly metamorphosed Mg-Fe rich alteration zone, the equivalent of a chloritic alteration zone found within massive sulphide deposits (Friesen et al. 1982). The presence of this mineral suggests that the rocks have undergone a strong Mg-Fe enrichment and a Na-Ca-K depletion. The cordierite is observed macroscopically as a spotted texture. This texture is termed dalmatianite and develops in chlorite-rich footwall alteration pipes below massive sulphide deposits in regionally metamorphosed areas or in the contact metamorphic aureole of a post volcanic intrusion (Riverin and Hodgson 1980). The cordierite forms during thermal prograde metamorphism (MacRae 1977) and is later replaced by mica and/or chlorite during retrograde metamorphism (Friesen and al. 1982). Therefore, the presence of cordierite is compatible to a volcanogenic alteration zone associated to a massive sulphide deposit. The dalmatianite texture also places it spatially in the VMS genetic model. The obliteration of the cordierite being crosscut by the type III veins (Fig. 1.8F) shows that the formation of cordierite preceded, at least partially, the gold mineralization at Comtois.

The volcanic rocks throughout the study area contain traces of andalusite. The andalusite is often observed as large sugar-like grains in a fine-grained sericite-quartz assemblage. Andalusite in other VMS deposits is recognized as the metamorphic equivalent of advanced argillic alteration such as a quartz-koalinite-pyrophillite assemblage (Gustafson and Hunt 1975; Hannington et al. 2002). The metamorphic contact aureole produced by the granitic intrusion contributed to the growth of the large grains of andalusite in a high Al_20_3 and high SiO_2 environments (Lemiere et al.1986).

Epidote is observed in two forms. It is observed as part of the type II veins mineral assemblage. The epidote-quartz-actinolite-albite-pyrite veins have been recognized as a prograde alteration in other VMS type deposits (Galley et al.2000). Epidote patches, locally observed at Comtois, represent the prograde epidote-quartz alteration style also consistent with VMS type deposits (Galley 1993). This alteration is usually very extensive laterally and is controlled by the primary permeability of the host rocks. The epidote, in veins and patches, is therefore representative of zones that were favourable for hydrothermal flow.

The type II veins are mainly composed of actinolite-quartz and are characteristically accompanied by an albite alteration halo. The albite represents a spilitization of the volcanic rocks as Ca, Mg and Fe migrate to the actinolite bearing veins (Tab 1.1). This migration of elements is produced by the flow of hydrothermal fluids in the deep convection cell that would eventually produce a massive sulphide lens higher up stratigraphically (Galley 1993). Actinolite is often found as an alteration mineral in high temperature intrusion related environments (Gustafson and Quiroga 1995; Dilles and Einaudi 1992) consistent with deep hydrothermal convection cells. Corundum was also observed in some veins, which is further evidence of a high temperature environment (Hemley et al. 1980).

The type III veins with a related silicic alteration envelope contain the gold mineralization. The gold is found as electrum in an Au:Ag ratio varying between 9:1 and 2:1. This ratio is compatible with ratios commonly recorded among high sulphidation massive sulphide deposits (Poulsen and Hannington 1996). There are also traces pyrrhotite, sphalerite and galena, which are common sulphides in VMS deposits. The majority of the mineralization is found within the veins. No massive sulphide lens has been discovered yet. It is suggested that the study area was located under a massive sulphide during the formation of the deposit. The massive sulphide lens has either been eroded, unformed, remobilised or unfound. The

	Host Rock	Alteration Zone	Transfer of Elements	Vein
Type II Veins	quartz plagioclase actinolite(±) biotite(±) muscovite(±)	albite quartz biotite(±) muscovite(±)	Ca→ Mg→ Fe→	actinolite epidote(±) quartz
Type III Veins	quartz plagioclase biotite	quartz sericite plagioclase	Fe→ ←Si	pyrite quartz chalcopyrite(±) pyrrhotite(±) sphalerite(±)

Tab. 1.1: Summary of major mineralogy for each vein type with their respective alteration zones and host rocks that illustrates the transfer of elements between host rock and hydrothermal fluids.

volcanic sequence is verticalized with a polarity to the north. Morphologically, the two enriched zones resemble stratigraphically concordant superimposed sulphide lenses typically found in VMS type deposits.

1.6 Conclusion

The geological setting of the Comtois deposit along with its hydrothermal alteration zones suggests that the mineralization is synvolcanic. The hydrothermal alterations distinguished by cordierite, andalusite and epidote indicate a metamorphosed altered zone typical of a VMS system. The cordierite mineralization spatially places the mapped area under a potential VMS. The thermal metamorphism, produced by the granitic intrusion, occurred after the mineralising event. However, the presence of large sugar-like andalusite grains, actinolite veins and corundum show that the hydrothermal fluids were abnormally hot. This leads to believe that the hydrothermal fluids that altered Comtois may have originated close to the granite before it's ascent. The genetic model may be a hybrid found between the VMS and porphyry deposit models.

Further drilling of the stratigraphically higher volcanic units may discover new massive sulphide lenses and important gold resources.

APPENDIX A

ANALYSIS OF VEIN MINERALOGY AND VEIN ALTERATION USING A SIEMENS D-5000 X-RAY DIFFRACTOMETER

A.1 Résumé

Les roches volcaniques de Comtois ont subi beaucoup d'altérations hydrothermales. Une étude de la minéralogie des veines et des altérations est essentielle pour comprendre l'histoire géologique de Comtois. Une meilleure compréhension des altérations produites par les veines pourrait mener à un modèle génétique.

Des petits échantillons représentatifs des veines et leurs enveloppes d'altération ont été prélever. Les échantillons ont été analyser par diffraction de rayon X. L'étude des résultats à permis d'identifier deux types de veines qui ont des altérations hydrothermales importantes. Les veines de type II sont des veines de quartz+actinote±épidote±pyrite. Ils ont produit une altération sodique des roches volcanique en lessivant le Ca, Mg et Fe. Cette altération sodique est définie par l'albite. Les veines de type III ont produit une silicification de la roche hôte.

D'autres minéraux d'altération importants pas directement reliés aux veines ont été identifiés dans les roches volcaniques. Ces minéraux sont la cordiérite et l'andalousite. La présence de ces minéraux démontre que les veines de types II et III ne sont pas les seules sources d'altérations hydrothermales.

A.2 Introduction

The volcanic rocks that occupy the Comtois deposit have undergone a large amount of hydrothermal alteration. An extensive study of these alterations have been undertaken to establish possible genetic models for the Comtois deposit.

Minor observations of the hydrothermal alterations have been described through thin section analysis under an optical microscope. These observations include the identification of cordierite, andalusite and other minerals that may be associated to a hydrothermal alteration. However, evolution of a pervasive alteration around a vein is difficult to observe within a single thin section.

X-ray diffraction allows a quantitative and qualitative analysis of the mineralogy of the sample. Analysis of small representative samples of a vein and the altered host rock by X-ray diffraction enables a view of the spatial relationship between the vein and the alteration of the host rock produced by the vein.

This study attempted to link alterations to particular vein types and to define any pre-existing alterations. It also hopes to shed some light on the possible genetic models.

A.2 Analytical Methods

Hand samples of the various veins found within the study area were taken with a portable rock saw. The samples are 2 cm thick slabs perpendicular to the vein orientation. Approximately 1 gram samples of the vein and host rock at various distances from the vein were extracted in the laboratory using a rock saw and wire cutters. Each 1 gram sample pulverised into a fine powder using a mil-ball grinder. A small 10 μg sample of the fine homogeneous powders are individually mounted on disks greased with Vaseline for adhesion. The prepared samples are then analysed overnight in a Siemens D-5000 X-ray diffractometer (fig. A.1).

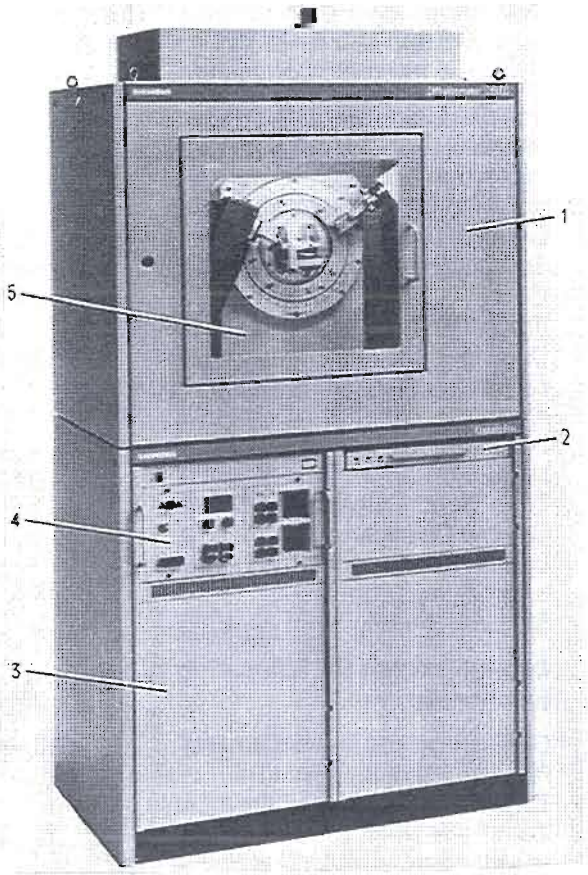

Fig. A.1: Siemens D5000 diffractometer
in a radiation protected box, mounted
on a cabinet.

Analysis of the powder by the diffractometer results in a spectrum of spikes. The various spikes and combination of spikes at specific wavelengths represent different minerals within the sample. The combination of the spectrums of each mineral results in the spectrum of the total sample. The relative height of the spikes for the various minerals represents the quantitative value of each mineral within the sample. The value of relative height for each sample is normalised to a percentage of the mineral found within the sample.

Fig. A.2: Photographs of hand samples with microsample locations for X-ray diffraction analysis

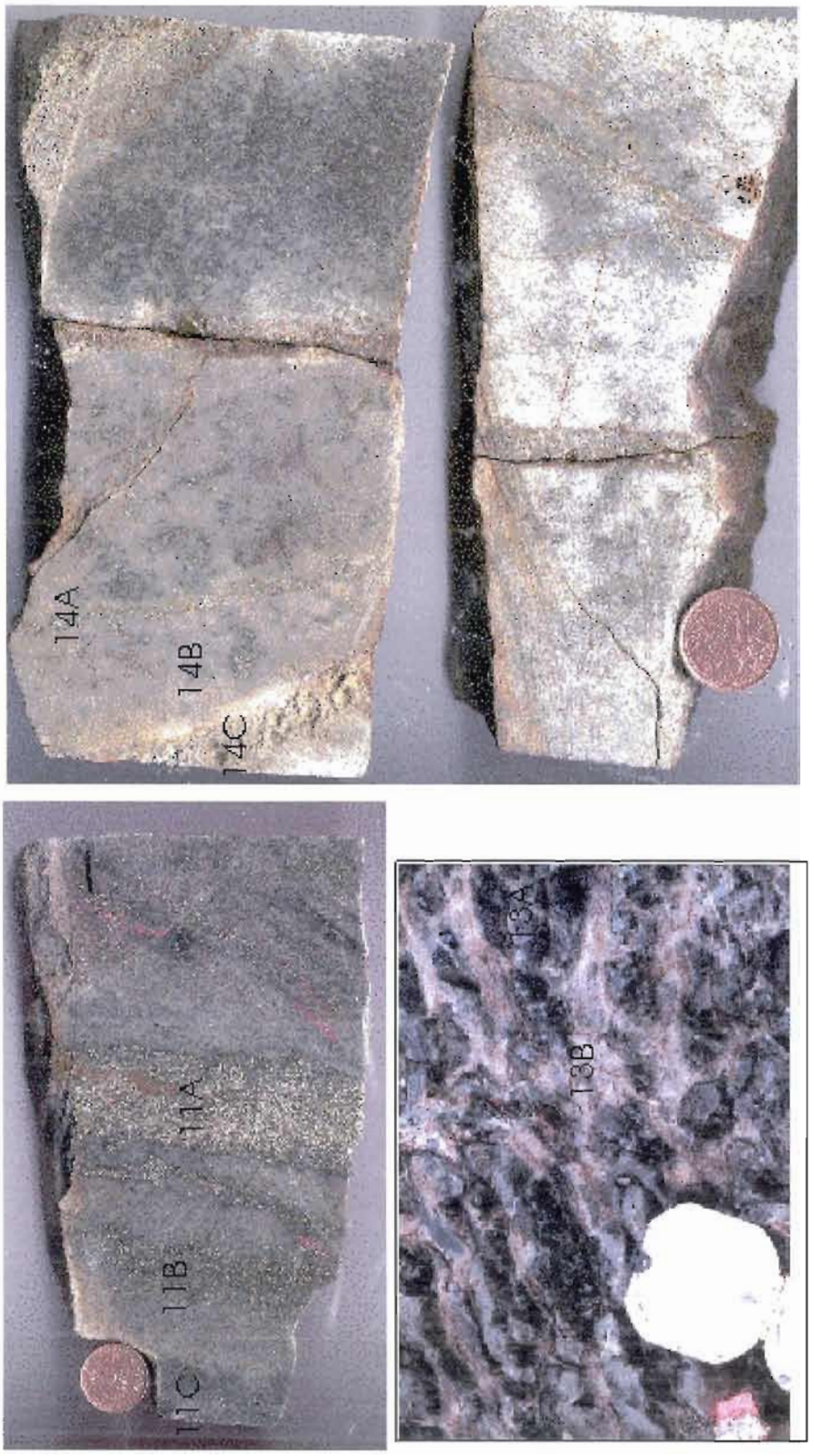

Fig.A.2 con't

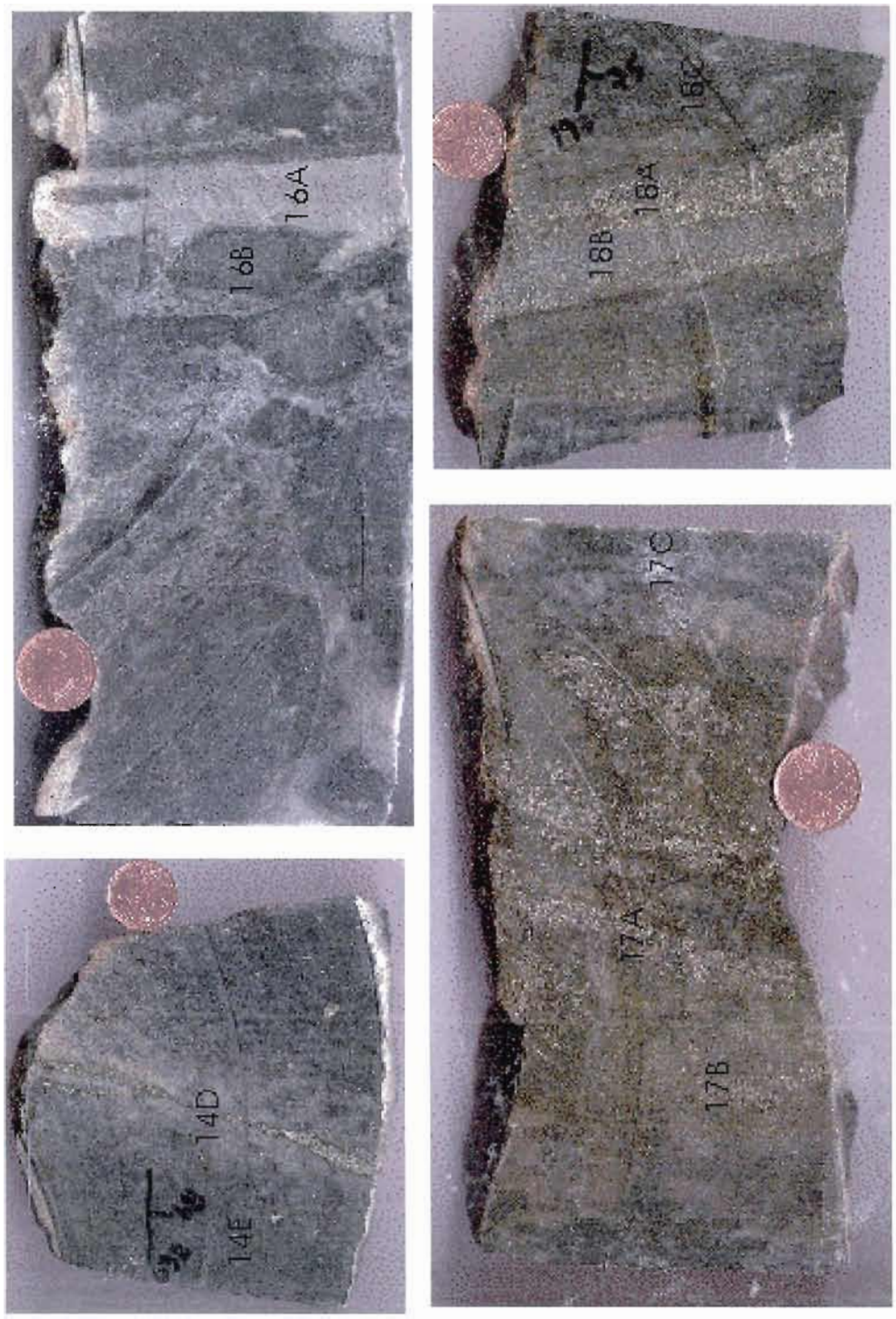

Fig A.2 con't

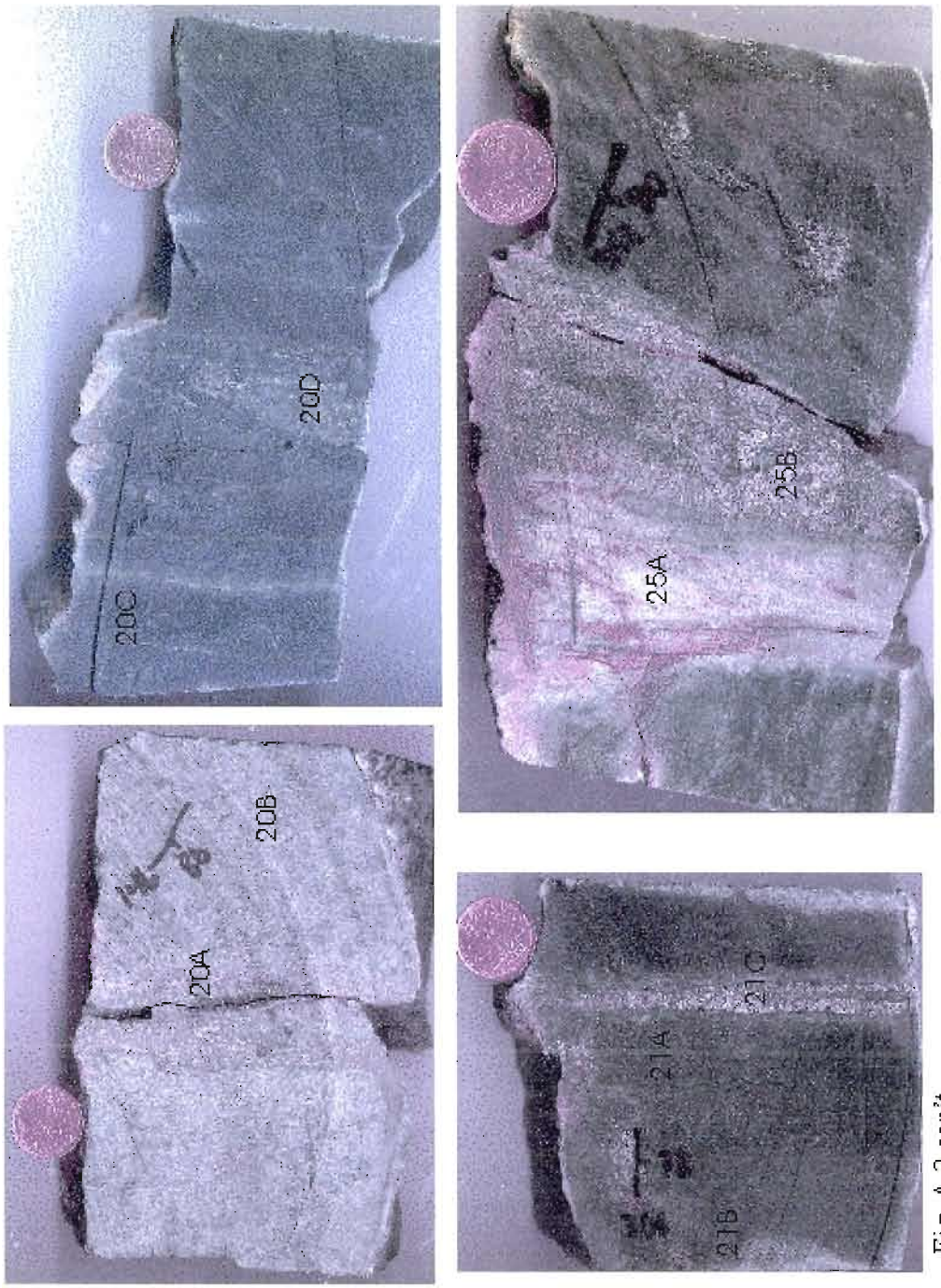

Fig A.2 con't

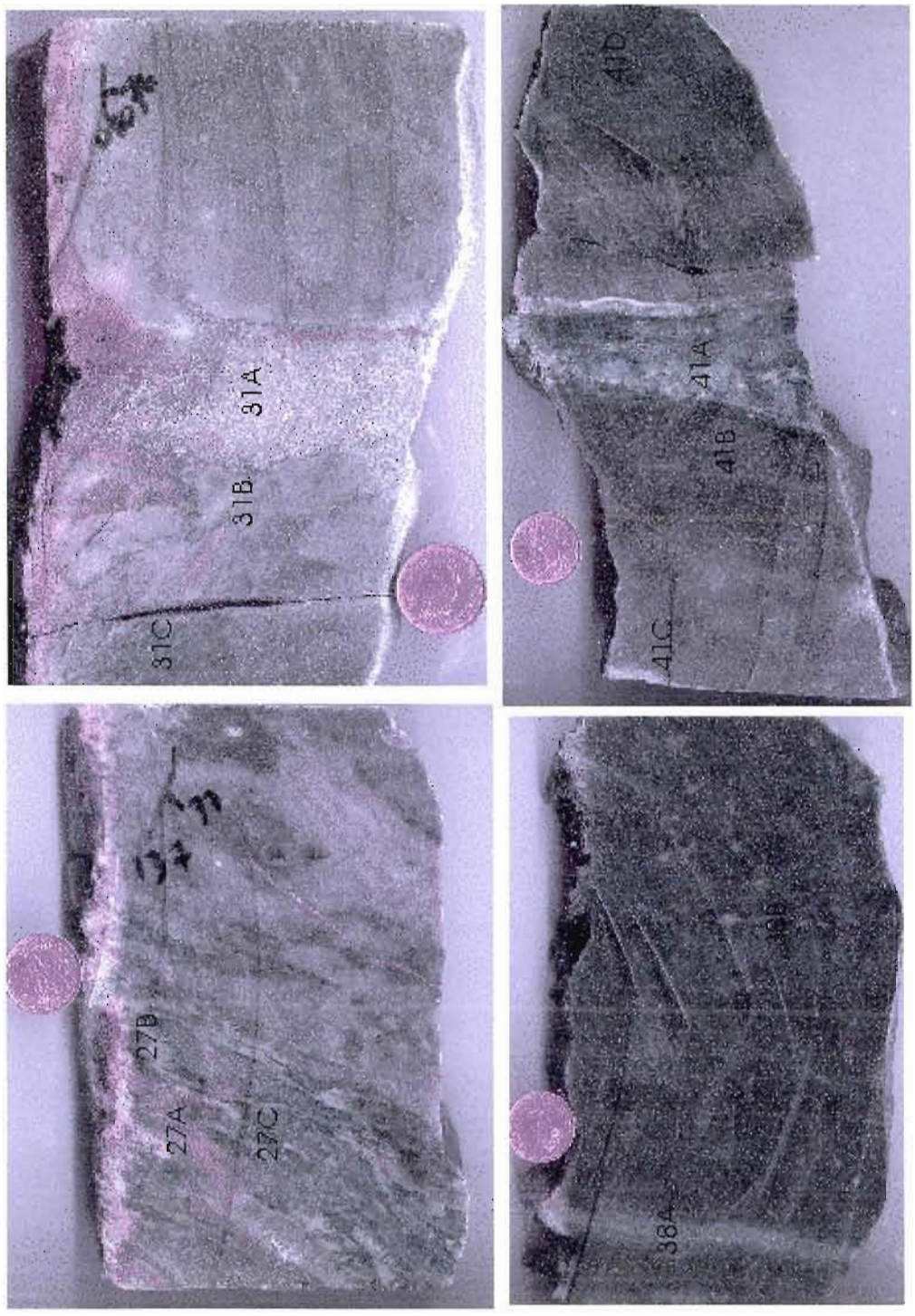

Fig. A.2 con't

	2 A		2 B		2 C		3 A		3 B		3 C		6 A		6 B		6 C	
	mes.	%	mes.	%	mes.	%	mes.	%	mes.	%	mes.	%	mes.	%	mes.	%	mes.	%
quartz	70	12	1075	51	369	33	11	1	34	3	209	27	57	7	338	34	125	10
plagio(albite)	41	7	384	18	605	55	564	37	680	59	61	7			542	53	887	75
microcline	62	11			33	3	111	7			76	9	290	37				
andalusite					22	2	14	1										
actinote	133	22	177	9			585	38	60	5	45	5	388	51			130	11
epidote	246	41			11	1					388	48						
cordierite			31	1											17	2		
magnetite	5	1			18	2												
pyrite	15	3	161	8	11	1	12	1	26	2	19	2	25	3	7	1	15	1
chalcopyrite			11	1														
pyrrhotite																		
mica																		
muscovite							167	10										
biotite			115	6											82	8		
chlorite	9	2	54	3	17	2	56	3	10	1	10	1	6	1	19	2	39	3
paragonite					8	1												
pyroxene																		
orthose																		
amphibole																		
piemontite																		
augite																		
sphalerite																		
Total	581	99	2008	97	1094	100	1520	98	810	70	808	99	766	99	1005	100	1196	100

Tab. A.1: Results of X-ray diffraction

	10 A		10 B		10 C		10 D		10 E		11 A		11 B		11 C		13 A		13 B	
	mes.	%	mes.	%	mes.	%	mes.	%	mes.	%	mes.	%	mes.	%	mes.	%	mes.	%	mes.	%
quartz	844	38	1381	57	1443	72	940	46	344	24	143	8	2828	87	132	15	46	6	827	52
plagio(albite)	386	18	196	8	84	4							45	1	253	28	126	17	405	25
microcline			10	1	5	1			6	1										
andalusite	55	3	216	9	138	7			66	5			50	2	8	1			14	1
actinote											77	4					483	64	58	4
epidote																				
cordierite							386	19												
magnetite	70	3	10	1	7	1			11	1	21	1								
pyrite	69	3	118	5	25	1	274	13	651	45	1446	83	31	1	101	11			30	2
chalcopyrite					5	1			44	3	26	1			16	2				
pyrrhotite																				
mica							24	1	207	14							30	4		
muscovite			333	14	246	12							300	9	367	41				
biotite	653	29																	244	15
chlorite	11	1	69	3	10	1	34	2	51	4					20	2	39	5	20	1
paragonite																				
pyroxene			49	2					17	1										
orthose							15	1	12	1										
amphibole																				
piemontite																				
augite																				
sphalerite	16	1	10	0	5	0	269	14	18	1	57	3								
Total	2104	96	2392	100	1968	100	1942	96	1427	100	1770	100	3254	100	897	100	724	96	1598	100

	14 A		14 B		14 C		14 D		14 E	
	mes.	%	mes.	%	mes.	%	mes.	%	mes.	%
quartz	761	38	1942	73	1907	70	2214	78	1544	61
plagio(albite)			80	3	177	7			275	11
microcline										
andalusite	16	1	111	4	88	3	183	6	103	4
actinote										
epidote										
cordierite										
magnetite										
pyrite	1226	61	112	4	41	2	116	4	33	1
chalcopyrite										
pyrrhotite									25	1
mica			416	16	495	18	193	7	536	21
muscovite										
biotite										
chlorite			9	1			26	1	8	1
paragonite										
pyroxene										
orthose										
amphibole										
piemontite										
augite										
sphalerite										
Total	2003	100	2670	101	2708	100	2732	96	2524	100

	16 A		16 B	
	mes.	%	mes.	%
quartz			17	2
plagio(albite)	53	5		
microcline				
andalusite				
actinote			488	66
epidote				
cordierite				
magnetite			50	7
pyrite			15	2
chalcopyrite				
pyrrhotite				
mica	1096	94		
muscovite				
biotite			32	4
chlorite	11	1	87	12
paragonite				
pyroxene				
orthose				
amphibole				
piemontite				
augite				
sphalerite				
Total	1160	100	689	93

	17 A		17 B		17 C	
	mes.	%	mes.	%	mes.	%
quartz	46	4	120	10	1991	78
plagio(albite)			257	20	180	7
microcline	45	4				
andalusite					193	8
actinote						
epidote						
cordierite						
magnetite	247	24				
pyrite	652	63	632	50		
chalcopyrite						
pyrrhotite						
mica			117	10	204	8
muscovite						
biotite						
chlorite	47	5	132	10		
paragonite						
pyroxene						
orthose						
amphibole						
piemontite						
augite						
sphalerite						
Total	1037	100	1258	100	2568	101

	18 A		18 B		18 C		21 A		21 B		21 C		20 A		20 B		20 C		20 D	
	mes.	%	mes.	%	mes.	%	mes.	%	mes.	%	mes.	%	mes.	%	mes.	%	mes.	%	mes.	%
quartz	489	20	389	9	277	13	483	46	1215	59	200	16	4210	81	1256	56	1012	44	29	2
plagio(albite)	139	6	220	11	512	23	131	13	232	11	31	1	61	1	405	18	313	14	8	1
microcline			8	1			30	3	54	3	21	1			112	5	41	2		
andalusite	9	1	182	9	36	2			2	1	9	1	655	13						
actinote	195	8									83	7							492	36
epidote							74	7									7	1	126	9
cordierite									202	10			7	1	15	1	280	12		
magnetite							20	2	162	8	30	2	10	1	36	2	81	4		
pyrite	1387	57	726	35	83	4	64	6			721	59	113	2	59	3	20	1	561	41
chalcopyrite											8	1								
pyrrhotite					82	4														
mica	79	3	487	23	1089	50	36	3	153	7									15	1
muscovite																				
biotite															116	5	129	6		
chlorite	120	5	71	3	107	5	103	10	28	1	92	8	10	1	108	5	48	2	72	5
paragonite													72	1						
pyroxene																				
orthose													41	1						
amphibole															141	6	374	16		
piemontite																				
augite																				
sphalerite																				
Total	2418	100	2083	91	2186	101	941	90	2048	100	1195	96	5179	102	2248	101	2305	102	1303	95

	25 A		25 B		27 A		27 B		27 C		31 A		31 B		31 C		38 A		38 B	
	mes.	%	mes.	%	mes.	%	mes.	%	mes.	%	mes.	%	mes.	%	mes.	%	mes.	%	mes.	%
quartz	83	5	632	42	2400	91	1318	62	1001	54	66	4	1481	72	1470	69	1178	89	478	37
plagio(albite)	1384	75	53	4			141	7											329	26
microcline	269	15							70	4										
andalusite	23	1											102	5					6	1
actinote			64	4			406	19	279	15							100	8	375	29
epidote			347	24					7	1										
cordierite																				
magnetite	29	2																		
pyrite	15	1	379	26			104	5	28	2	1530	96	54	3	220	10				
chalcopyrite																				
pyrrhotite																				
mica					214	8	125	6									6	1	76	6
muscovite													407	20	352	17				
biotite																				
chlorite	18	1			18	1	27	1					8	1	88	4	5	1	8	1
paragonite																				
pyroxene																				
orthose																				
amphibole																				
piemontite									60	3										
augite									378	21							272			
sphalerite																				
Total	1821	100	1475	100	2632	100	2121	100	1823	100	1596	100	2052	101	2130	100	1561	99	1272	100

	41 A		41 B		41 C		41 D	
	mes.	%	mes.	%	mes.	%	mes.	%
quartz	40	5	37	4	398	18	809	47
plagio(albite)			6	1	752	34	241	14
microcline					35	2	53	3
andalusite								
actinote	535	73	656	71			423	25
epidote	132	18						
cordierite								
magnetite								
pyrite	5	1					142	8
chalcopyrite								
pyrrhotite								
mica	4	1	178	19	1030	46	35	2
muscovite								
biotite								
chlorite	16	2	29	3	6	1		
paragonite								
pyroxene								
orthose								
amphibole								
piemontite								
augite	158							
sphalerite								
Total	890	100	906	98	2221	101	1703	99

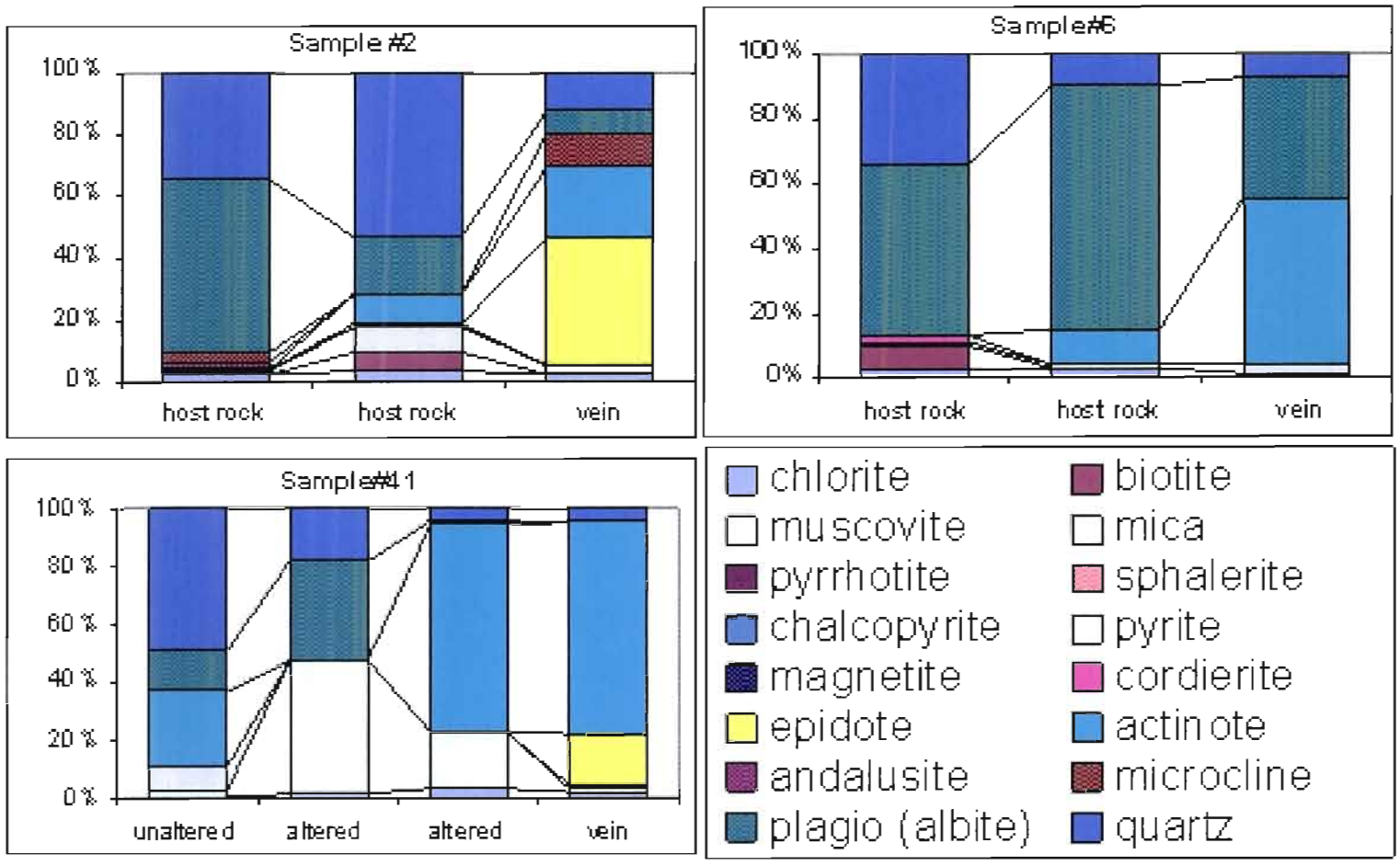

Fig. A.3: Examples of X-ray diffraction analysis of Type II veins

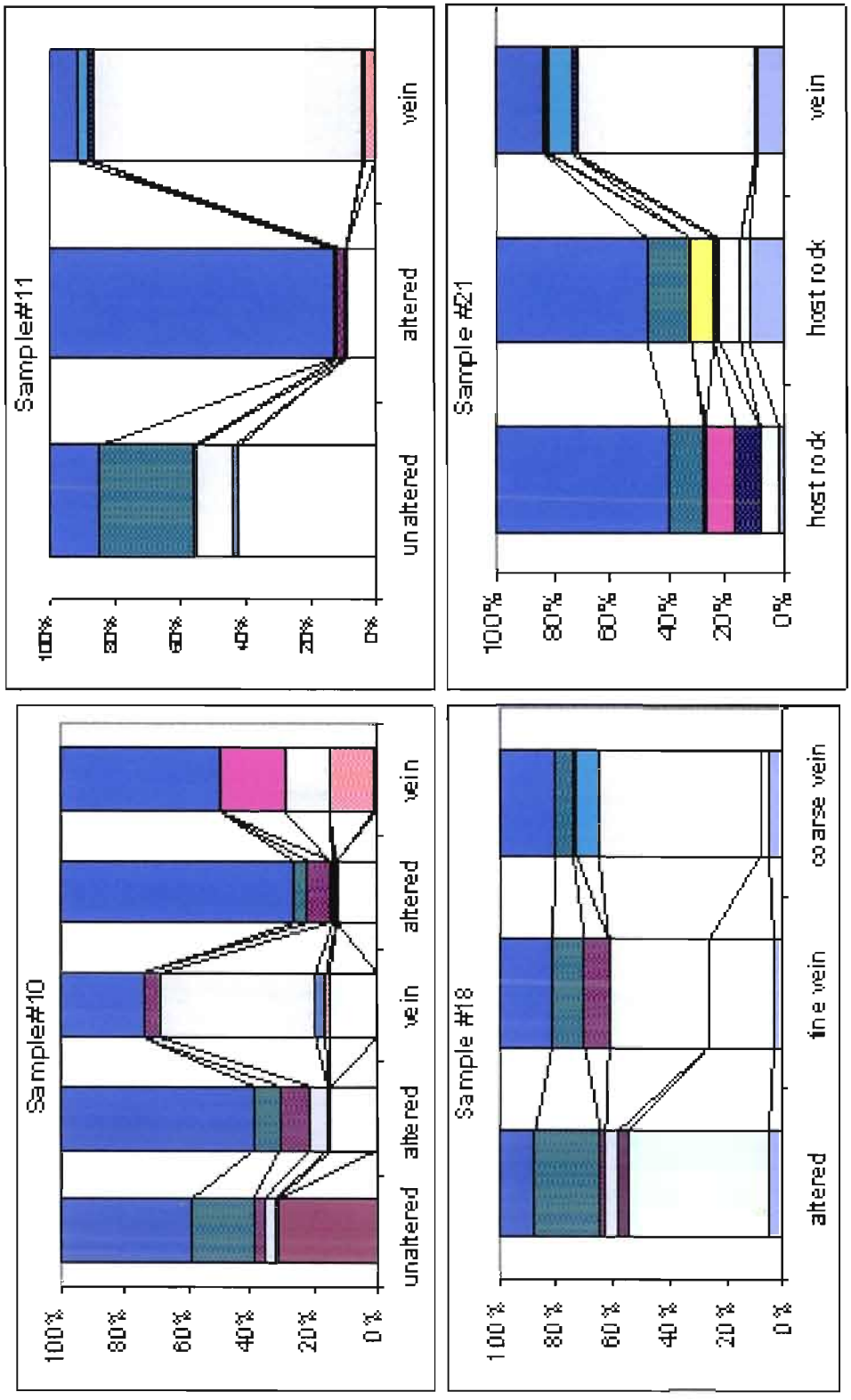

Fig A.4: Examples of X-ray diffraction analysis of Type III veins

A.4 Discussion

Histograms of the X-ray diffraction results within a hand sample allows for observation of the alteration of the host rock produced by the incorporation of the vein at a more convenient scale. Three types of veins are identified within the study area:

- Type I: Quartz Veins
- Type II: Quartz-Actinote+/-Epidote+/-Pyrite Veins
- Type III: Pyrite-Quartz+/-Chalcopyrite+/-Electrum Veins

The type I veins are 1-2mm thick quartz veins with no observable alteration. They are found within both mafic and felsic volcanic rocks with distinct orientations for each respective lithology. They seem to be remnants of the cooling volcanic rocks under different structural constraints.

The type II veins are found within both mafic and felsic volcanic rocks and are orientated 60N and 100N. They vary in thickness, ranging between 1-20mm, demonstrating a pinch and swell characteristic. They are composed of actinote and quartz and have a particular alteration envelop (fig.A.3). They occasionally contain pyrite and/or epidote, depending where they are localised on the property. The alteration envelope is enriched in albite and depleted in quartz in comparison to the host rock outside of the alteration envelope. It is also noted the actinote and epidote is not found pervasively found in the alteration envelop, they are restrained within the vein.

The type III veins found in both mafic and felsic volcanic rocks and have a distinct preferential orientation of 120N. Their thickness varies from 1-25mm and is mainly composed of pyrite. Small amounts of quartz and traces of chalcopyrite, pyrrhotite and sphalerite are also found within the type III veins (fig.A.4). The presence of gold is assumed but is not observed in the samples taken with X-ray diffraction in this case. The type III veins are occasionally

accompanied with an alteration envelope enriched in quartz. It is noted that the type III veins found in samples with important gold grades all have a quartz rich alteration envelop.

Andalusite and cordierite have been identified in thin section. However, analysis by x-ray diffraction has identified traces of cordierite and andalusite in many samples not observed in thin section. This is either due to a small mineralogy and/or to minute quantities because of being completely obliterated by subsequent alterations. Compilation of these traces of important hydrothermal minerals has identified a spatial relationship for cordierite and epidote. Cordierite is only found in the host rocks located in western half of the study area. Epidote is only found in the type II veins located in the western third of the study area.

A.5 Conclusion

Analysis of the veins by x-ray diffraction confirmed that 2 types of veins have important hydrothermal alteration. The type II veins produce a sodic alteration of the host rock by leaching Ca, Mg and Fe. The resulting alteration zone is defined by albite. The gold-bearing type III veins produce a silicification of the host rock and remove the Fe to crystallize pyrite found decimated in the alteration zone. The biotite, losing its Fe recrystalizes into a white mica.

X-ray diffraction also confirmed the presence of andalusite throughout the study area and cordierite in the western portion of this same area. This fact proves that hydrothermal alterations had affected the volcanic rocks other than those produced by vein types II and III. A spatial relationship for cordierite and epidote was recognized with x-ray diffraction analysis. Cordierite and epidote are limited to the western portion of the study area. This finding indicates a possible zoning of the regional alteration zones, which may help pinpoint further important mineralised zones.

	Host Rock	Alteration Zone	Transfer of Elements	Vein
Type II Veins	quartz plagioclase actinolite(±) biotite(±) muscovite(±)	albite quartz biotite(±) muscovite(±)	Ca→ Mg→ Fe→	actinolite epidote(±) quartz
Type III Veins	quartz plagioclase biotite	quartz sericite plagioclase	Fe→ ←Si	pyrite quartz chalcopyrite(±) pyrrhotite(±) sphalerite(±)

Tab. A.2: Summary of major mineralogy for each vein type with their respective alteration zones and host rocks that illustrates the transfer of elements between host rock and hydrothermal fluids.

A.6 Spectrum results of X-ray diffraction analysis

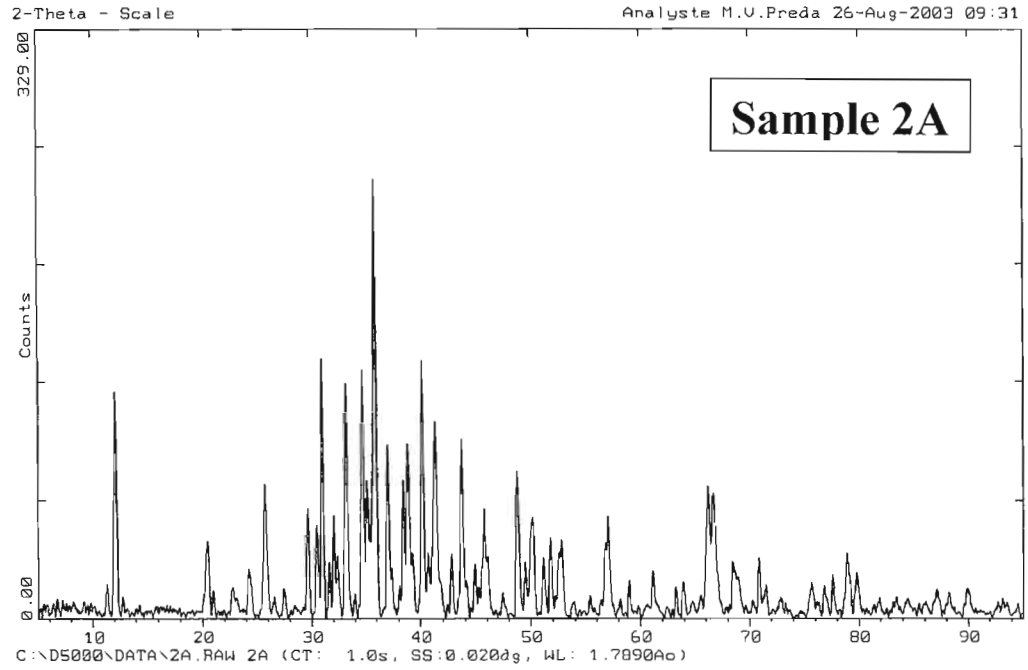

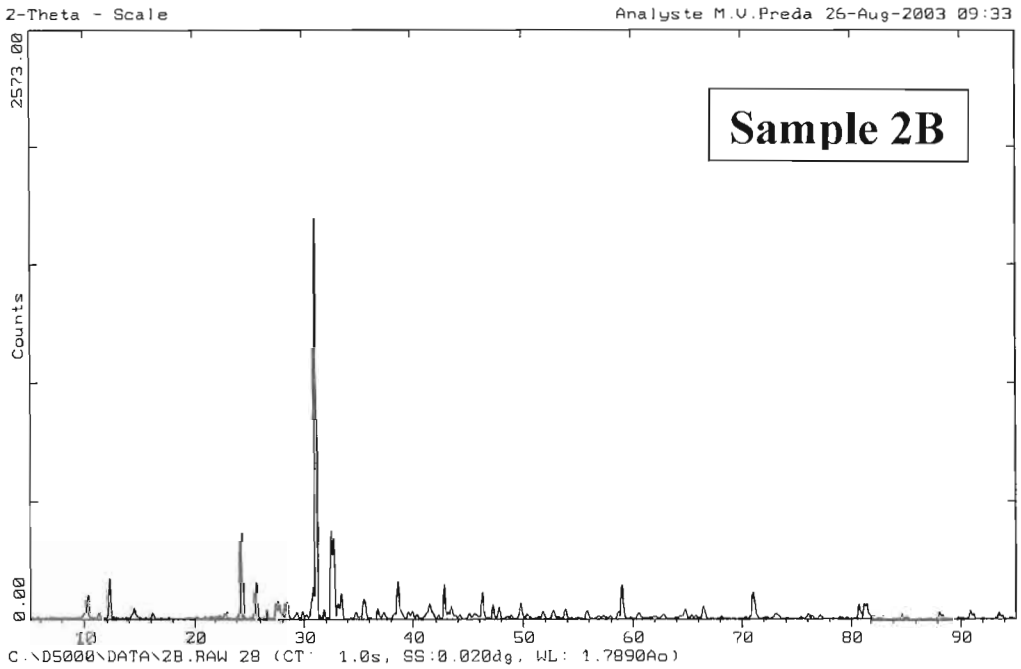

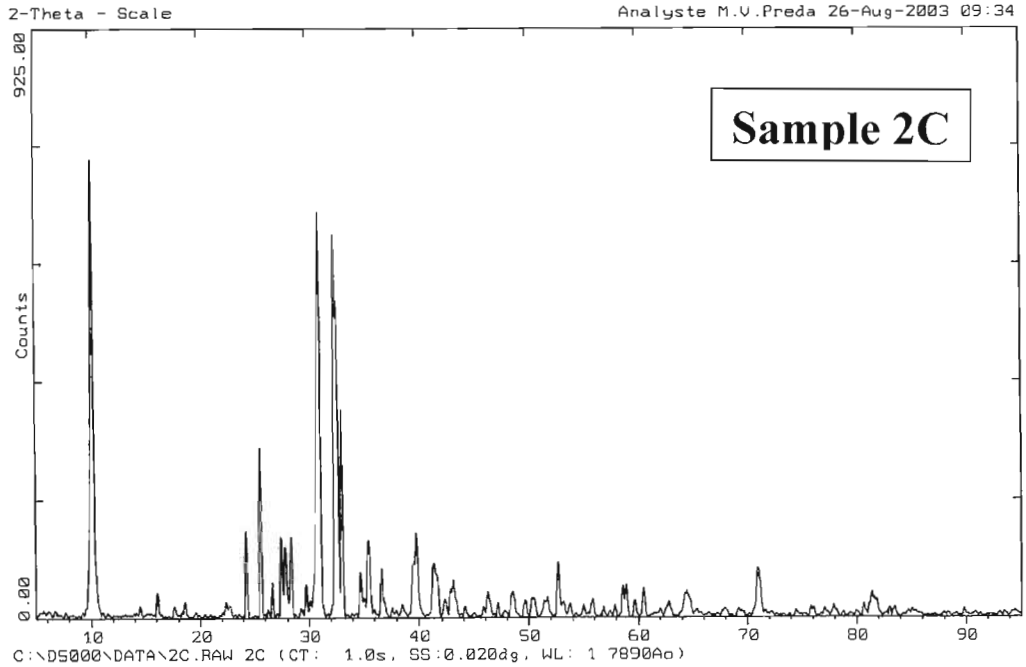
2-Theta - Scale
Analyste M.V.Preda 26-Aug-2003 09:34
925.00
Counts
0.00
Sample 2C
10
20
30
40
50
60
70
80
90
C:\D5000\DATA\2C.RAW 2C (CT: 1.0s, SS:0.020dg, WL: 1.7890Ao)

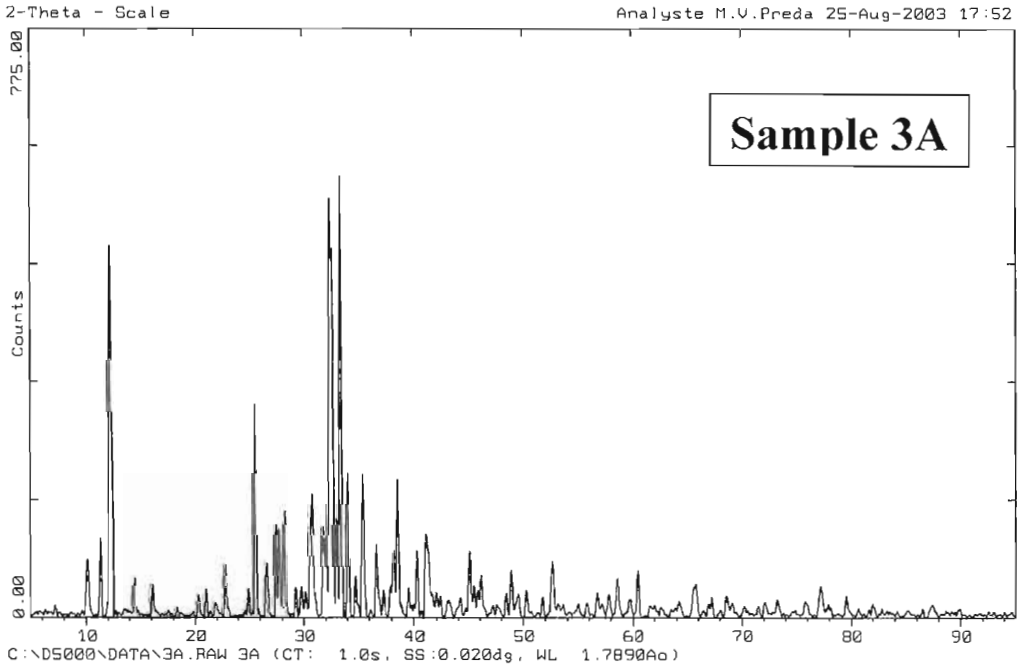
2-Theta - Scale
Analyste M.V.Preda 25-Aug-2003 17:52
775.00
Counts
0.00
Sample 3A
10
20
30
40
50
60
70
80
90
C:\D5000\DATA\3A.RAW 3A (CT: 1.0s, SS:0.020dg, WL: 1.7890Ao)

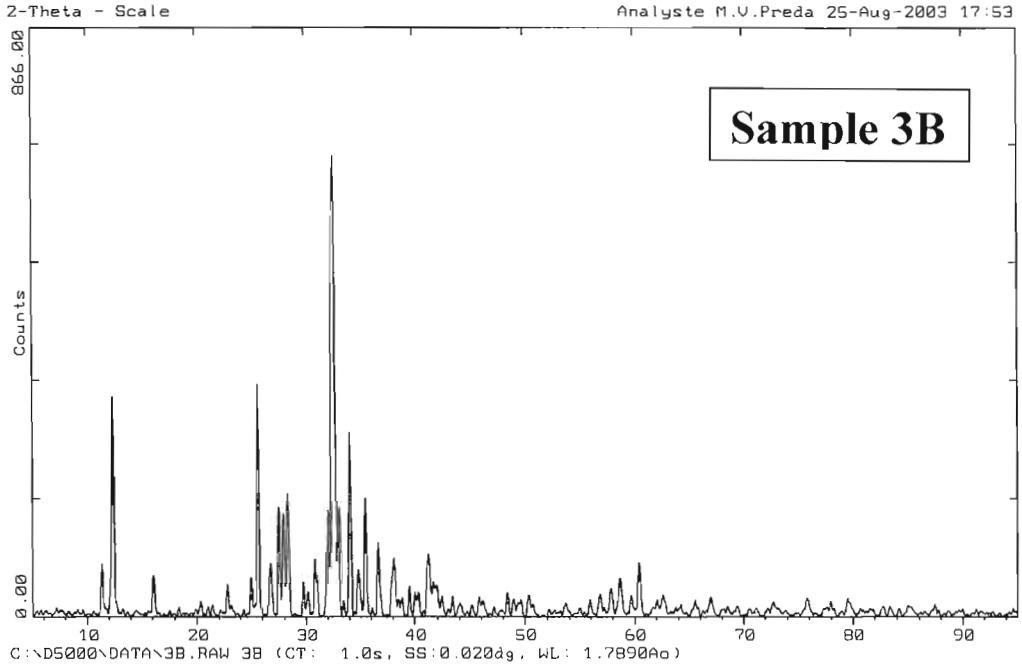
2-Theta - Scale
Analyste M.V.Preda 25-Aug-2003 17:53
866.00
Counts
0.00
Sample 3B
10
20
30
40
50
60
70
80
90
C:\D5000\DATA\3B.RAW 3B (CT: 1.0s, SS:0.020dg, WL: 1.7890Ao)

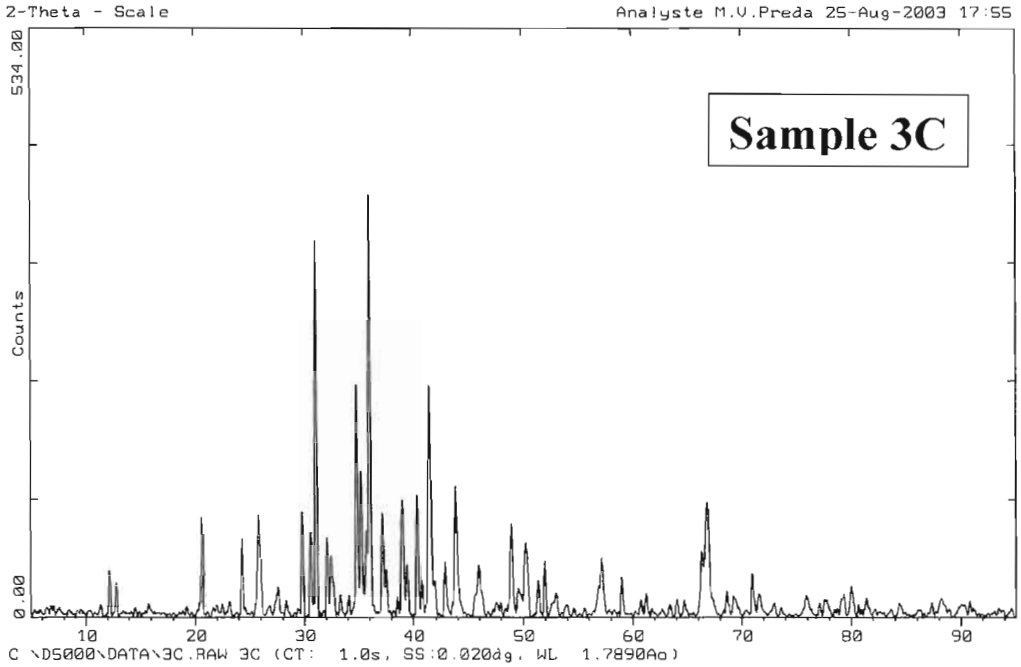
2-Theta - Scale
Analyste M.V.Preda 25-Aug-2003 17:55
534.00
Counts
0.00
Sample 3C
10
20
30
40
50
60
70
80
90
C \D5000\DATA\3C.RAW 3C (CT: 1.0s, SS:0.020dg, WL 1.7890Ao)

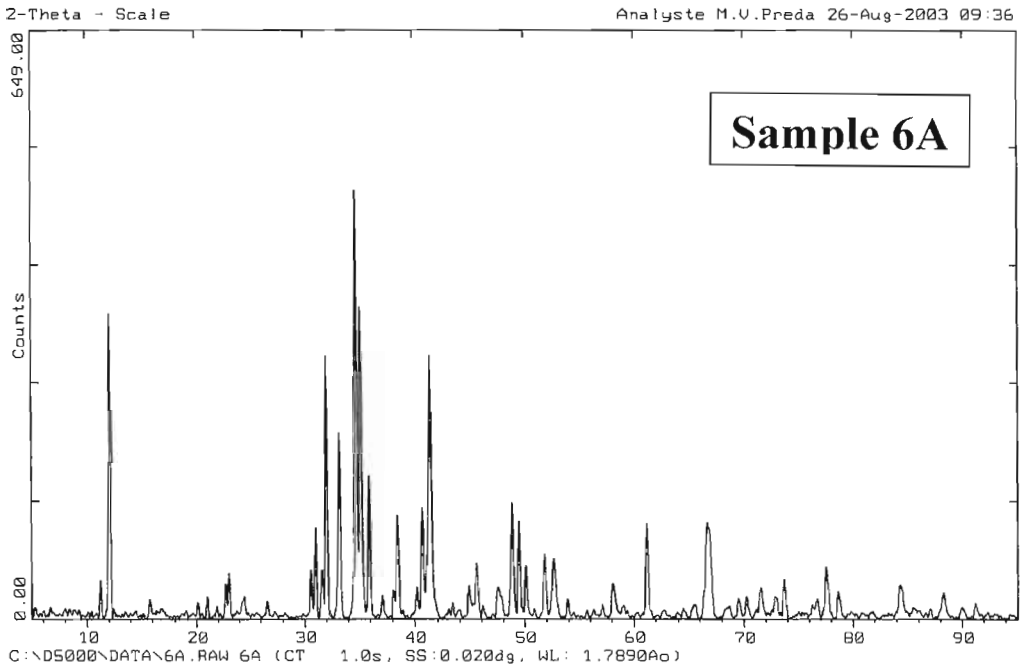
2-Theta - Scale
Analyste M.V.Preda 26-Aug-2003 09:36
649.00
Counts
0.00
Sample 6A
10
20
30
40
50
60
70
80
90
C:\D5000\DATA\6A.RAW 6A (CT 1.0s, SS:0.020dg, WL: 1.7890Ao)

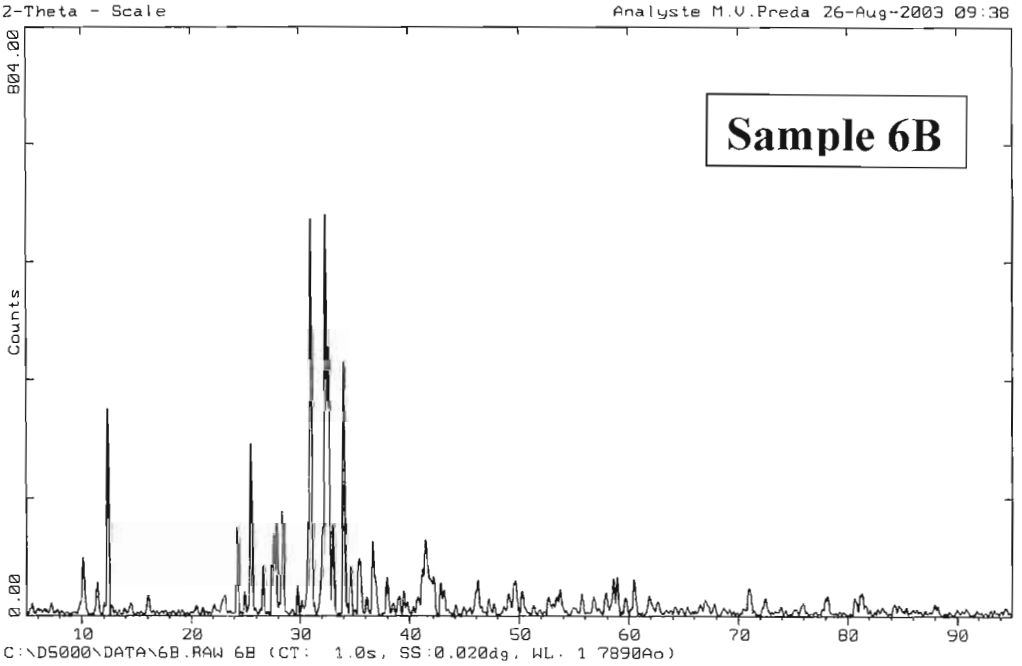
2-Theta - Scale
Analyste M.V.Preda 26-Aug-2003 09:38
804.00
Counts
0.00
Sample 6B
10
20
30
40
50
60
70
80
90
C:\D5000\DATA\6B.RAW 6B (CT: 1.0s, SS:0.020dg, WL: 1.7890Ao)

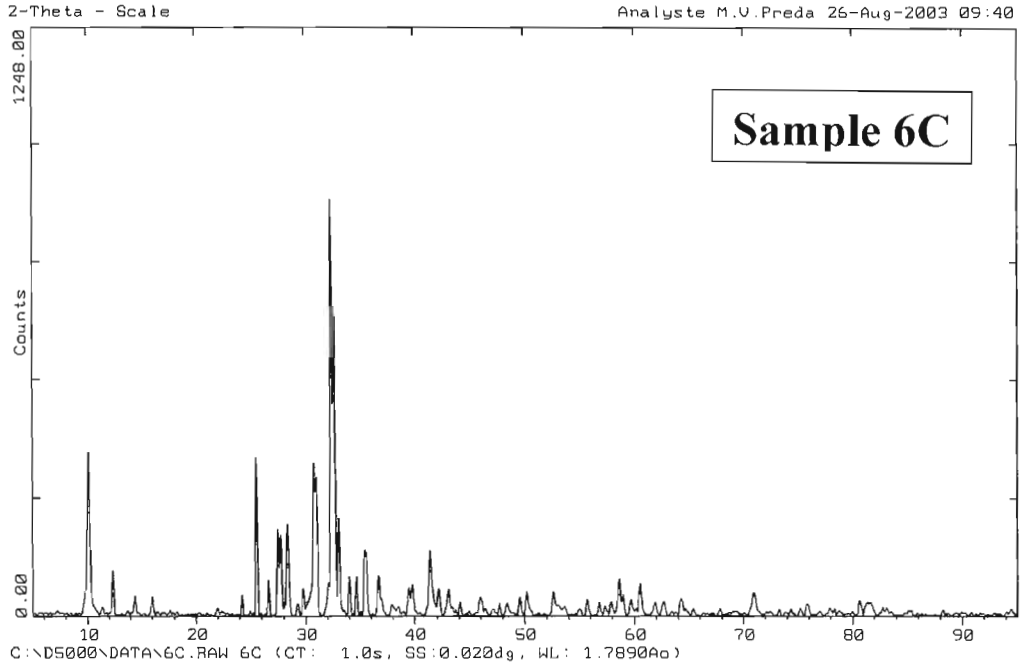
2-Theta - Scale
Analyste M.V.Preda 26-Aug-2003 09:40
1248.00
Counts
0.00
Sample 6C
10
20
30
40
50
60
70
80
90
C:\DS000\DATA\6C.RAW 6C (CT: 1.0s, SS:0.020dg, WL: 1.7890Ao)

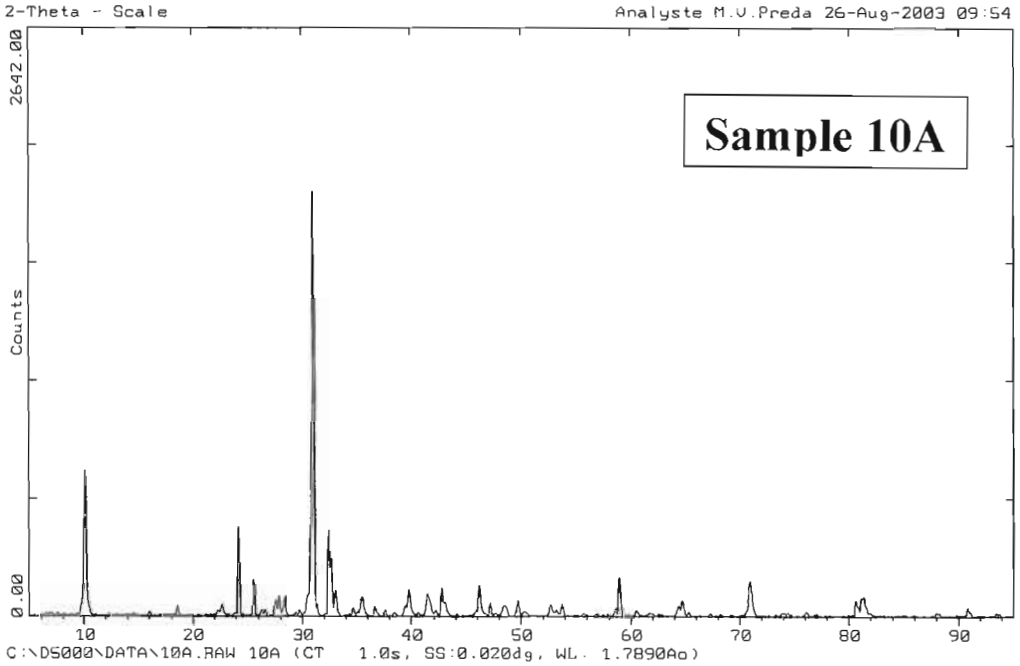
2-Theta - Scale
Analyste M.V.Preda 26-Aug-2003 09:54
2642.00
Counts
0.00
Sample 10A
10
20
30
40
50
60
70
80
90
C:\DS000\DATA\10A.RAW 10A (CT 1.0s, SS:0.020dg, WL: 1.7890Ao)

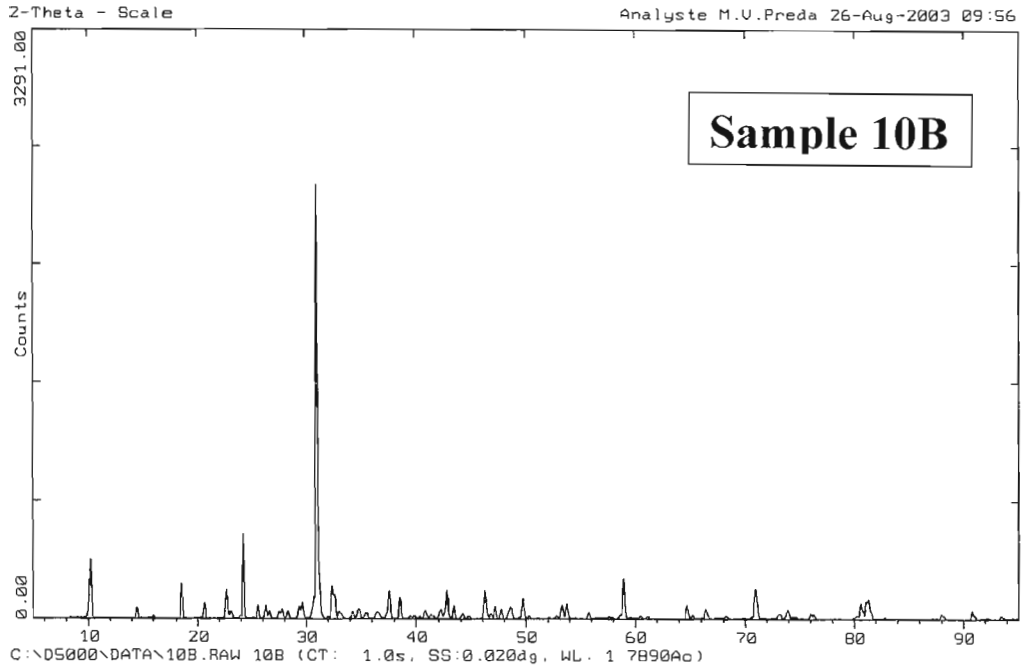
2-Theta - Scale
Analyste M.V.Preda 26-Aug-2003 09:56
3291.00
Counts
0.00
Sample 10B
10
20
30
40
50
60
70
80
90
C:\D5000\DATA\10B.RAW 10B (CT: 1.0s, SS:0.020dg, WL: 1.7890Ao)

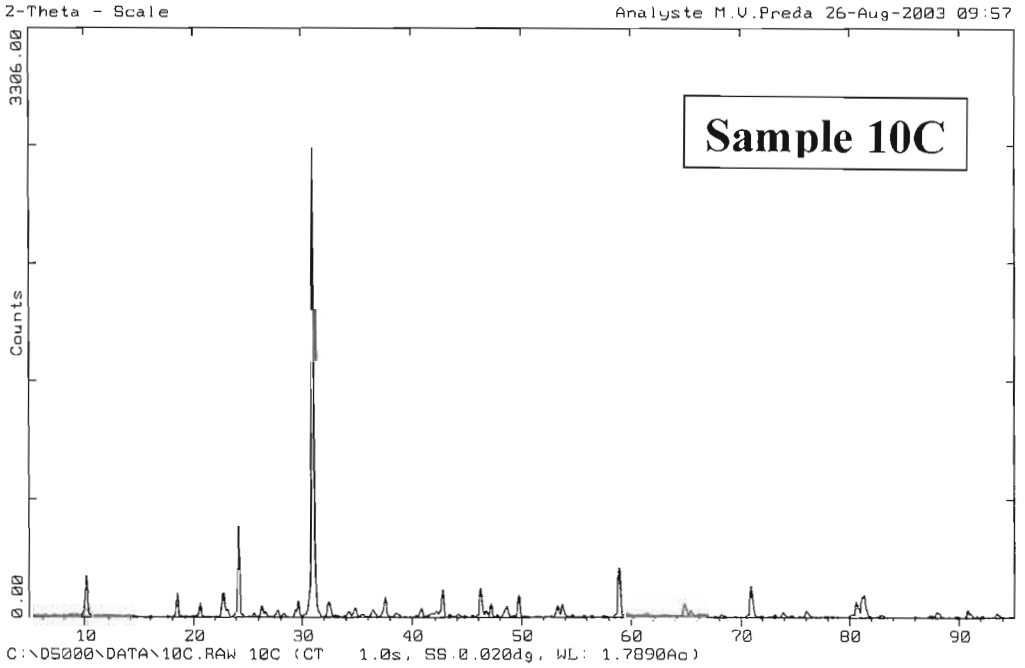
2-Theta - Scale
Analyste M.V.Preda 26-Aug-2003 09:57
3306.00
Counts
0.00
Sample 10C
10
20
30
40
50
60
70
80
90
C:\D5000\DATA\10C.RAW 10C (CT 1.0s, SS:0.020dg, WL: 1.7890Ao)

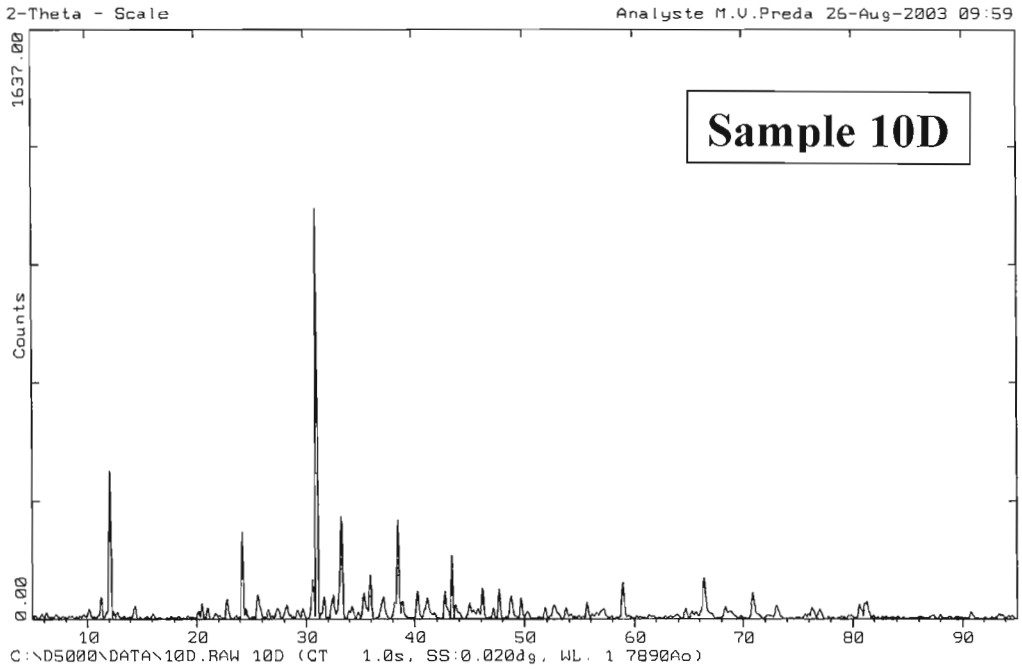
2-Theta - Scale
Analyste M.V.Preda 26-Aug-2003 09:59
1637.00
Counts
0.00
Sample 10D
10
20
30
40
50
60
70
80
90
C:\D5000\DATA\10D.RAW 10D (CT 1.0s, SS:0.020dg, WL. 1.7890Ao)

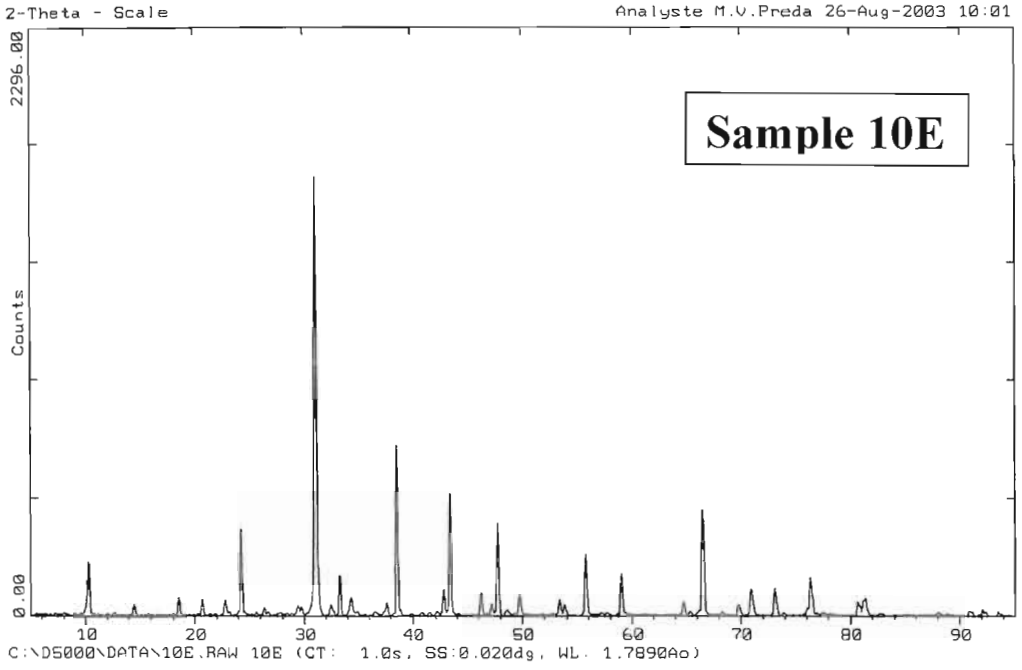
2-Theta - Scale
Analyste M.V.Preda 26-Aug-2003 10:01
2296.00
Counts
0.00
Sample 10E
10
20
30
40
50
60
70
80
90
C:\D5000\DATA\10E.RAW 10E (CT: 1.0s, SS:0.020dg, WL. 1.7890Ao)

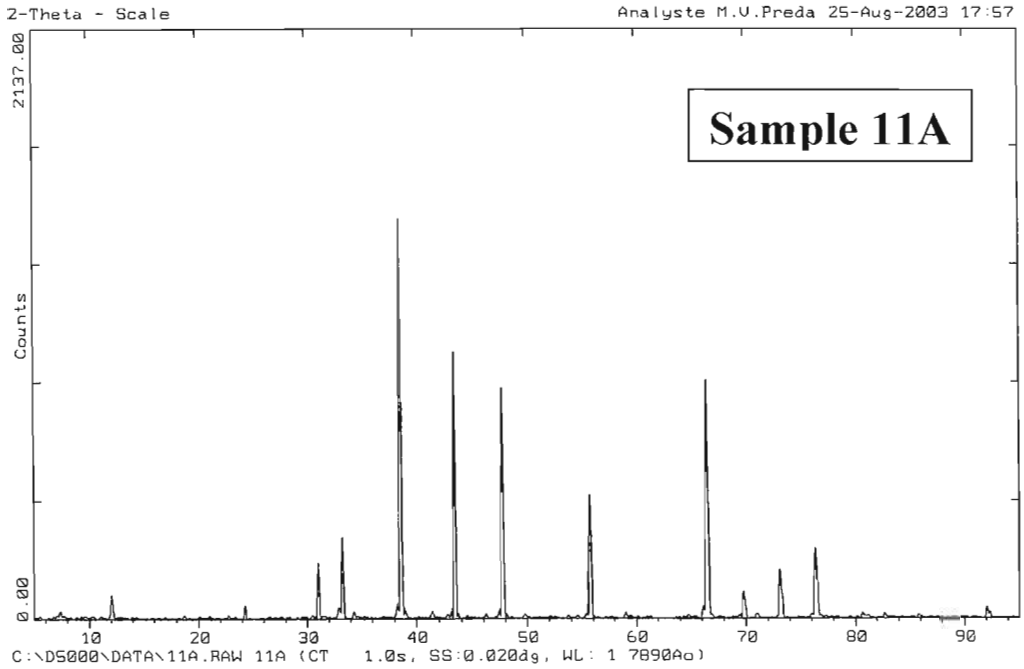
2-Theta - Scale
Analyste M.V.Preda 25-Aug-2003 17:57
2137.00
Counts
0.00
Sample 11A
10
20
30
40
50
60
70
80
90
C:\DS000\DATA\11A.RAW 11A (CT 1.0s, SS:0.020dg, WL: 1 7890Ao)

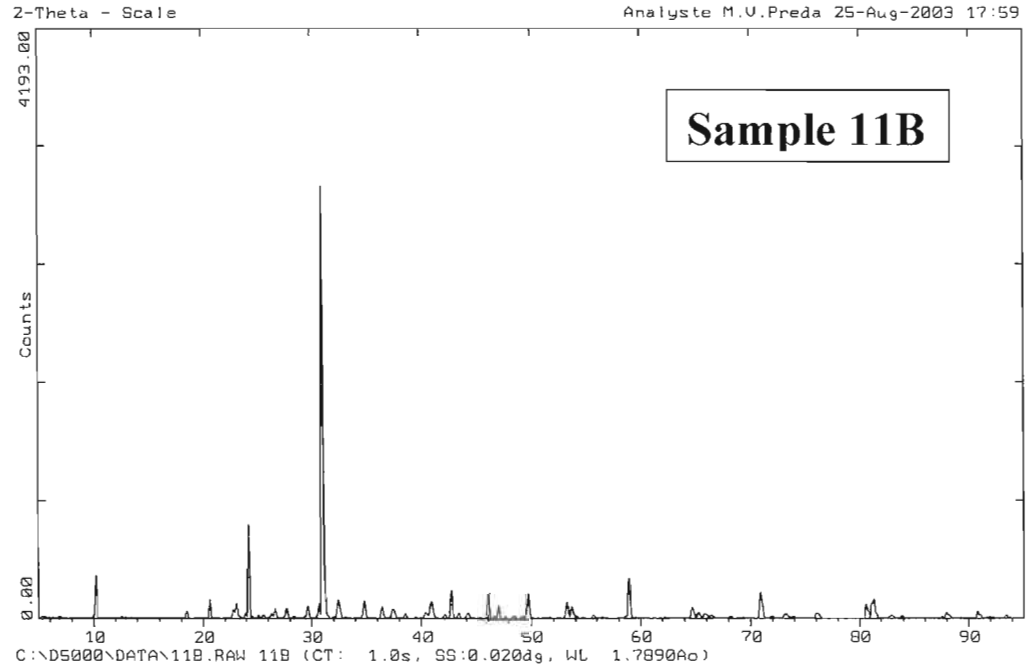
2-Theta - Scale
Analyste M.V.Preda 25-Aug-2003 17:59
4193.00
Counts
0.00
Sample 11B
10
20
30
40
50
60
70
80
90
C:\DS000\DATA\11B.RAW 11B (CT: 1.0s, SS:0.020dg, WL 1.7890Ao)

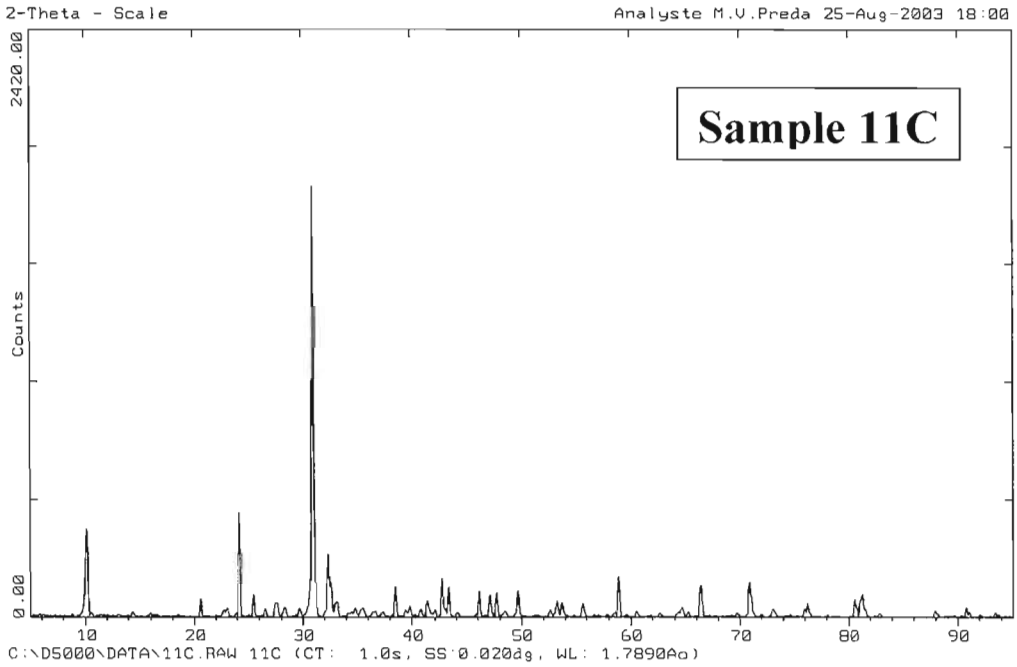
2-Theta - Scale
Analyste M.V.Preda 25-Aug-2003 18:00
2420.00
Counts
0.00
Sample 11C
10
20
30
40
50
60
70
80
90
C:\D5000\DATA\11C.RAW 11C (CT: 1.0s, SS:0.020dg, WL: 1.7890Ao)

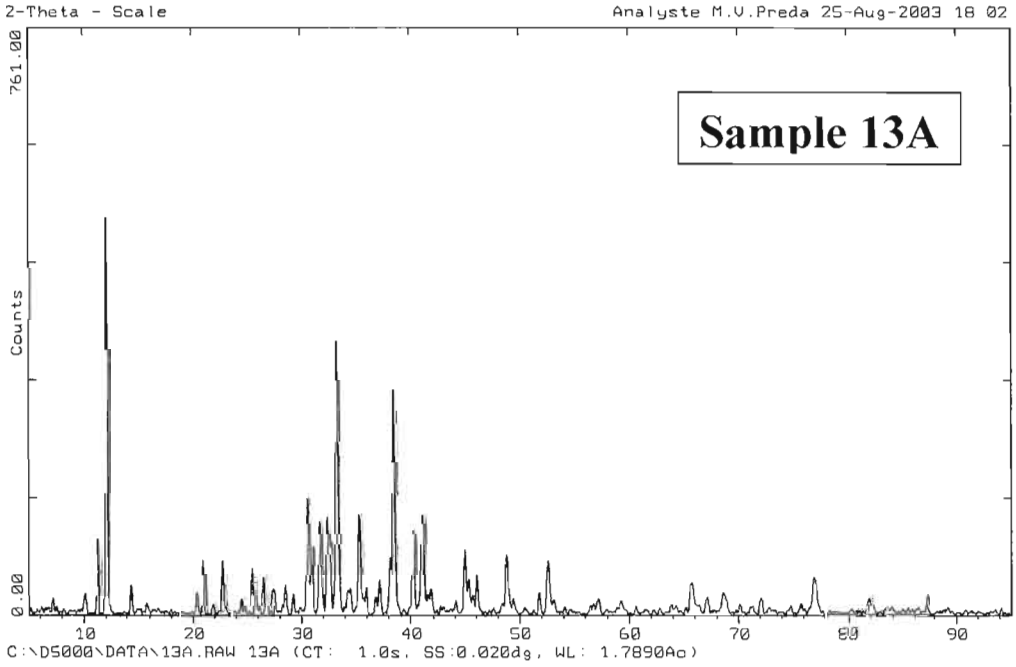
2-Theta - Scale
Analyste M.V.Preda 25-Aug-2003 18 02
761.00
Counts
0.00
Sample 13A
10
20
30
40
50
60
70
80
90
C:\D5000\DATA\13A.RAW 13A (CT: 1.0s, SS:0.020dg, WL: 1.7890Ao)

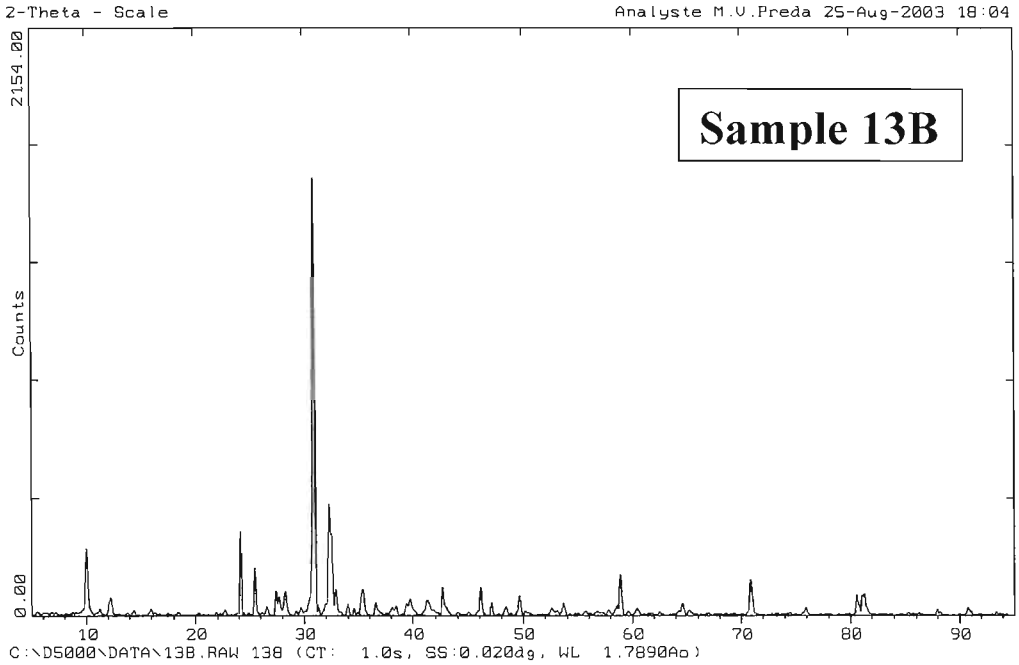
2-Theta - Scale
Analyste M.V.Preda 25-Aug-2003 18:04
2154.00
Counts
0.00
Sample 13B
10
20
30
40
50
60
70
80
90
C:\D5000\DATA\13B.RAW 13B (CT: 1.0s, SS:0.020dg, WL 1.7890Ao)

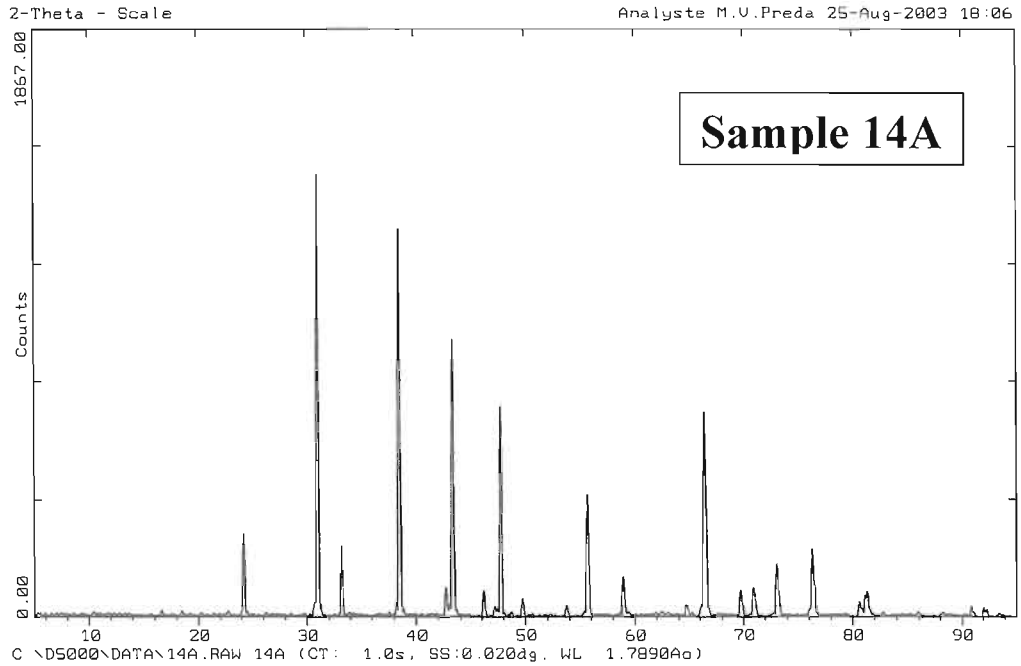
2-Theta - Scale
Analyste M.V.Preda 25-Aug-2003 18:06
1867.00
Counts
0.00
Sample 14A
10
20
30
40
50
60
70
80
90
C \D5000\DATA\14A.RAW 14A (CT: 1.0s, SS:0.020dg, WL 1.7890Ao)

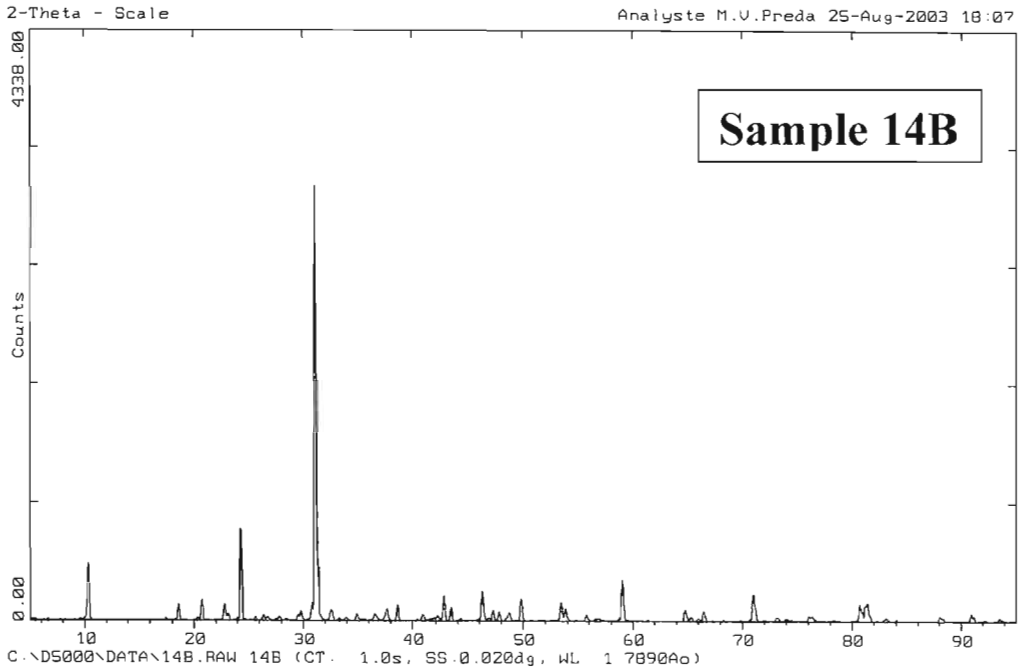
2-Theta - Scale
Analyste M.V.Preda 25-Aug-2003 18:07
4338.00
Counts
0.00
Sample 14B
10
20
30
40
50
60
70
80
90
C:\DS000\DATA\14B.RAW 14B (CT: 1.0s, SS:0.020dg, WL 1 7890Ao)

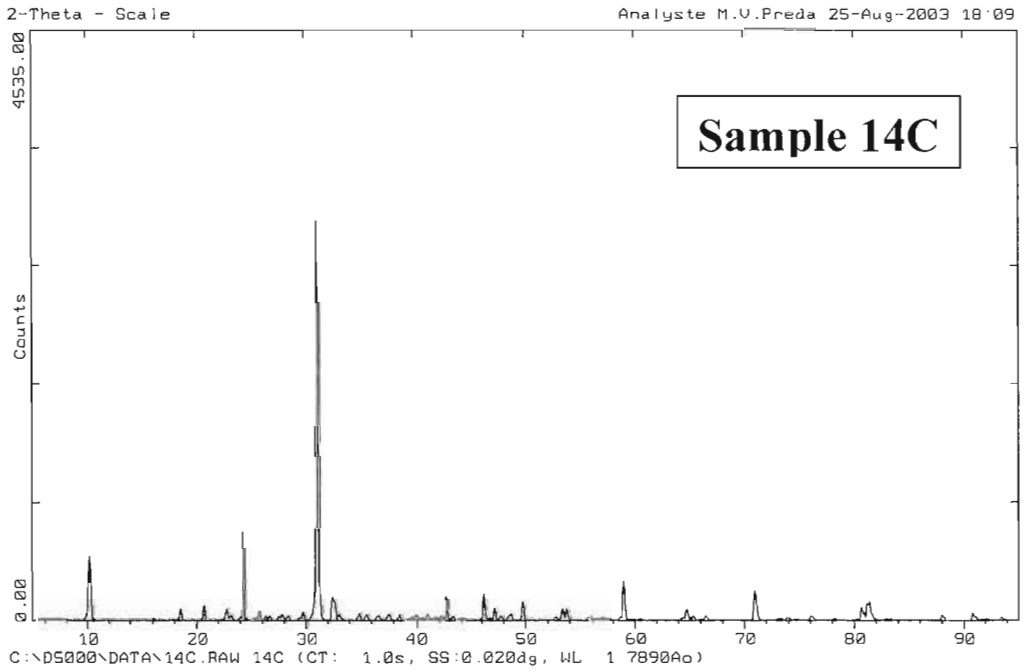
2-Theta - Scale
Analyste M.V.Preda 25-Aug-2003 18:09
4535.00
Counts
0.00
Sample 14C
10
20
30
40
50
60
70
80
90
C:\DS000\DATA\14C.RAW 14C (CT: 1.0s, SS:0.020dg, WL 1 7890Ao)

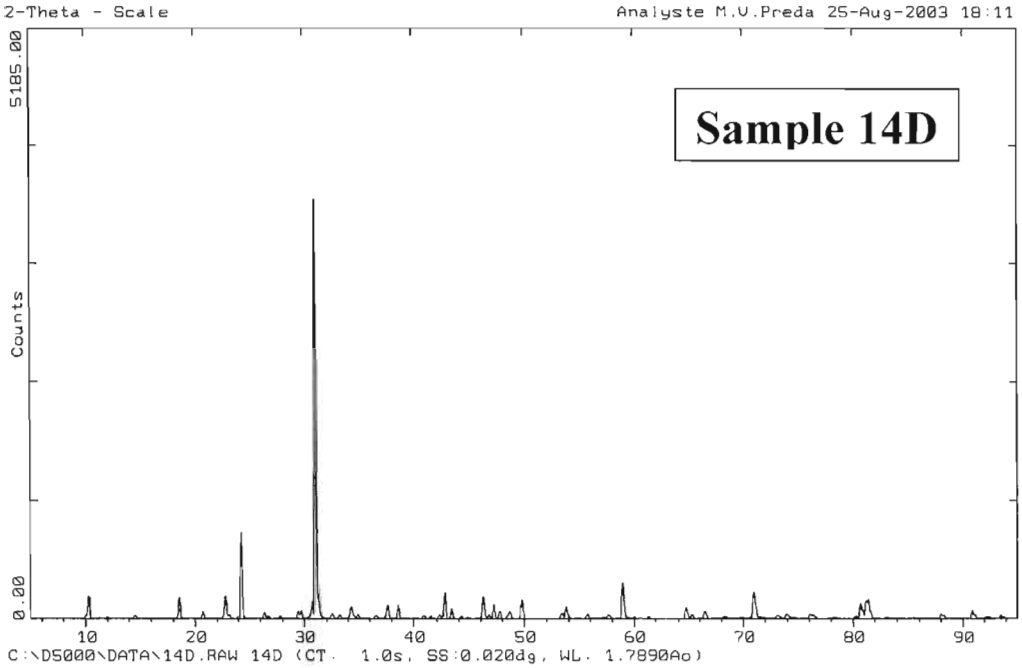
2-Theta - Scale
Analyste M.V.Preda 25-Aug-2003 18:11
5185.00
Counts
0.00
Sample 14D
10
20
30
40
50
60
70
80
90
C:\D5000\DATA\14D.RAW 14D (CT: 1.0s, SS:0.020dg, WL: 1.7890Ao)

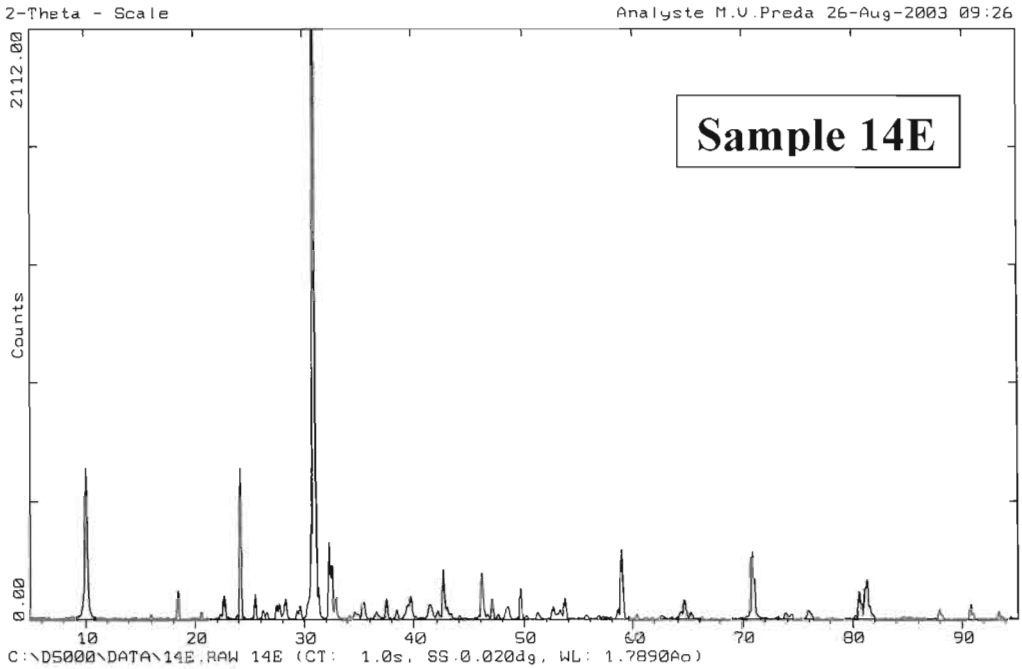
2-Theta - Scale
Analyste M.V.Preda 26-Aug-2003 09:26
2112.00
Counts
0.00
Sample 14E
10
20
30
40
50
60
70
80
90
C:\D5000\DATA\14E.RAW 14E (CT: 1.0s, SS:0.020dg, WL: 1.7890Ao)

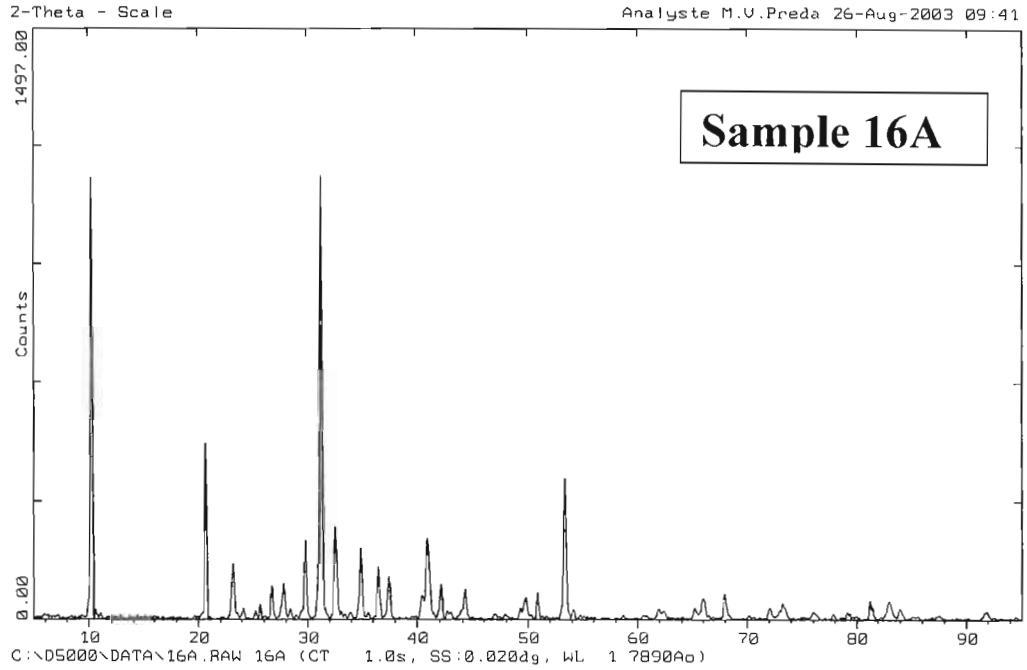
2-Theta - Scale
Analyste M.V.Preda 26-Aug-2003 09:41
1497.00
Counts
0.00
Sample 16A
10
20
30
40
50
60
70
80
90
C:\D5000\DATA\16A.RAW 16A (CT 1.0s, SS:0.020dg, WL 1 7890Ao)

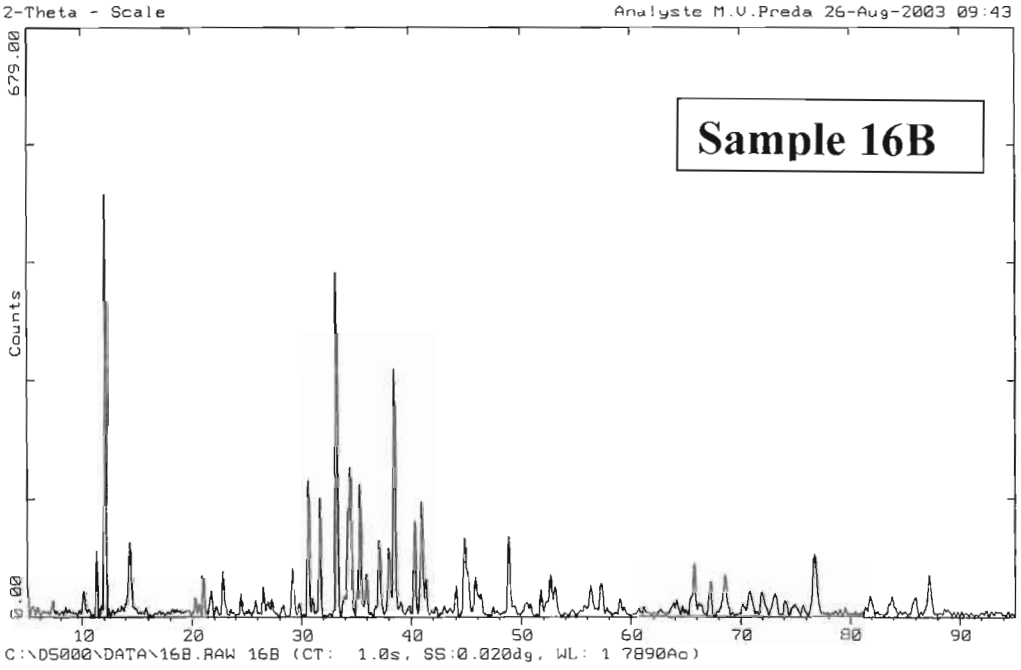
2-Theta - Scale
Analyste M.V.Preda 26-Aug-2003 09:43
679.00
Counts
0.00
Sample 16B
10
20
30
40
50
60
70
80
90
C:\D5000\DATA\16B.RAW 16B (CT: 1.0s, SS:0.020dg, WL: 1 7890Ao)

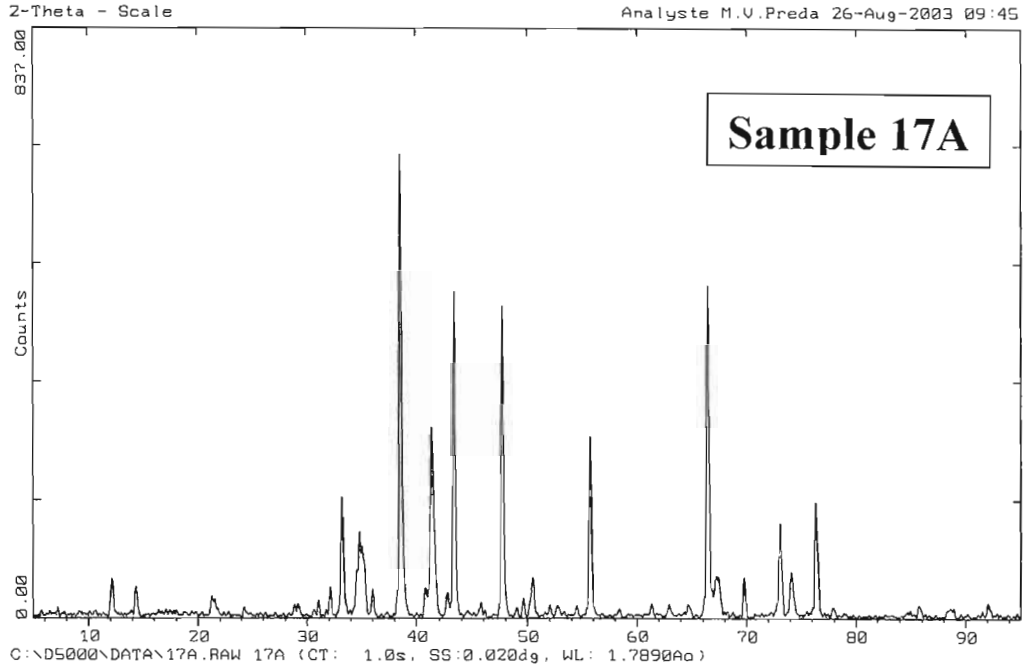
2-Theta - Scale
Analyste M.V.Preda 26-Aug-2003 09:45
837.00
Counts
0.00
Sample 17A
10
20
30
40
50
60
70
80
90
C:\D5000\DATA\17A.RAW 17A (CT: 1.0s, SS:0.020dg, WL: 1.7890Ao)

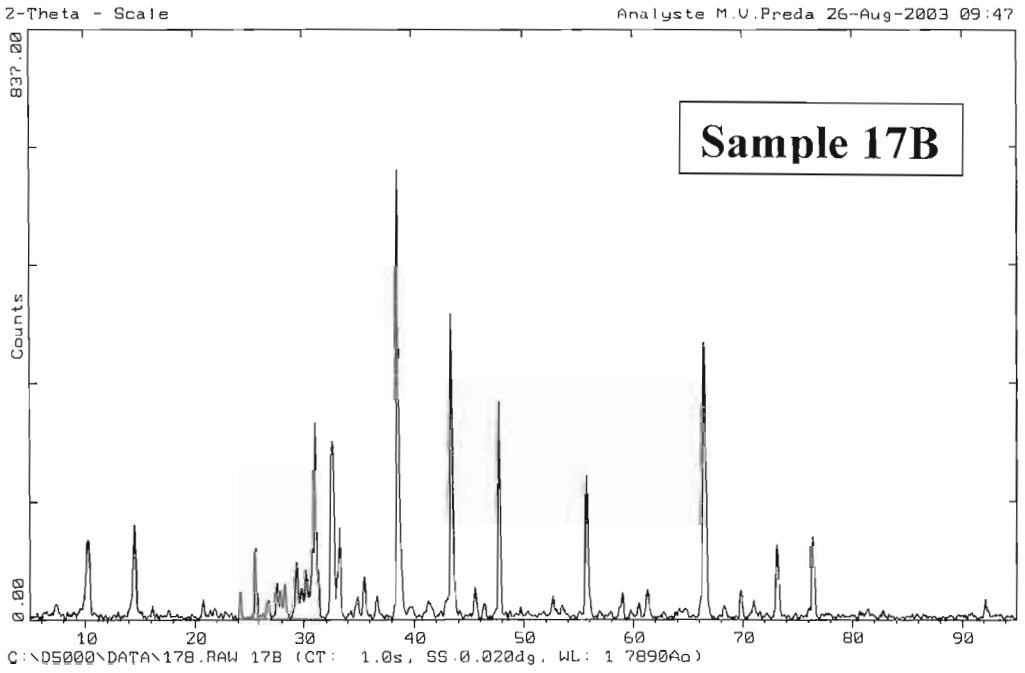
2-Theta - Scale
Analyste M.V.Preda 26-Aug-2003 09:47
837.00
Counts
0.00
Sample 17B
10
20
30
40
50
60
70
80
90
C:\D5000\DATA\17B.RAW 17B (CT: 1.0s, SS:0.020dg, WL: 1.7890Ao)

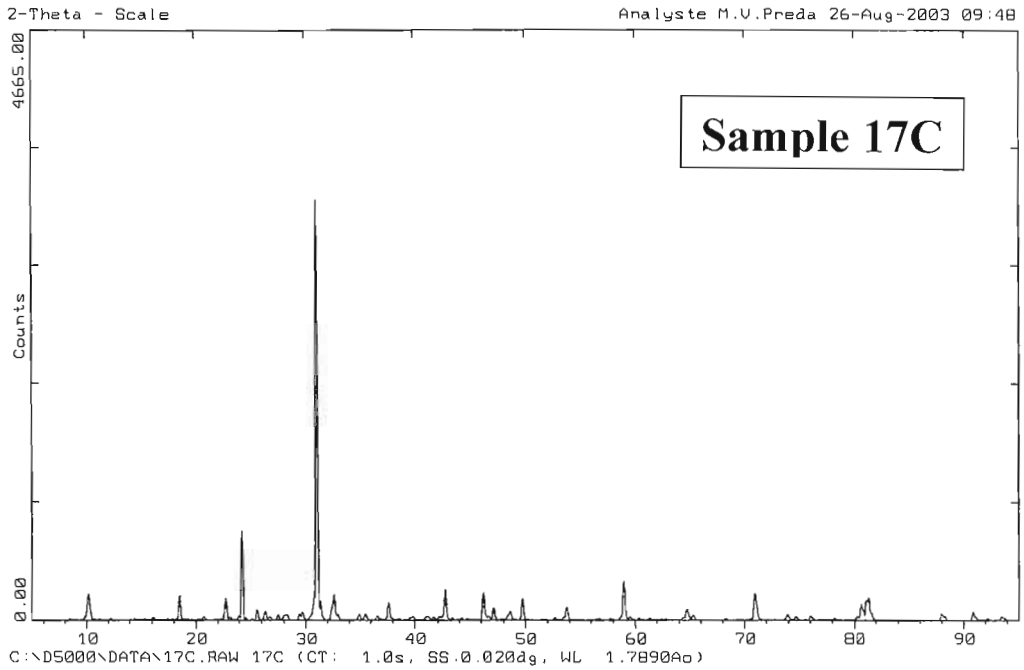
2-Theta - Scale
Analyste M.V.Preda 26-Aug-2003 09:48
4665.00
Counts
0.00
Sample 17C
10
20
30
40
50
60
70
80
90
C:\D5000\DATA\17C.RAW 17C (CT: 1.0s, SS:0.020dg, WL 1.7890Ao)

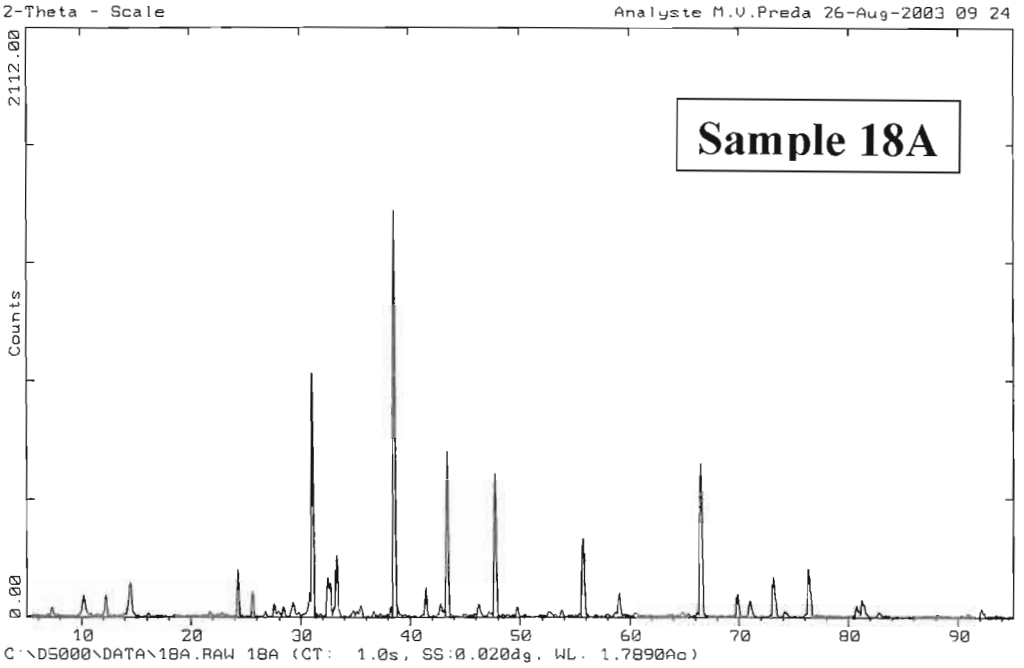
2-Theta - Scale
Analyste M.V.Preda 26-Aug-2003 09 24
2112.00
Counts
0.00
Sample 18A
10
20
30
40
50
60
70
80
90
C:\D5000\DATA\18A.RAW 18A (CT: 1.0s, SS:0.020dg, WL. 1.7890Ao)

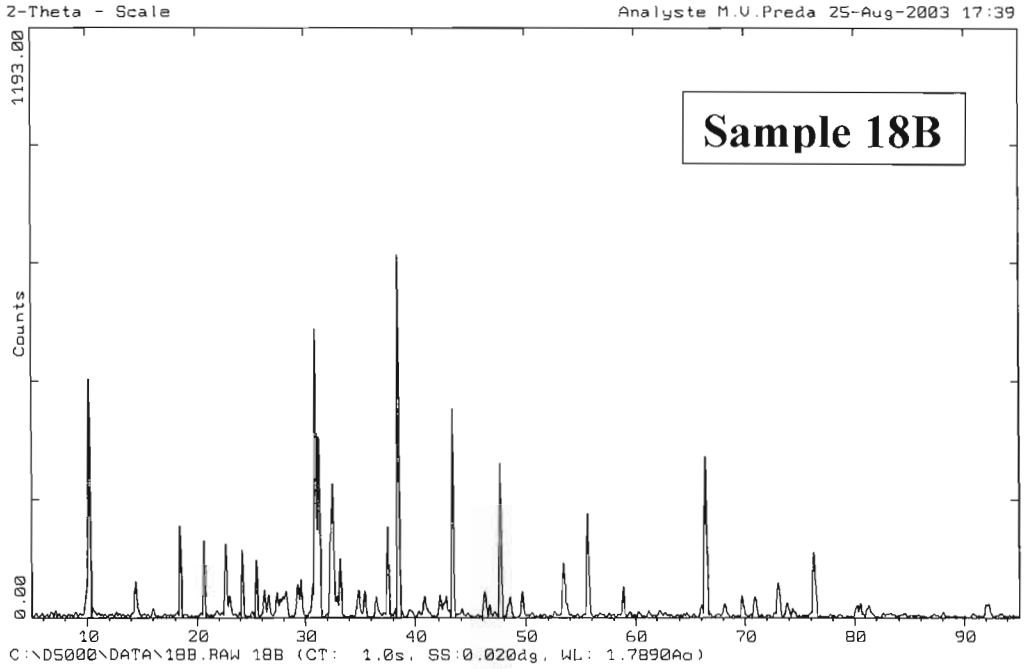
2-Theta - Scale
Analyste M.V.Preda 25-Aug-2003 17:39
1193.00
Counts
0.00
Sample 18B
10
20
30
40
50
60
70
80
90
C:\D5000\DATA\18B.RAW 18B (CT: 1.0s, SS:0.020dg, WL: 1.7890Ao)

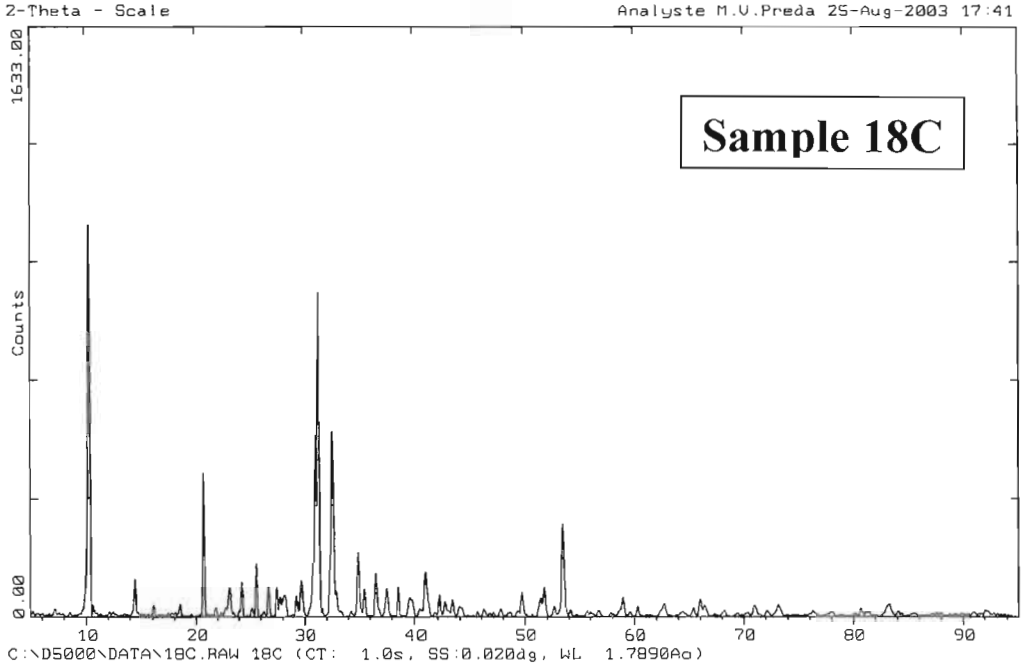
2-Theta - Scale
Analyste M.V.Preda 25-Aug-2003 17:41
1633.00
Counts
0.00
Sample 18C
10
20
30
40
50
60
70
80
90
C:\D5000\DATA\18C.RAW 18C (CT: 1.0s, SS:0.020dg, WL 1.7890Ao)

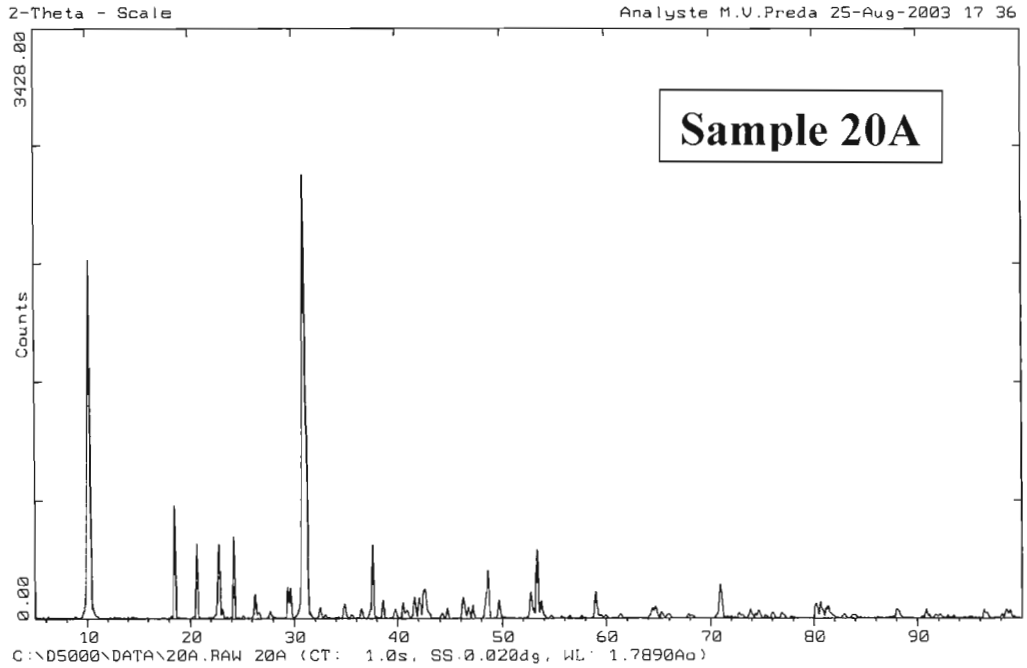
2-Theta - Scale
Analyste M.V.Preda 25-Aug-2003 17 36
3428.00
Counts
0.00
Sample 20A
10
20
30
40
50
60
70
80
90
C:\D5000\DATA\20A.RAW 20A (CT: 1.0s, SS:0.020dg, WL: 1.7890Ao)

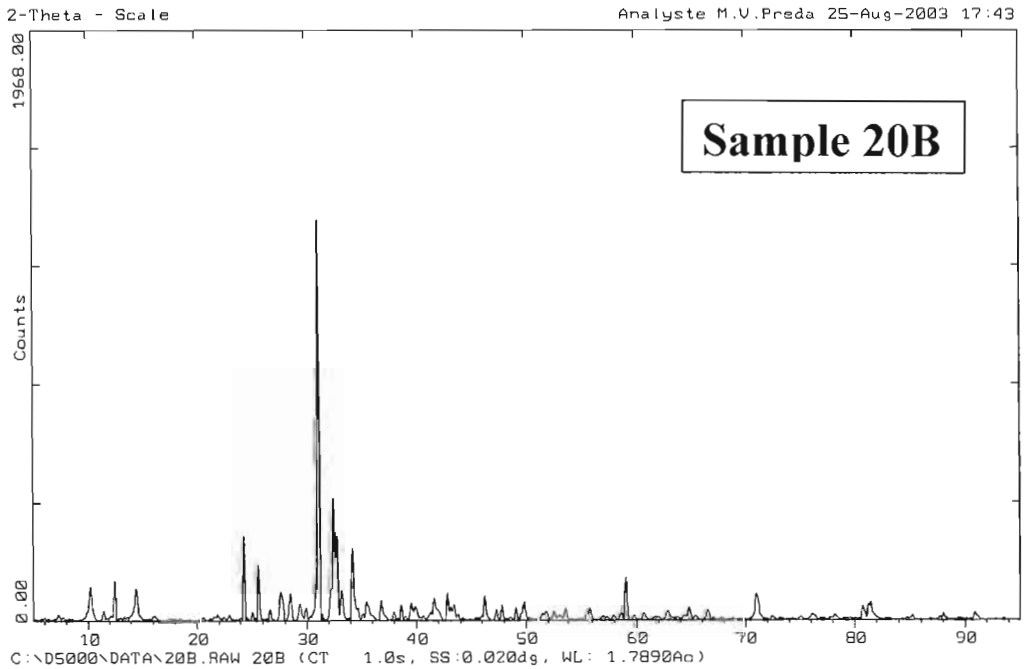
2-Theta - Scale
Analyste M.V.Preda 25-Aug-2003 17:43
1968.00
Counts
0.00
Sample 20B
10
20
30
40
50
60
70
80
90
C:\D5000\DATA\20B.RAW 20B (CT 1.0s, SS:0.020dg, WL: 1.7890Ao)

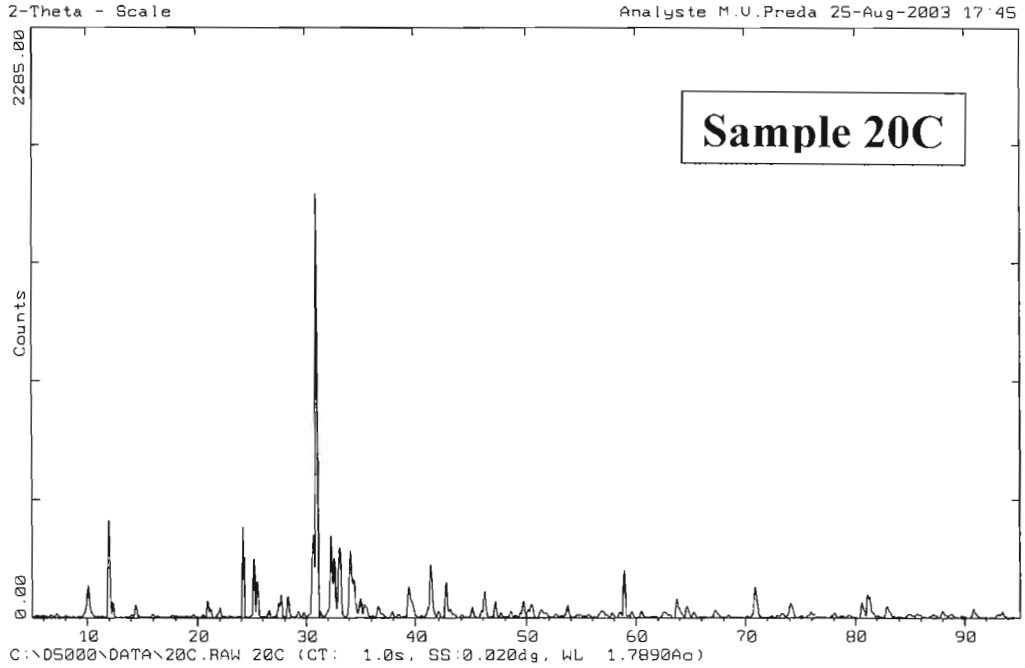
2-Theta - Scale
Analyste M.U.Preda 25-Aug-2003 17:45
2285.00
Counts
0.00
Sample 20C
10
20
30
40
50
60
70
80
90
C:\DS000\DATA\20C.RAW 20C (CT: 1.0s, SS:0.020dg, WL 1.7890Ao)

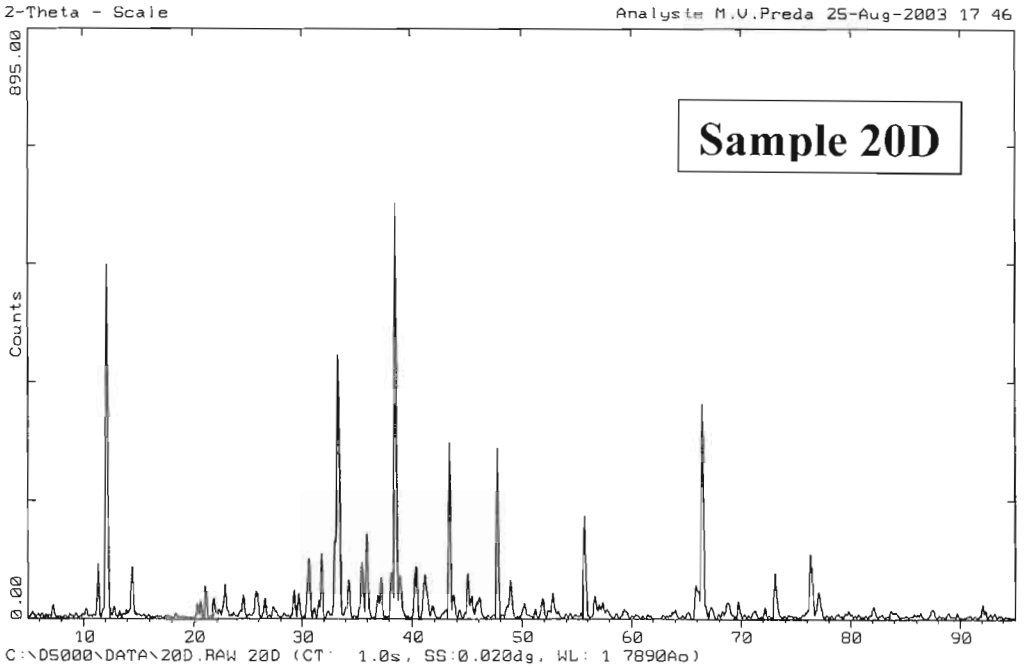
2-Theta - Scale
Analyste M.U.Preda 25-Aug-2003 17 46
895.00
Counts
0.00
Sample 20D
10
20
30
40
50
60
70
80
90
C:\DS000\DATA\20D.RAW 20D (CT: 1.0s, SS:0.020dg, WL: 1 7890Ao)

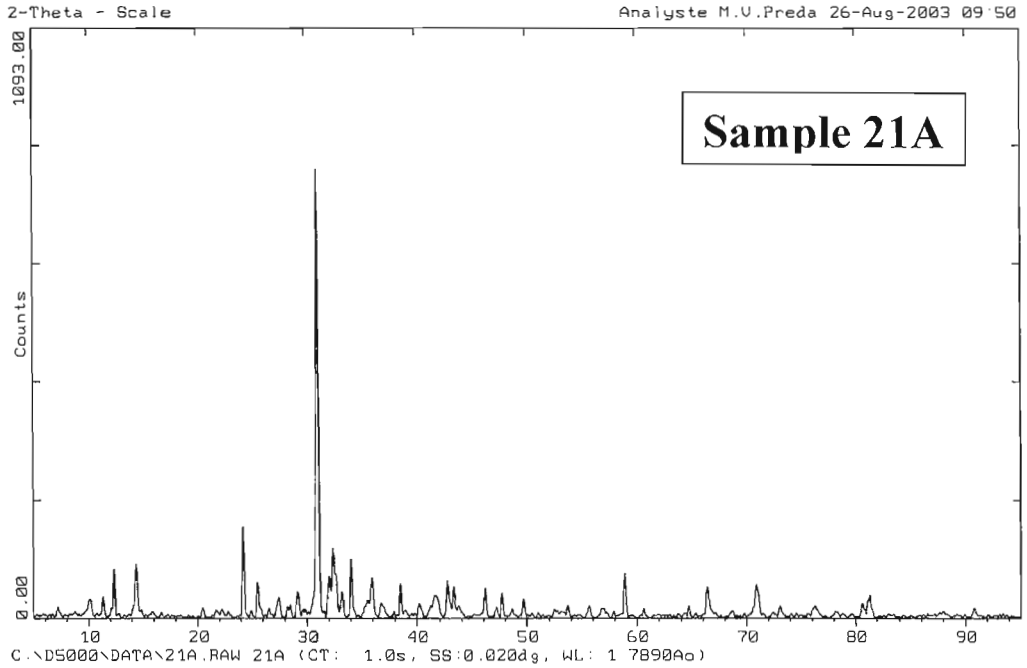
2-Theta - Scale
Analyste M.V.Preda 26-Aug-2003 09:50
1093.00
Counts
0.00
Sample 21A
10
20
30
40
50
60
70
80
90
C:\D5000\DATA\21A.RAW 21A (CT: 1.0s, SS:0.020dg, WL: 1.7890Ao)

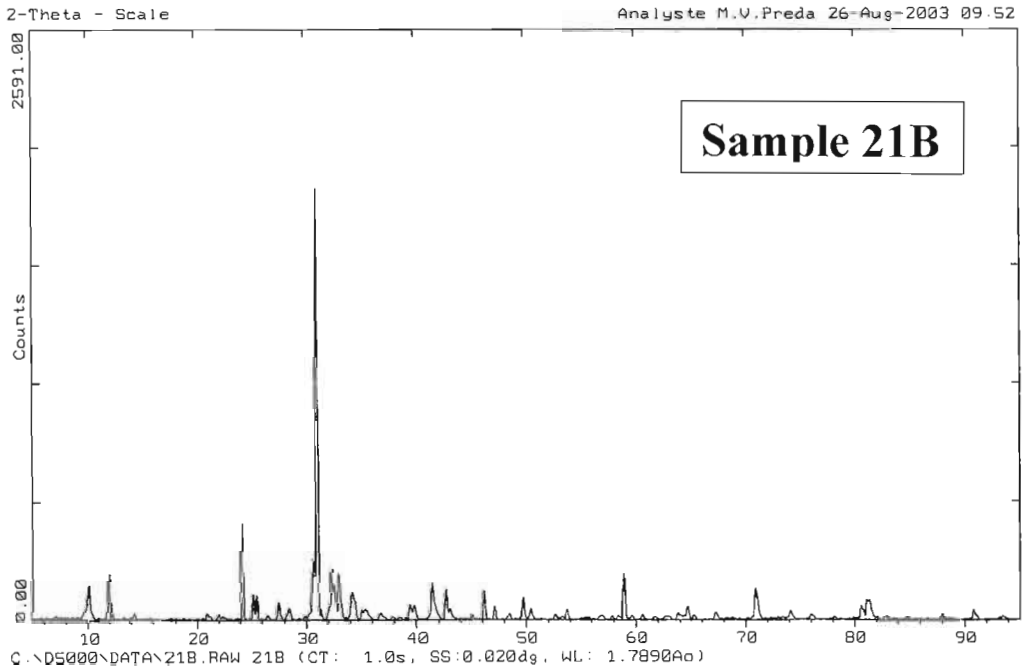
2-Theta - Scale
Analyste M.V.Preda 26-Aug-2003 09:52
2591.00
Counts
0.00
Sample 21B
10
20
30
40
50
60
70
80
90
C:\D5000\DATA\21B.RAW 21B (CT: 1.0s, SS:0.020dg, WL: 1.7890Ao)

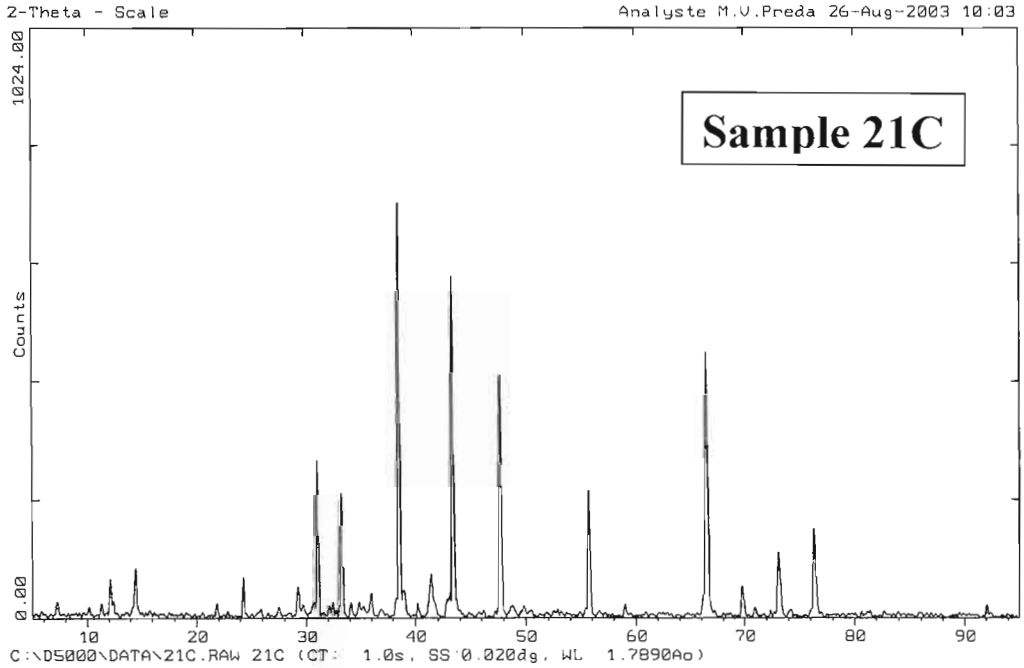
2-Theta - Scale
Analyste M.V.Preda 26-Aug-2003 10:03
1024.00
Counts
0.00
Sample 21C
10
20
30
40
50
60
70
80
90
C:\D5000\DATA\21C.RAW 21C (CT: 1.0s, SS:0.020dg, WL: 1.7890Ao)

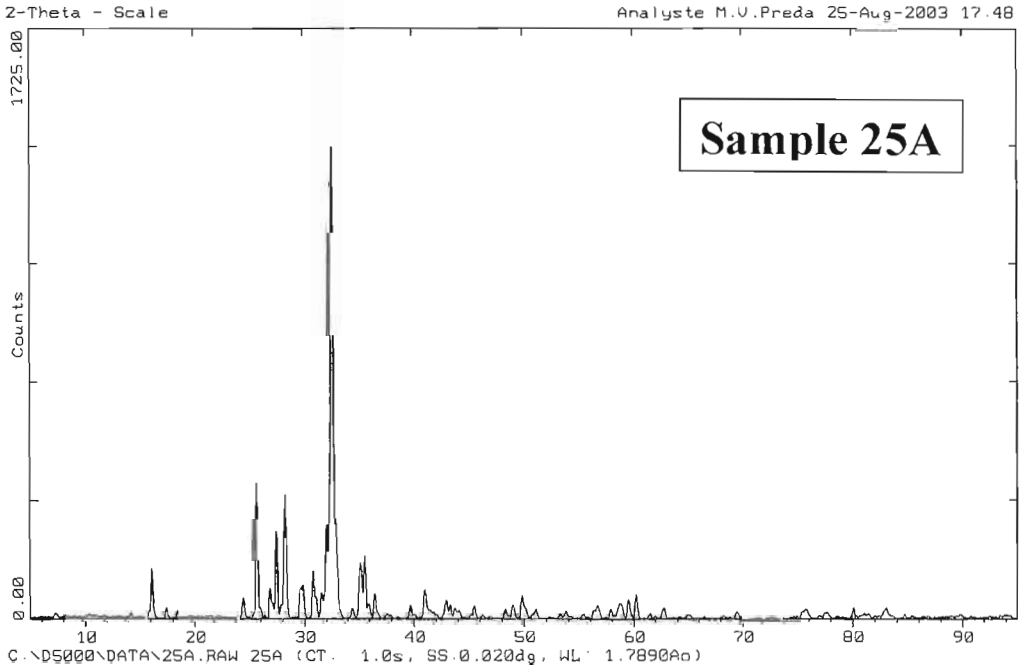
2-Theta - Scale
Analyste M.V.Preda 25-Aug-2003 17:48
1725.00
Counts
0.00
Sample 25A
10
20
30
40
50
60
70
80
90
C:\D5000\DATA\25A.RAW 25A (CT: 1.0s, SS:0.020dg, WL: 1.7890Ao)

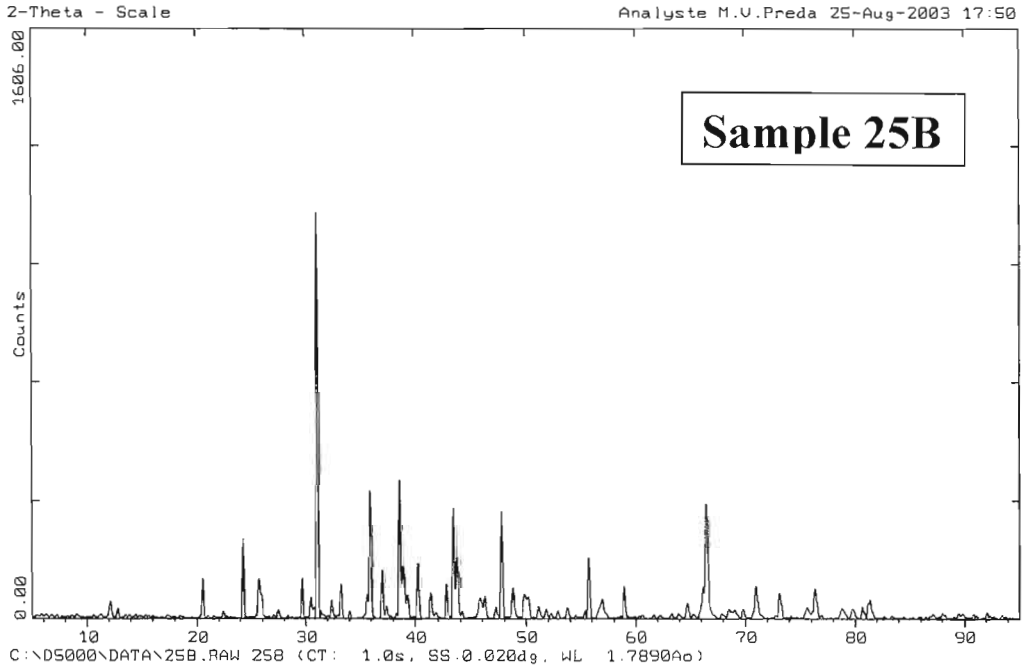
2-Theta - Scale
Analyste M.V.Preda 25-Aug-2003 17:50
1606.00
Counts
0.00
Sample 25B
10
20
30
40
50
60
70
80
90
C:\D5000\DATA\25B.RAW 25B (CT: 1.0s, SS:0.020dg, WL 1.7890Ao)

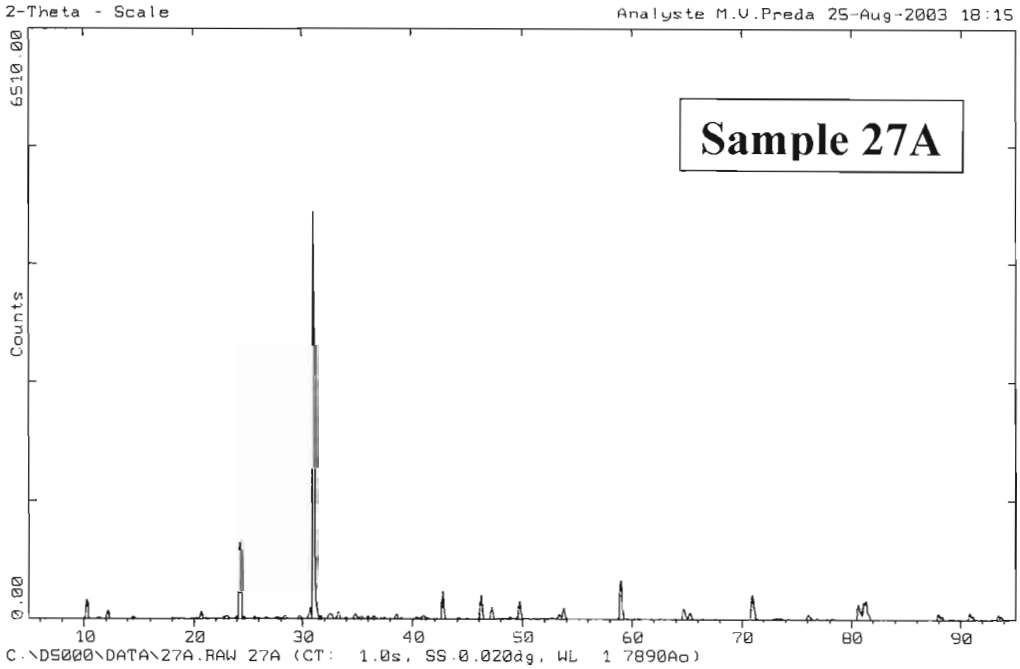
2-Theta - Scale
Analyste M.V.Preda 25-Aug-2003 18:15
6510.00
Counts
0.00
Sample 27A
10
20
30
40
50
60
70
80
90
C:\D5000\DATA\27A.RAW 27A (CT: 1.0s, SS:0.020dg, WL 1.7890Ao)

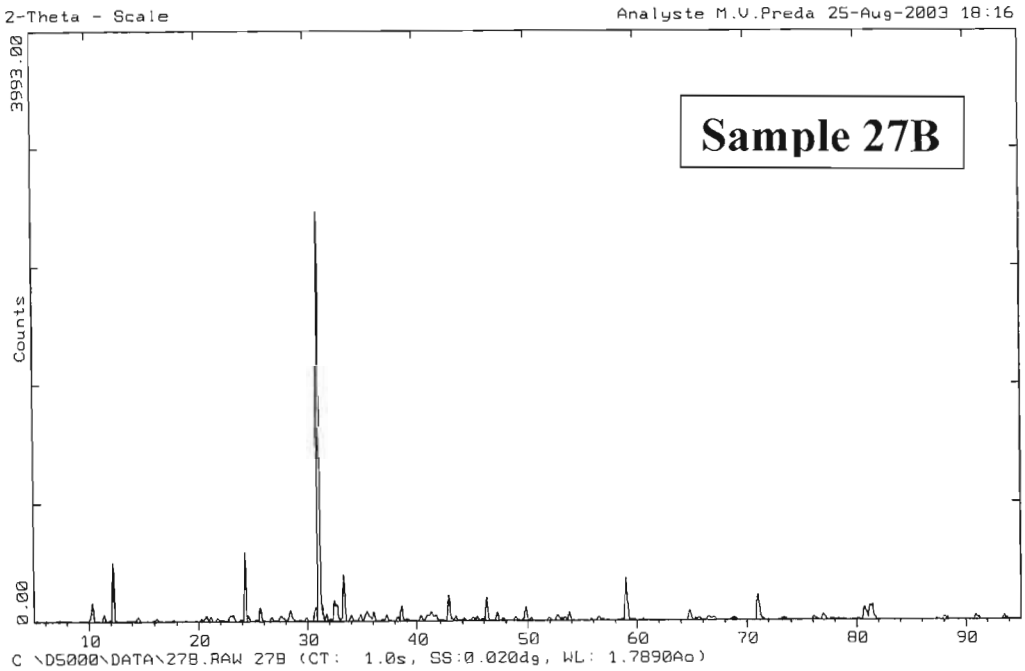
2-Theta - Scale
Analyste M.V.Preda 25-Aug-2003 18:16
3993.00
Counts
0.00
Sample 27B
10
20
30
40
50
60
70
80
90
C \D5000\DATA\27B.RAW 27B (CT: 1.0s, SS:0.020dg, WL: 1.7890Ao)

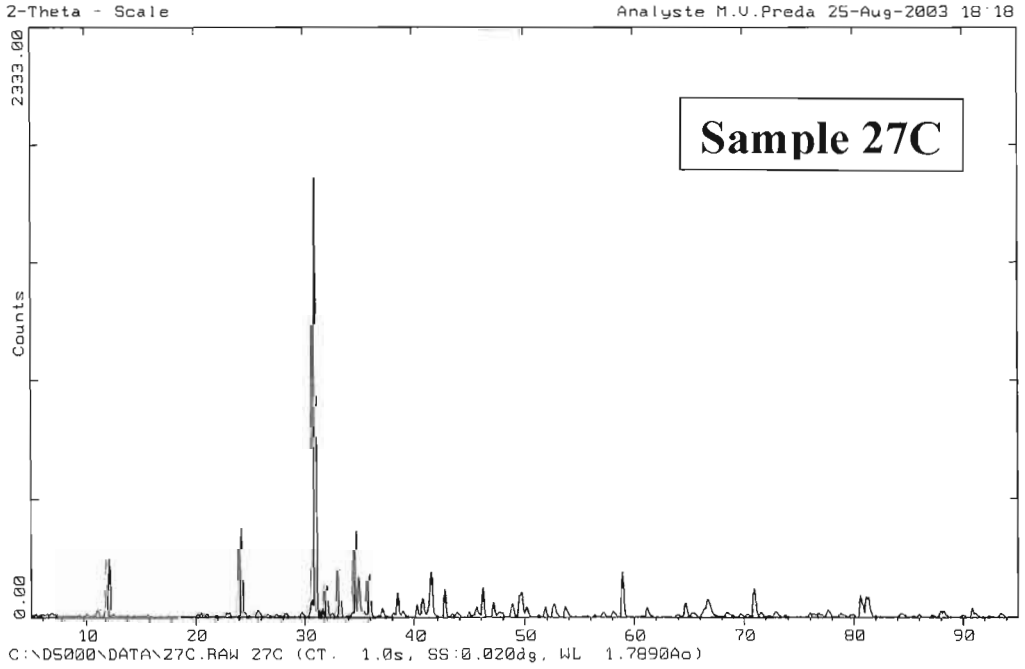
2-Theta - Scale
Analyste M.V.Preda 25-Aug-2003 18:18
2333.00
Counts
0.00
Sample 27C
10
20
30
40
50
60
70
80
90
C:\D5000\DATA\27C.RAW 27C (CT: 1.0s, SS:0.020dg, WL 1.7890Ao)

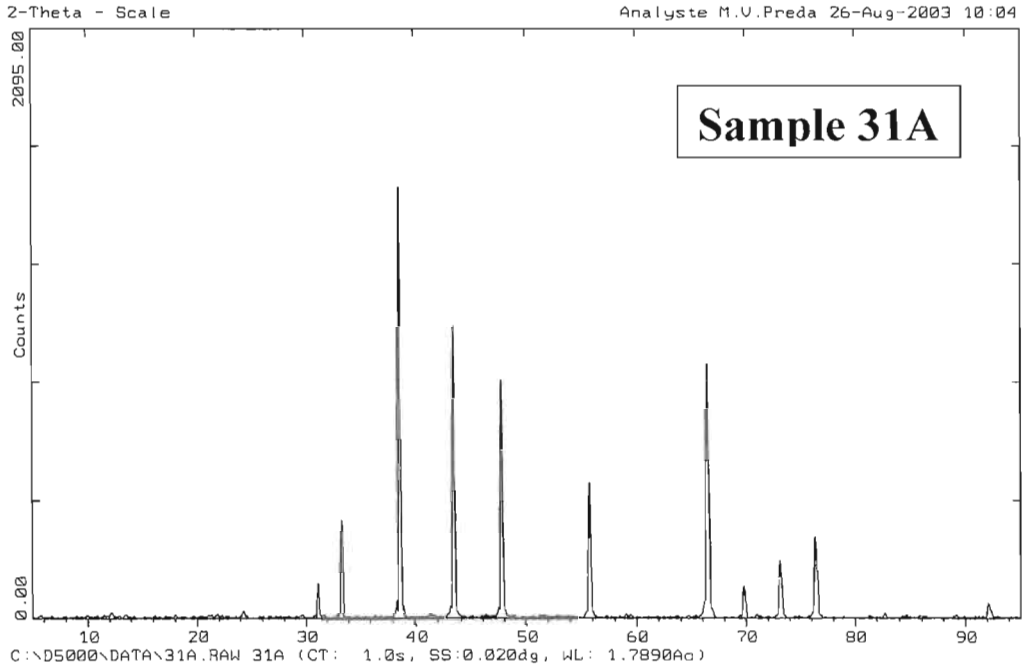
2-Theta - Scale
Analyste M.V.Preda 26-Aug-2003 10:04
2095.00
Counts
0.00
Sample 31A
10
20
30
40
50
60
70
80
90
C:\D5000\DATA\31A.RAW 31A (CT: 1.0s, SS:0.020dg, WL: 1.7890Ao)

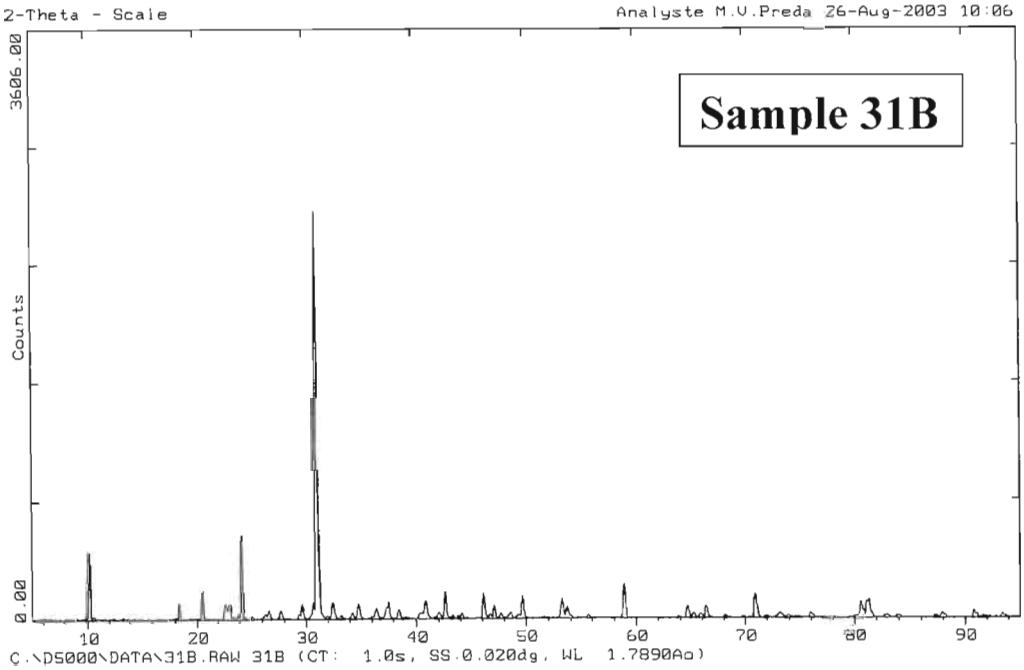
2-Theta - Scale
Analyste M.V.Preda 26-Aug-2003 10:06
3606.00
Counts
0.00
Sample 31B
10
20
30
40
50
60
70
80
90
C:\D5000\DATA\31B.RAW 31B (CT: 1.0s, SS:0.020dg, WL: 1.7890Ao)

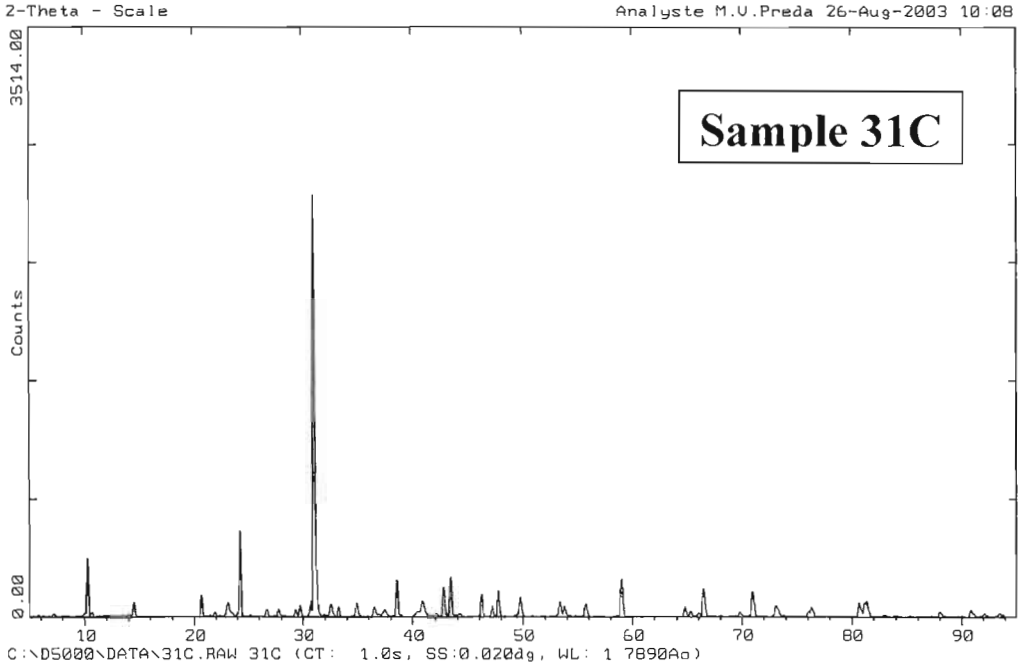
2-Theta - Scale
Analyste M.U.Preda 26-Aug-2003 10:08
3514.00
Counts
0.00
Sample 31C
10
20
30
40
50
60
70
80
90
C:\D5000\DATA\31C.RAW 31C (CT: 1.0s, SS:0.020dg, WL: 1.7890Ao)

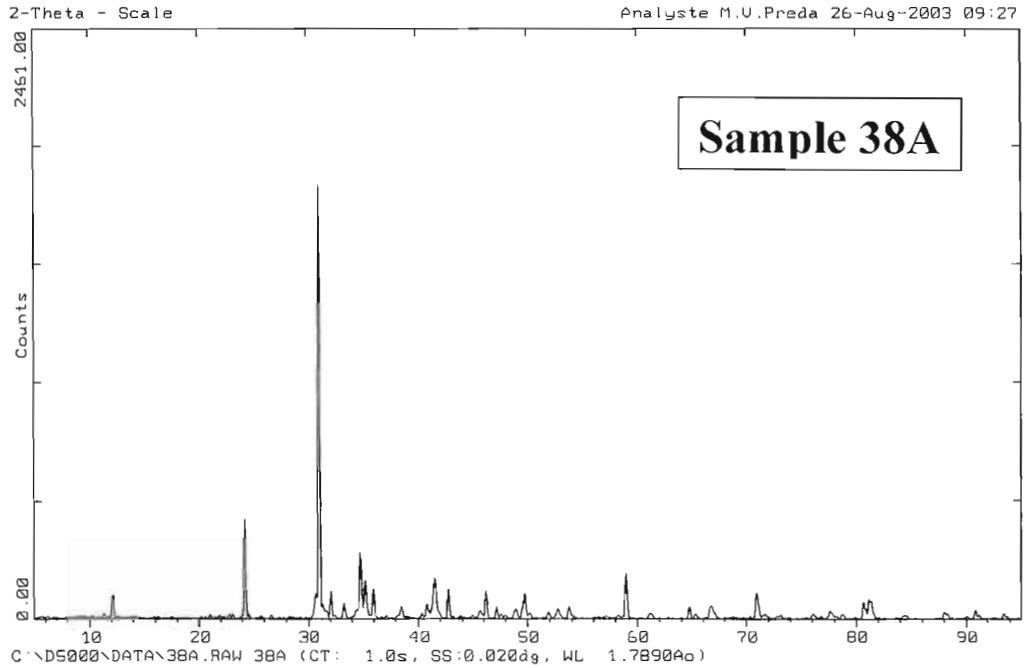
2-Theta - Scale
Analyste M.U.Preda 26-Aug-2003 09:27
2451.00
Counts
0.00
Sample 38A
10
20
30
40
50
60
70
80
90
C:\D5000\DATA\38A.RAW 38A (CT: 1.0s, SS:0.020dg, WL: 1.7890Ao)

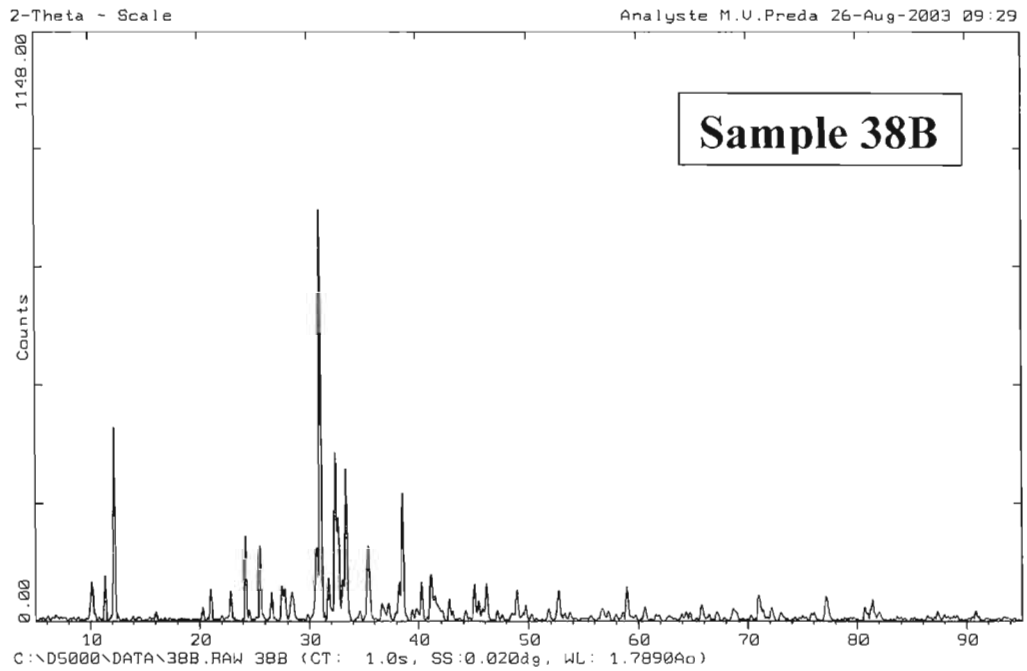
2-Theta - Scale
Analyste M.V.Preda 26-Aug-2003 09:29
1148.00
0.00
Counts
Sample 38B
10
20
30
40
50
60
70
80
90
C:\D5000\DATA\38B.RAW 38B (CT: 1.0s, SS:0.020dg, WL: 1.7890Ao)

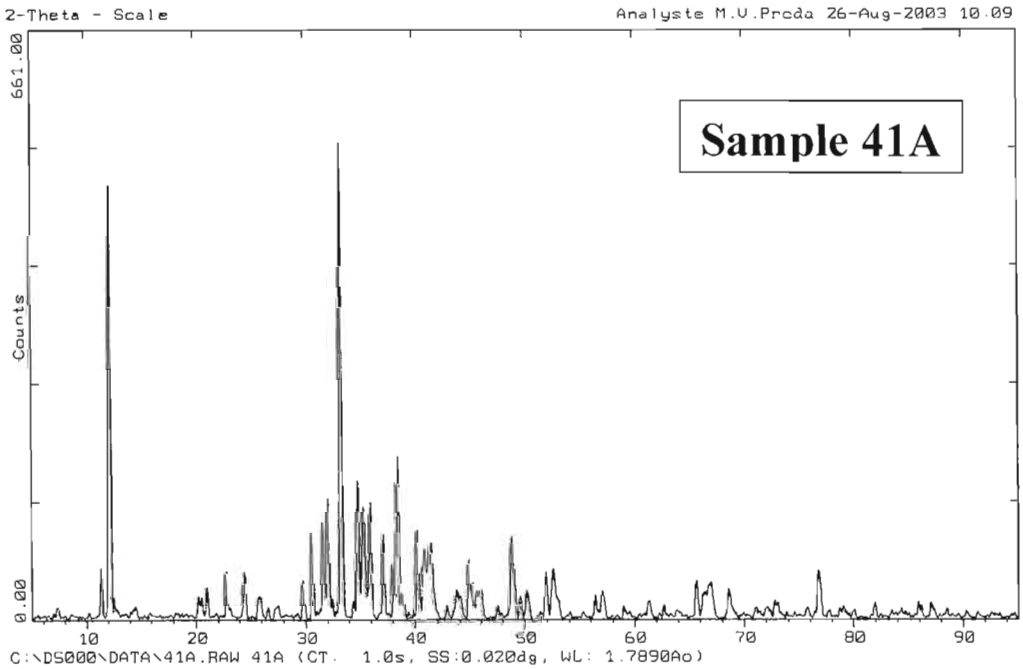
2-Theta - Scale
Analyste M.V.Preda 26-Aug-2003 10:09
661.00
0.00
Counts
Sample 41A
10
20
30
40
50
60
70
80
90
C:\D5000\DATA\41A.RAW 41A (CT: 1.0s, SS:0.020dg, WL: 1.7890Ao)

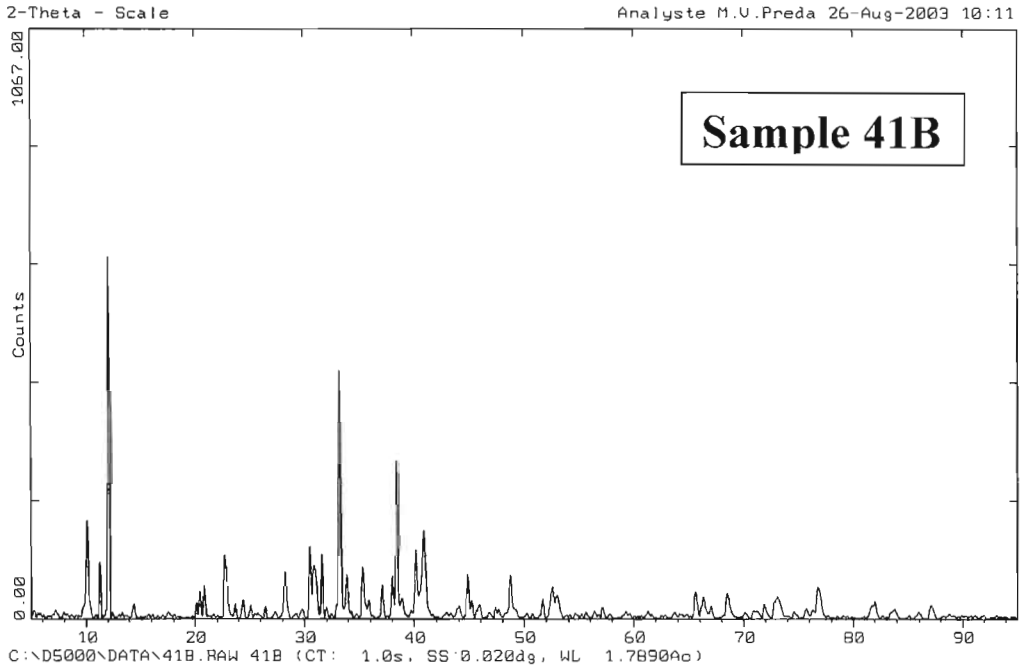
2-Theta - Scale
Analyste M.V.Preda 26-Aug-2003 10:11
1067.00
Counts
0.00
Sample 41B
10
20
30
40
50
60
70
80
90
C:\D5000\DATA\41B.RAW 41B (CT: 1.0s, SS:0.020dg, WL 1.7890Ao)

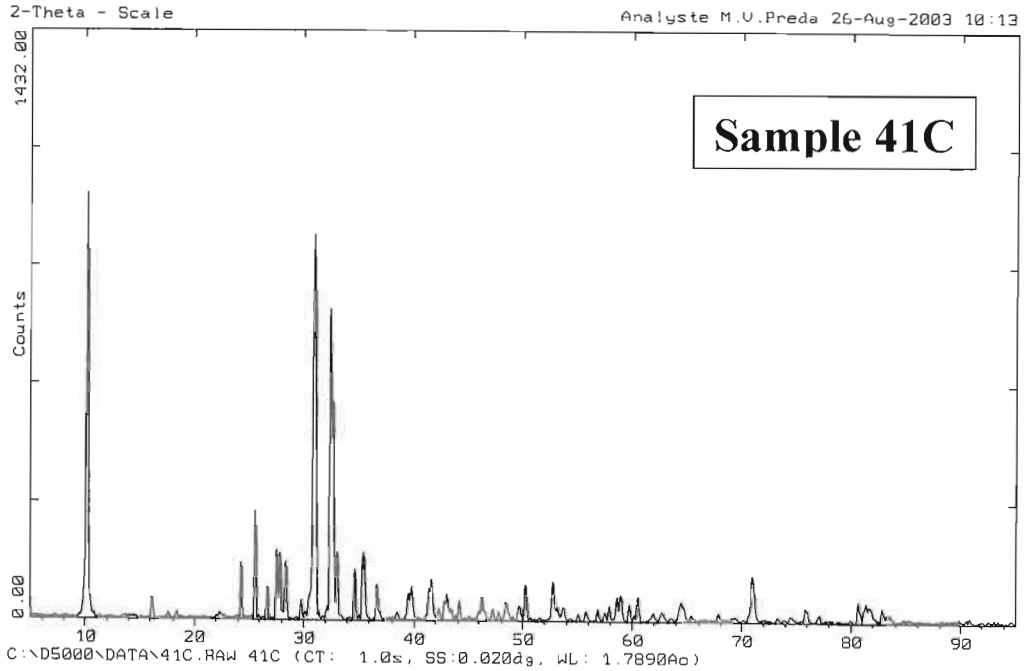
2-Theta - Scale
Analyste M.V.Preda 26-Aug-2003 10:13
1432.00
Counts
0.00
Sample 41C
10
20
30
40
50
60
70
80
90
C:\D5000\DATA\41C.RAW 41C (CT: 1.0s, SS:0.020dg, WL: 1.7890Ao)

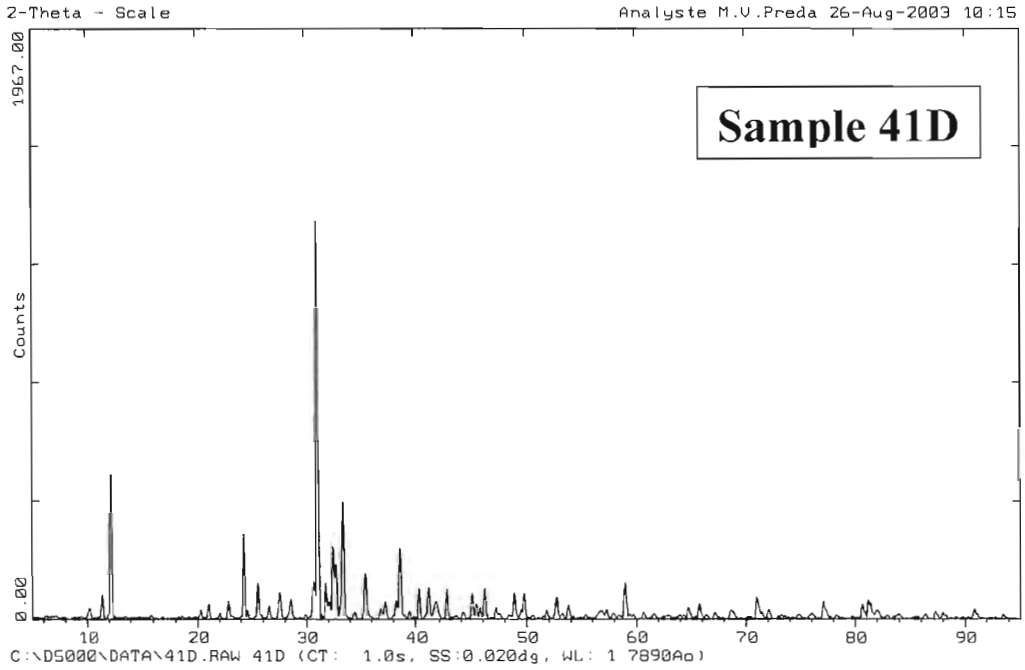
2-Theta - Scale
Analyste M.V.Preda 26-Aug-2003 10:15
1967.00
Counts
0.00
Sample 41D
10
20
30
40
50
60
70
80
90
C:\D5000\DATA\41D.RAW 41D (CT: 1.0s, SS:0.020dg, WL: 1 7890Ao)

APPENDIX B

ANALYSIS OF MINERALIZED PYRITE VEINS BY ELECTRON MICROSCOPE

B.1 Rérumé

La minéralisation aurifère de Comtois est retrouvée dans des veines de pyrite+quartz±chalcopyrite. Il est essentiel de comprendre dans quelle association minéralogique se retrouve l'or et de déterminer la composition des grains d'or pour les fins d'une interpretation.

Des lames minces polies des veines minéralisées ont été observées par un microscope a balayage électronique. Les résultats ont démontré que l'or est emprisonné dans la pyrite et dans ses fractures. Cet or est sous forme d'électrum. Le ratio or : argent de l'électrum varie de 1 : 2 à 9 : 1. Ce ratio est conforme aux dépôts de types épithermaux.

B.1 Introduction

The Comtois auriferous deposit is mainly composed of mineralized pyrite+/-chalcopyrite veins. The genetic model is unclear but geological evidence suggests either a VMS, skarn or shear zone type deposit.

The gold seems to be found within the pyrite+/-chalcopyrite veins. This is assumed because all samples with important gold values contain a pyrite+/-chalcopyrite vein. However, gold has not been observed in thin section using an optical microscope. Therefore, analysis of the pyrite+/-chalcopyrite veins with an electron microscope was essential to observe the gold mineralization. The results confirmed the presence of the gold within the pyrite+/-chalcopyrite veins and gave valuable information concerning the genetic model.

B.2 Analytical Methods

Small thin section sized samples were prepared in the laboratory using a rock saw. Polished thin sections were prepared by Petrographic International in Saskatchewan, Canada. The thin sections were then thoroughly examined and described with an optical microscope prior to any preparation for electron microscope analysis. Areas of interest were chosen and circled with a marker to later be observed with the electron microscope. The microscope is Hitachi S-2300 Scanning Electron Microscope (fig. B.1). It is equipped with an IXRF computing system and Kevex Quantum SeLi Rx detector for low atomic numbers. It's count time for the Rx spectrum is 50 seconds with 40% dead time. It is equipped with a Gini type backscatter detector and a filament voltage of 20KV.

The thin section was then coated with a thin coat of carbon to charge the minerals on the thin section. This is done to enhance the visibility of the minerals by the electron microscope. The thin sections were individually mounted in the electron microscope. The microscope was then sealed and flooded with liquid nitrogen to establish a vacuum within the electron microscope. The circles of interest were then found and observed at magnifications not possible with an

optical microscope. Colour is not an element that is visible with an electron microscope. However, the relative densities of the minerals are observed. The density of the minerals is proportionate to the luminosity of the image received by the microscope. The mineral of interest is gold which is very dense, therefore very bright. The very bright grains were then selected with pinpoint accuracy and analysed with the electron microscope. Digital photographs of the areas of interest were also taken with the electron microscope.

B.3 Results

Analysis of the thin section by the electron microscope found electrum grains associated with the pyrite of the mineralised veins. The electrum is located in the pyrite grains and the pyrite fractures. The gold:silver ratio of the electrum varies from 1:2 to 9:1 (fig. B.2 + B.3). Analysis of 730 portions of core samples by ICPAS show an average Au:Ag ratio of 1:3 to 9:1 (fig. B.4).

Fig. B.1: Hitachi S-2300 scanning electron microscope

Thin Section	Component	Concentration
10a	Te	65.5
	Au	15.9
	Bi	17.9
10a	Ag	8.5
	Au	91.5
14x	Ag	50.5
	Au	49.5
14x	Ag	49.0
	Au	51.0
11a	Ag	25.0
	Au	75.0
11b	Ag	64.0
	Au	36.0
11b	Ag	11.4
	Au	88.6
39b	Ag	38.5
	Au	61.5
39b	Ag	43.6
	Au	56.4
39b	Ag	39.6
	Au	60.4
39b	Ag	43.5
	Au	56.5

Tab. B.1: Results of electrum grains analysis under electron microscope

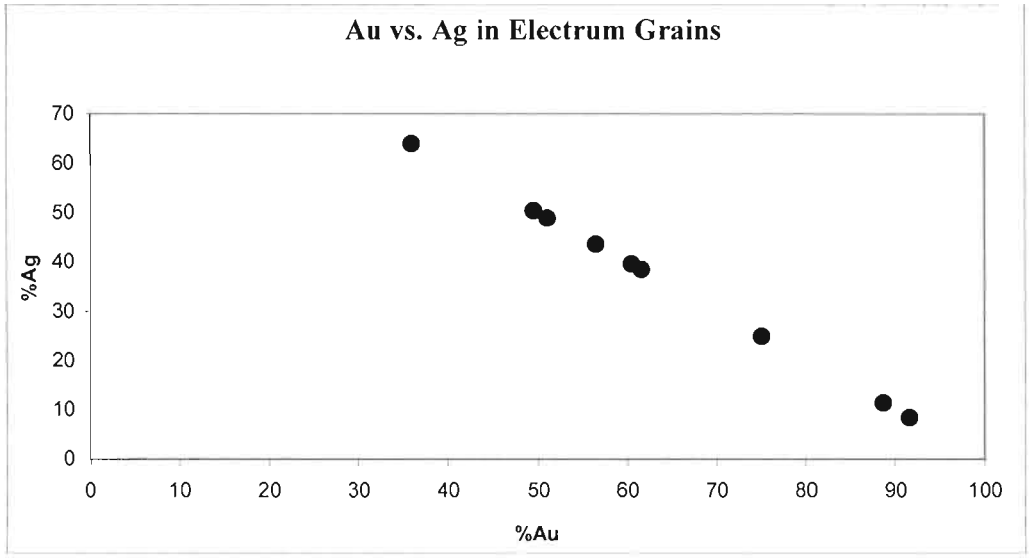

Fig. B.2: Analysis of electrum grains by electron microscope

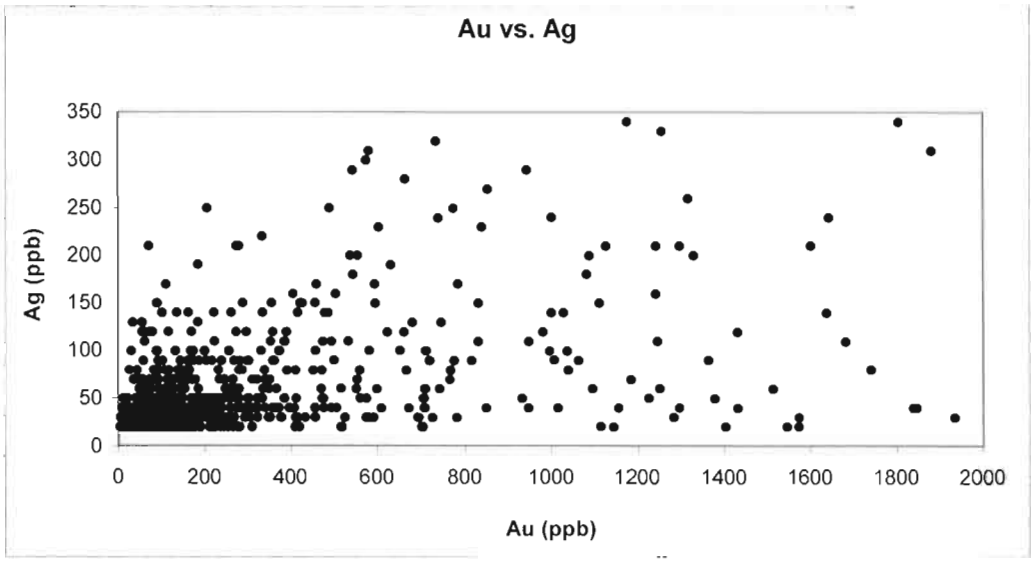

Fig. B.3: Analysis of 730 portions of core samples by ICPAS

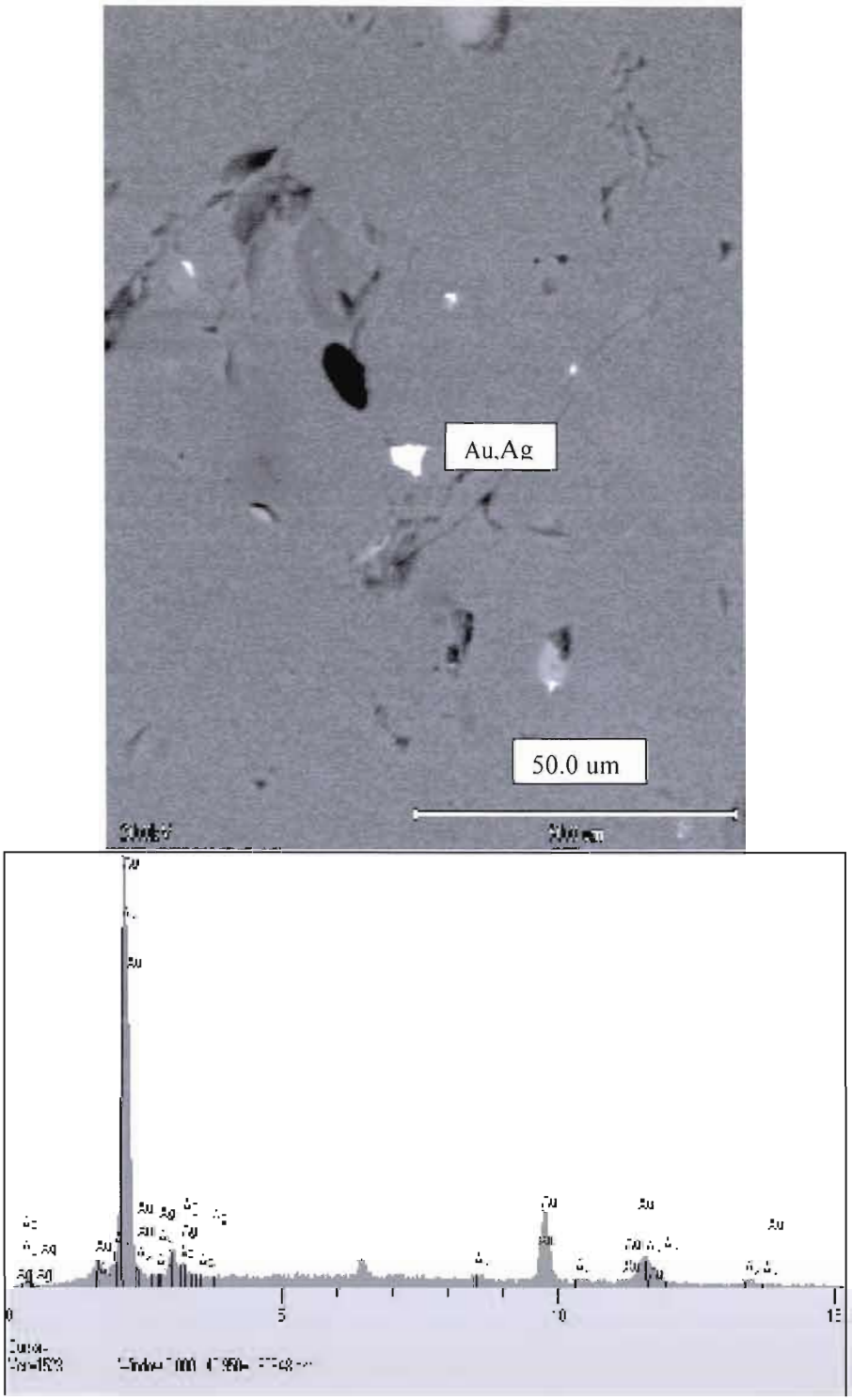

Fig. B.4: Thin Section 11b.1 and spectrum; gold locked in pyrite

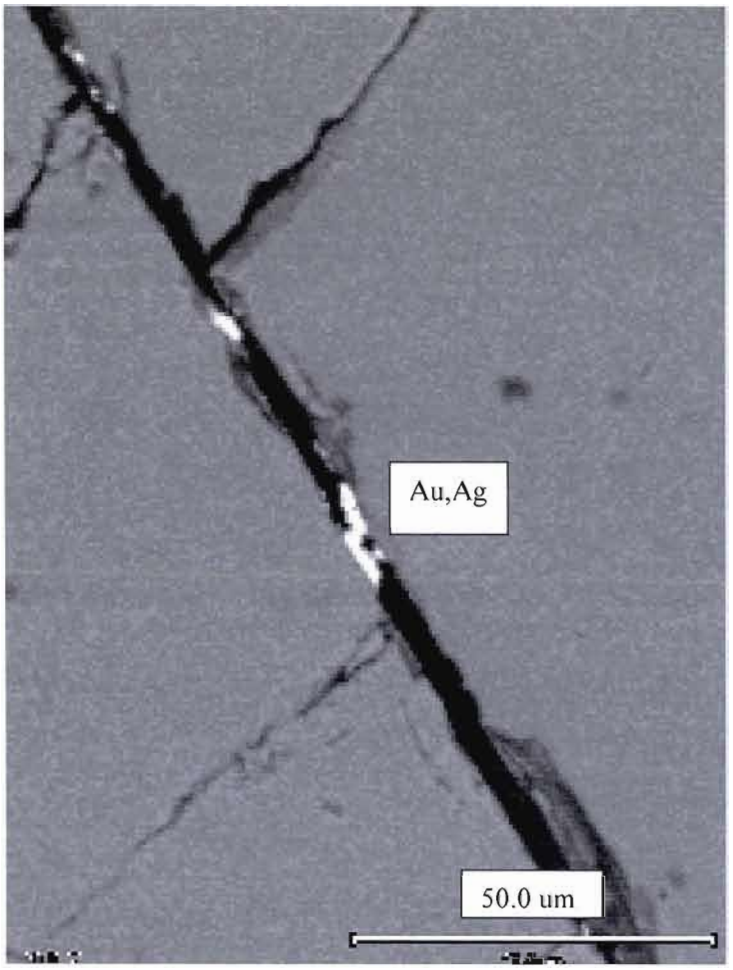

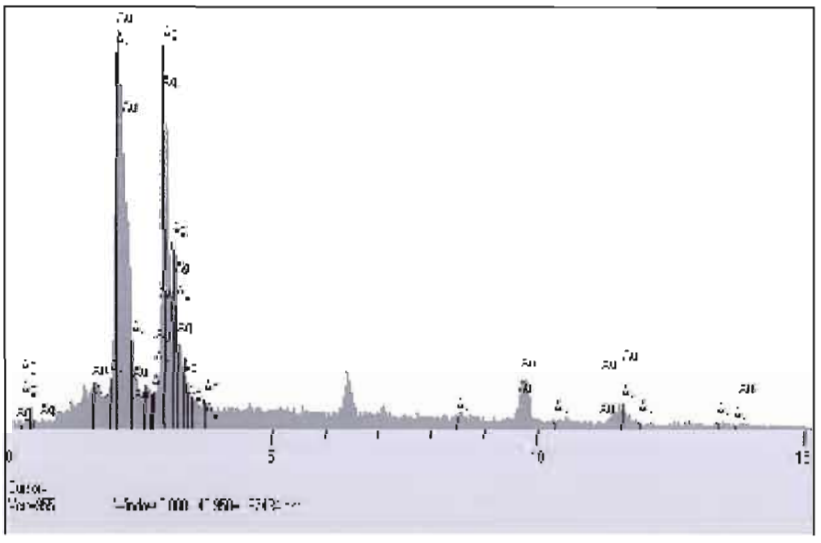

Fig.B.5: Thin Section 11b.2 and spectrum; gold in pyrite fracture

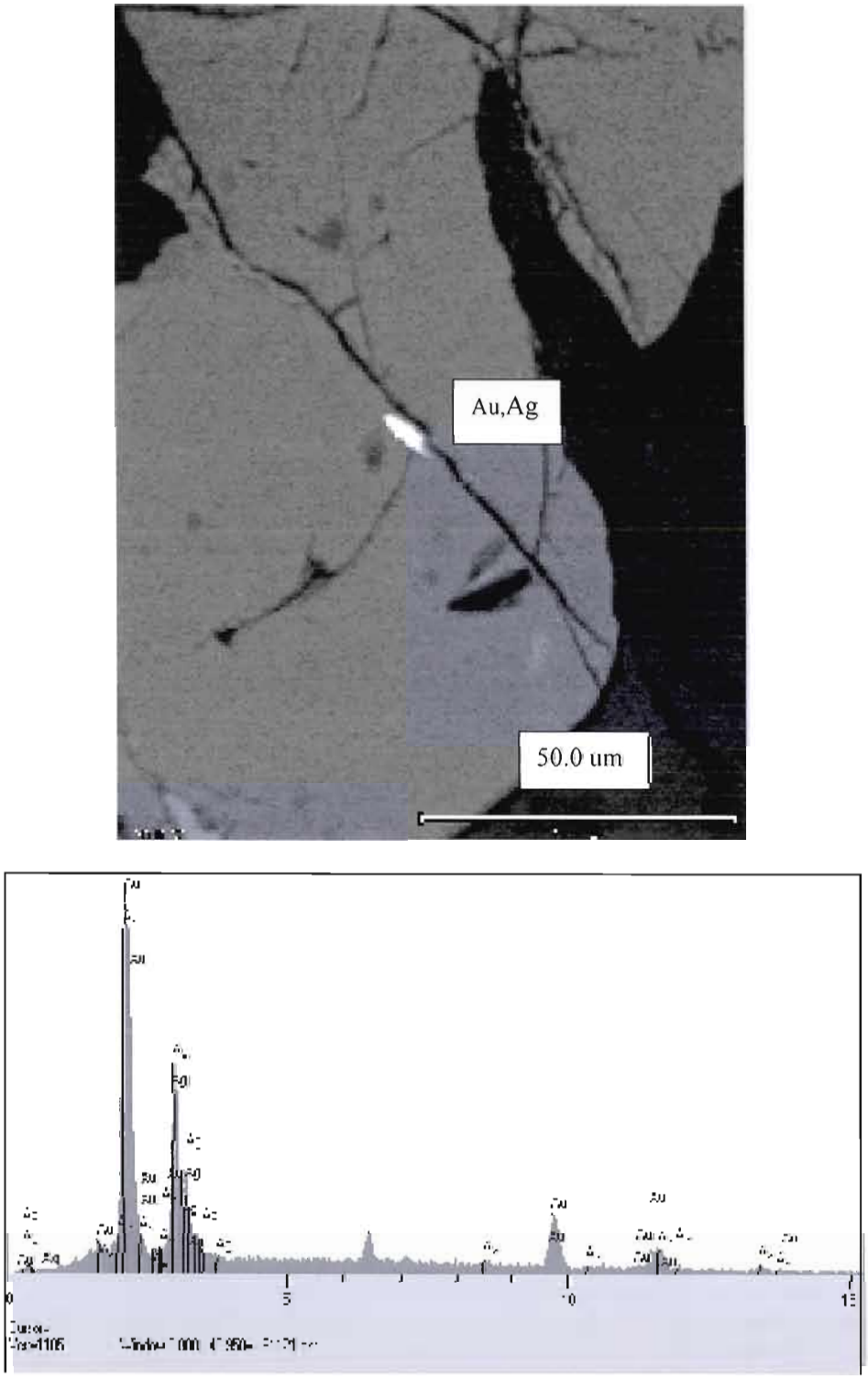

Fig. B.6: Thin Section 14x.1 and spectrum; gold in pyrite fracture

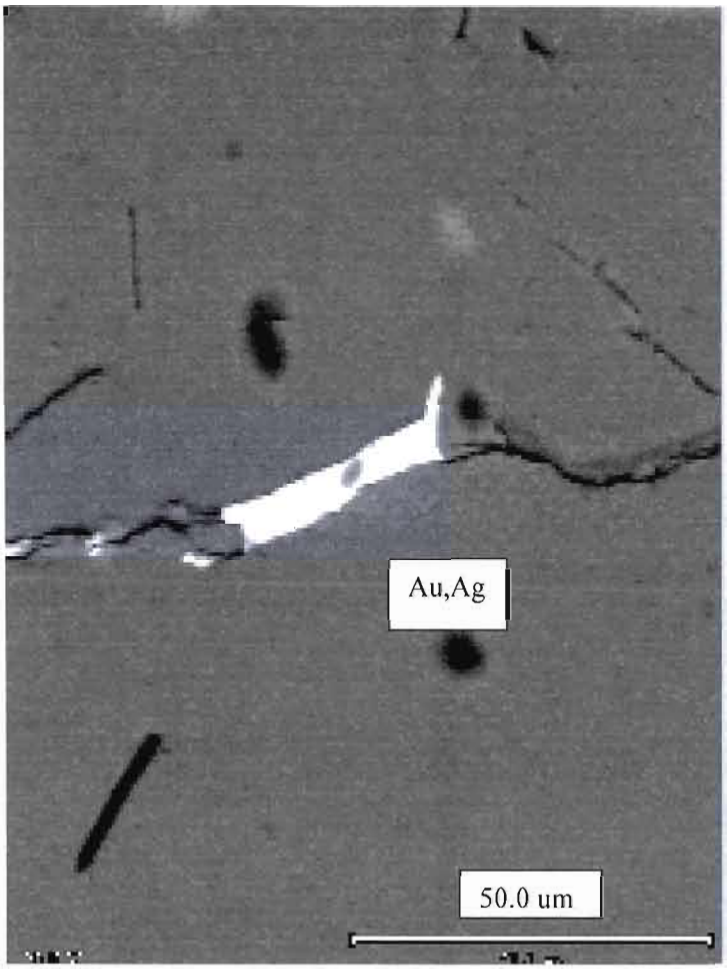

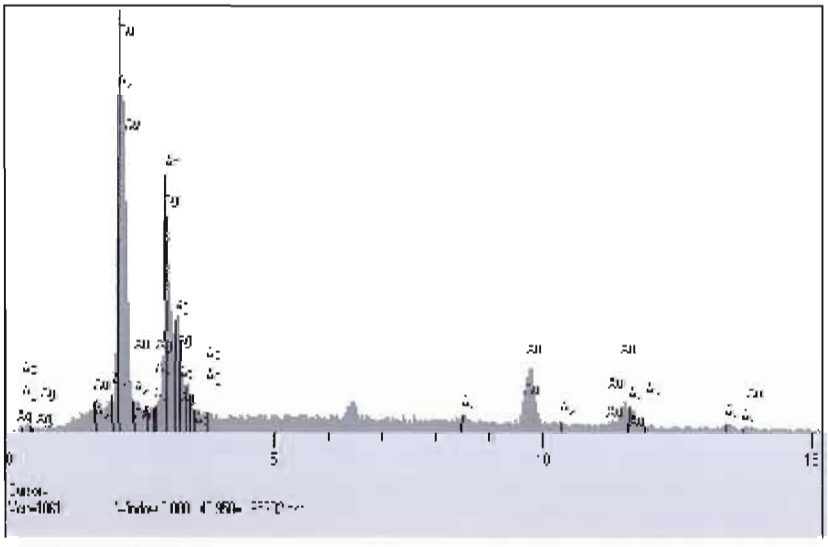

Fig.B.7: Thin Section 14.x.2 and spectrum; gold in pyrite fracture

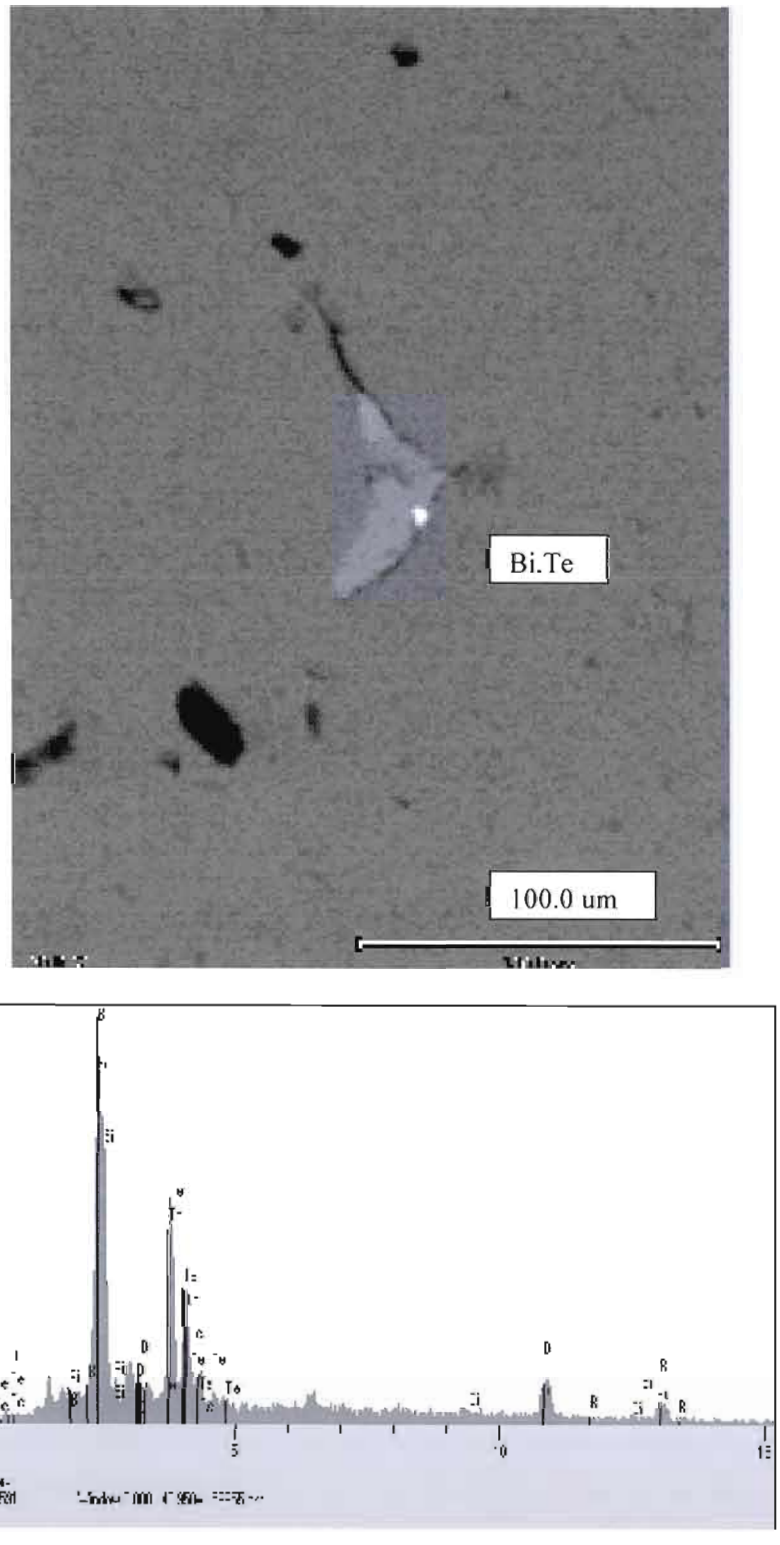

Fig.B.8: Thin Section 31b.1 and spectrum; BiTe locked in pyrite

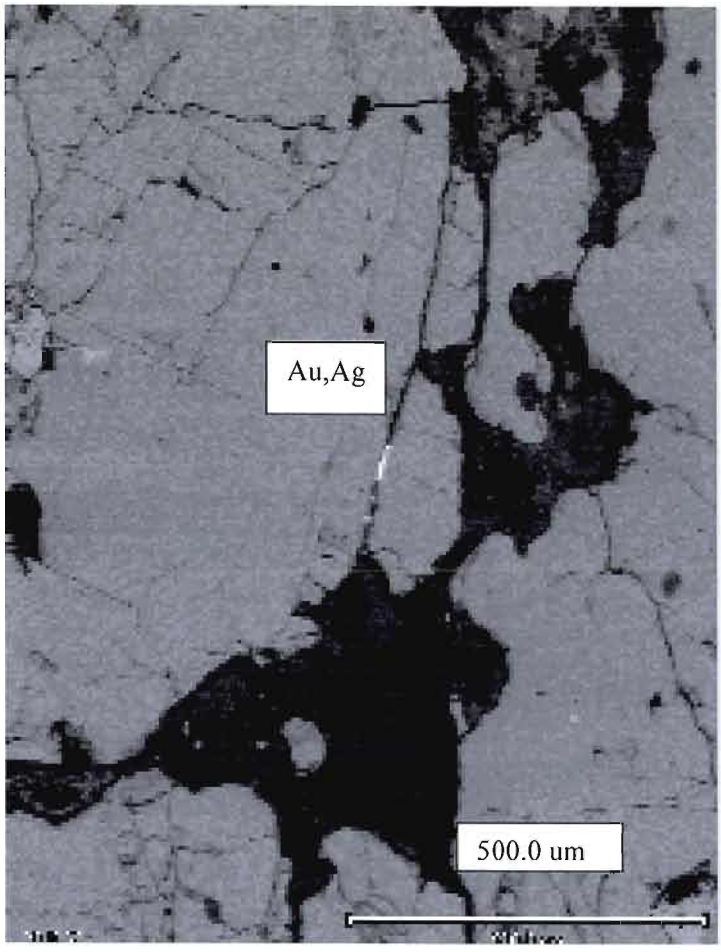

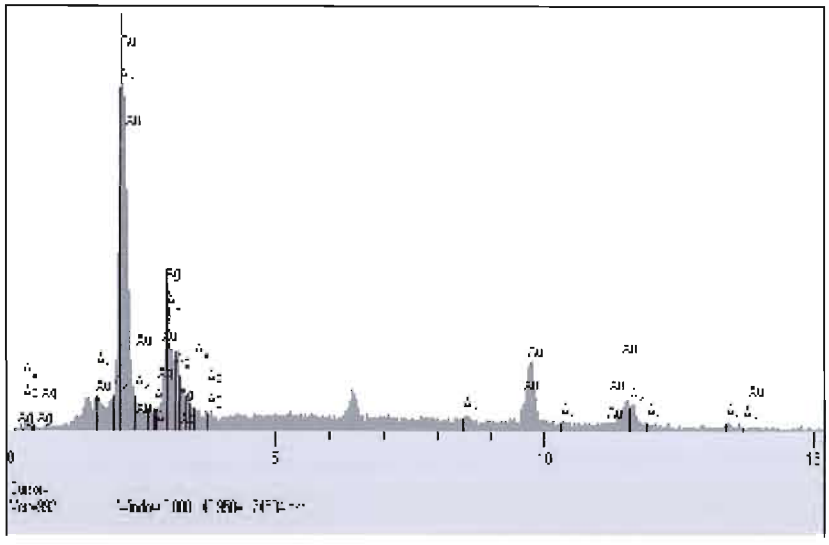

Fig.B.9: Thin Section 31b.2 and spectrum; gold in pyrite fracture

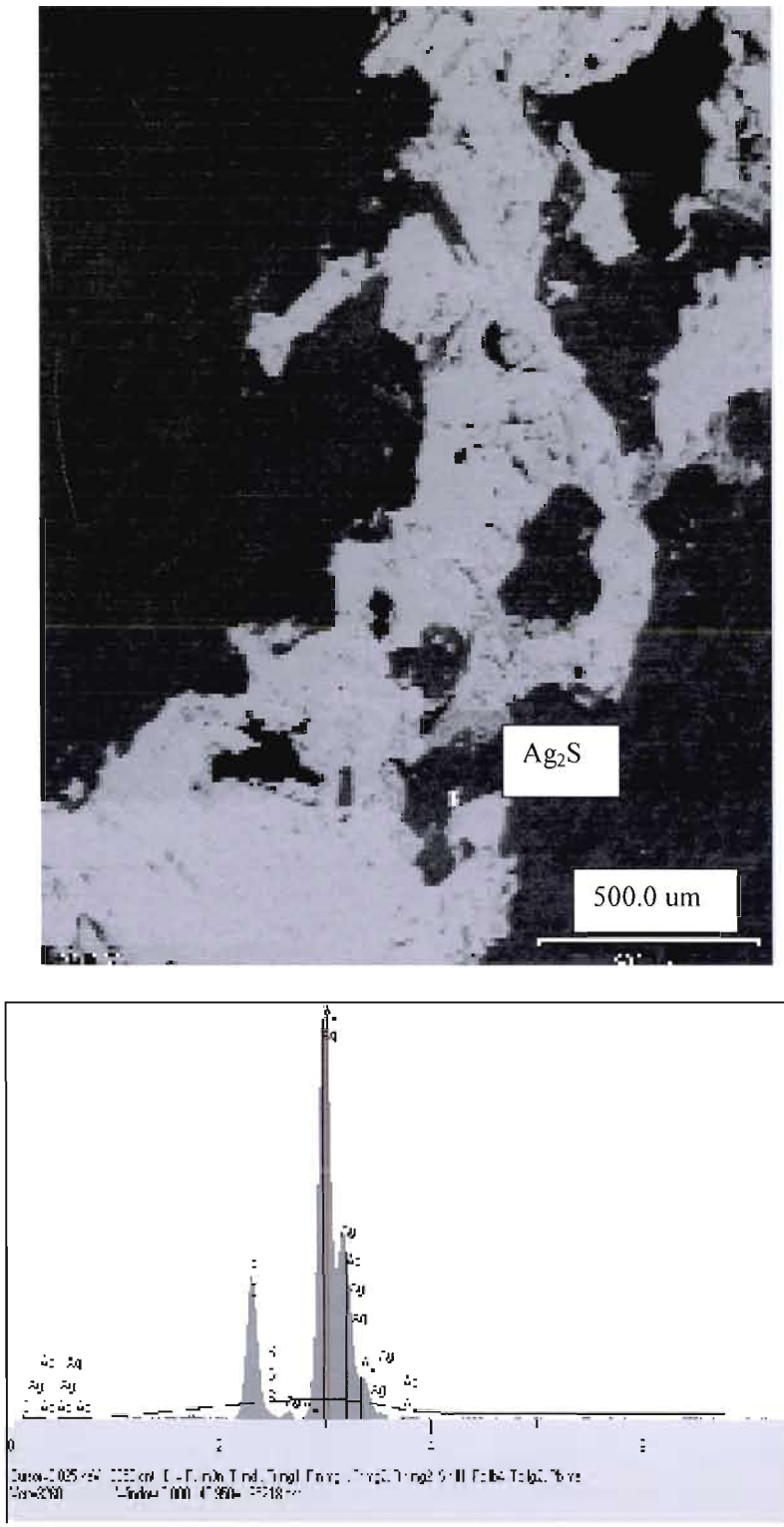

Fig. B.10: Thin Section 39.1 and spectrum; Argentite

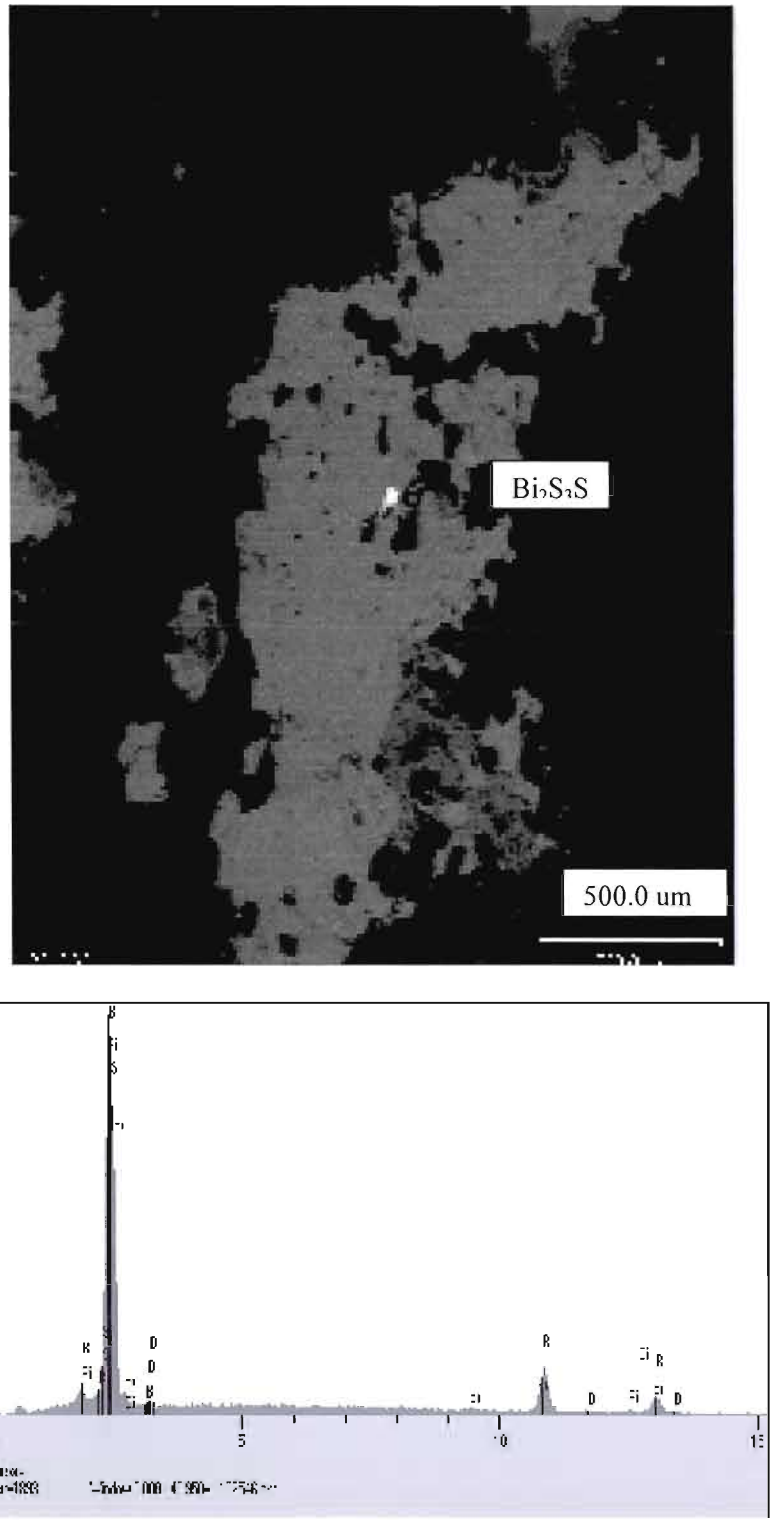

Fig. B.11: Thin Section 39.2 and spectrum; Bismuthinite locked in pyrite

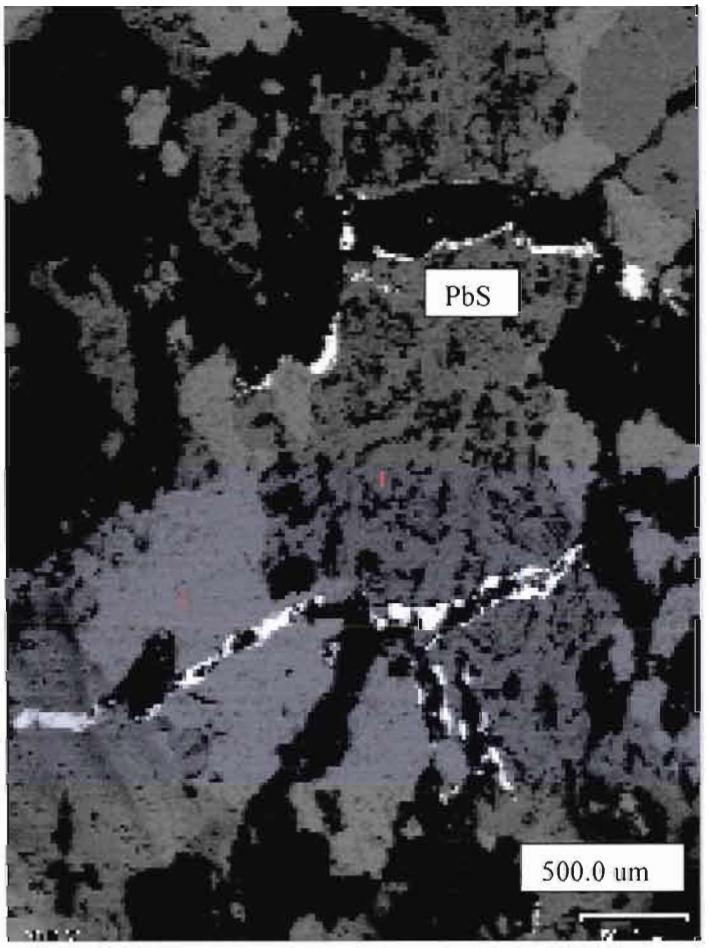

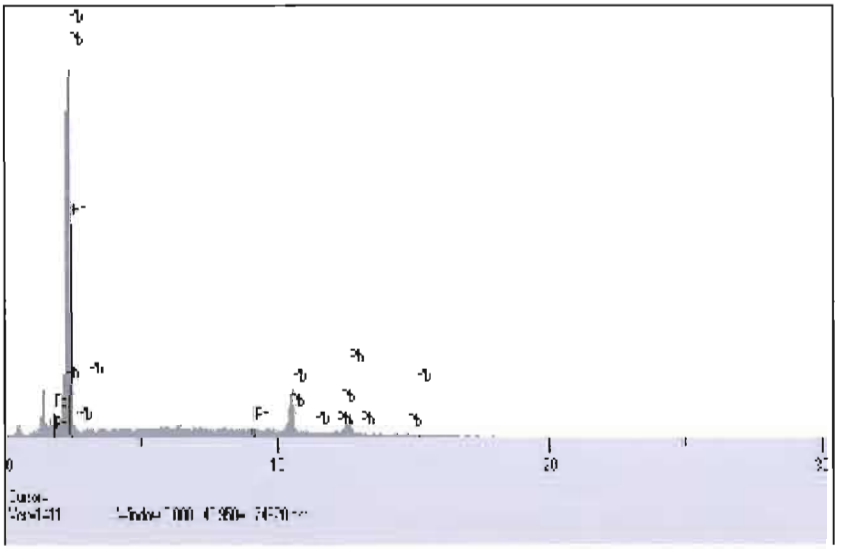

Fig. B.12: Thin Section 39.3 and spectrum; galena and pyrite

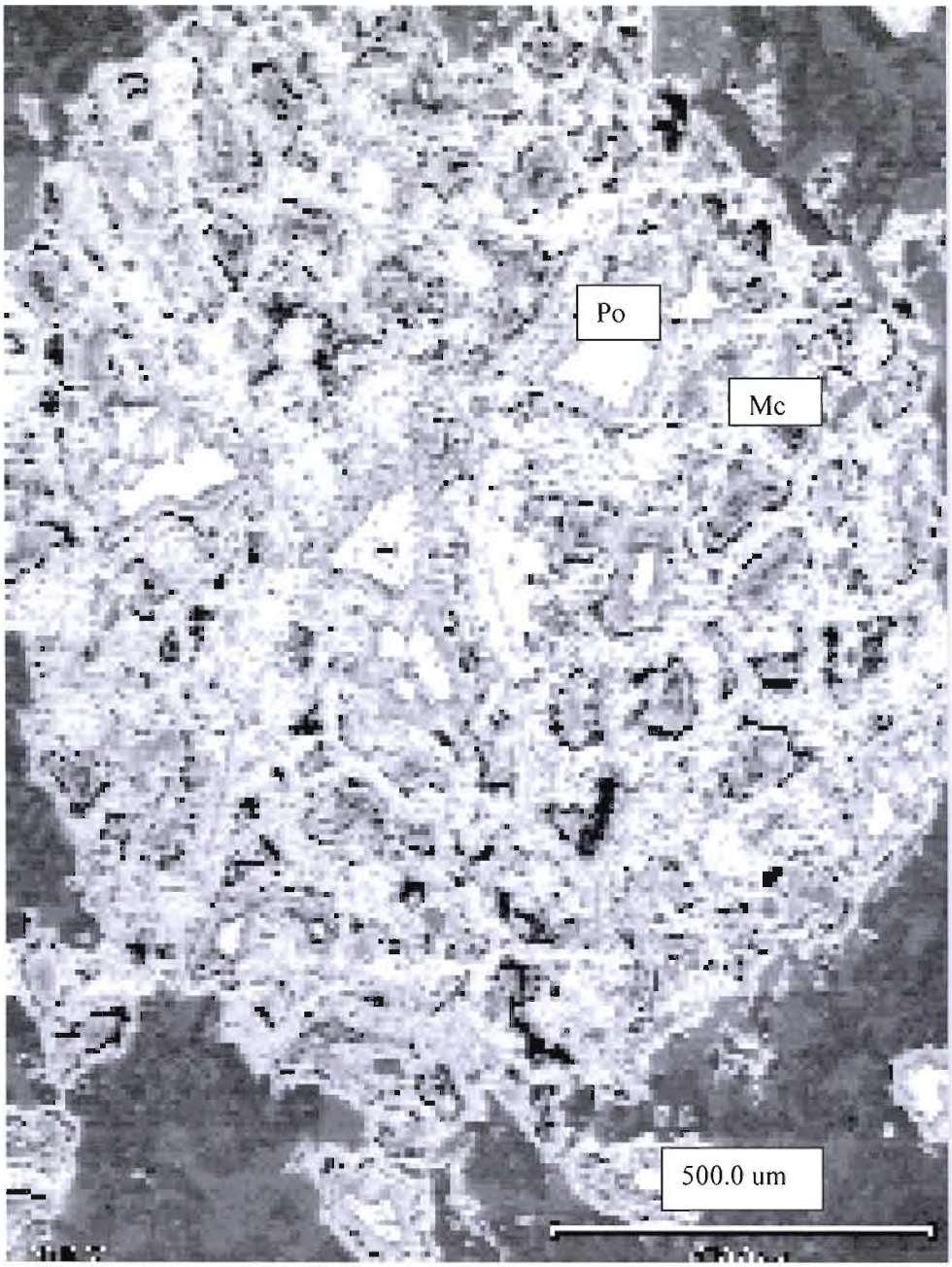

Fig. B.13: Thin Section 2b; pyrrhotite and marcasite (superficial alteration)

B.4 Discussion and Conclusion

Observation of samples of the pyrite+/-chalcopyrite veins under an electron microscope confirmed that the gold bearing grains are found within the pyrite+/-chalcopyrite veins.

Further observation concluded that the gold bearing grains are associated with pyrite. The gold is found locked within the pyrite (fig. B.4 and B.6) and within the pyrite fractures (Fig. B.5, B.7 and B.9). No gold was observed within the chalcopyrite grains.

Other heavy elements were identified that escaped observation under the optical microscope. Native lead (Pb) was discovered associated with pyrite (Fig. B.12). Grains of BiTe were also observed in the same environment as the electrum grains (Fig. B.8 and B.11). The BiTe grains are occasionally gold bearing (Tab. B.1 sample 10a). Rare grains of argentite have also been observed locally.

Analysis of the gold bearing grains showed the grains to be Au,Ag (Electrum). The ratio of Au:Ag varies from 9:1 to 1:2 (fig B.2). Au:Ag ratios for primary gold deposits such as shear zone deposits vary from 5:1 to 9:1 (Robert, 1995). In comparison, the electrum grains of the Comtois deposit contain too much silver to be coherent with a shear zone genetic model. Epithermal type deposit (Poulsen, 1995) such as gold rich VMS type deposits better fit the Au:Ag ratio of the Comtois deposit.

APPENDIX C

Au (ppb) and Ag (ppm) Results from ICPAS Analysis of Core Samples Performed by Chimitec, Bondar Clegg Ltd. for Maude Lake Exploration

C.1 Preparation of Samples by Chimitec, Bondar Clegg LTD.

- The full sample is ground to a –10 sized mesh
- 250 grams of the –10 mesh powder is extracted
- The 250 grams is then pulverised to a 95% -150 sized mesh
- Resulting powder is then analysed by ICPAS for all wanted elements except for Au
- For Au 30 grams of the –150 powder is analysed by pyro-analysis-AA
- Limit of detection for Au is 5 pp

Sample ID	Au30	Au g/t	Ag
77001	282	0,28	0,2
77003	674	0,67	0,4
77004	174	0,17	0,3
77005	354	0,35	0,3
77006	255	0,26	0,2
77007	225	0,23	0,4
77008	52	0,05	0,5
77009	170	0,17	1,2
77010	81	0,08	0,4
77011	139	0,14	0,4
77013	520	0,52	0,2
77015	133	0,13	0,2
77016	52	0,05	0,3
77017	84	0,08	0,3
77019	77	0,08	0,2
77021	79	0,08	0,2
77022	151	0,15	0,2
77023	67	0,07	0,4
77024	223	0,22	1,4
77025	39	0,04	0,4
77026	192	0,19	0,4
77028	31	0,03	0,4
77029	35	0,04	0,3
77030	22	0,02	0,5
77031	189	0,19	0,5
77032	103	0,10	0,2
77034	92	0,09	0,3
77040	110	0,11	0,2
77041	87	0,09	0,2
77043	240	0,24	0,4
77044	601	0,60	0,6
77045	137	0,14	0,5
77046	127	0,13	0,4
77048	153	0,15	0,3
77049	91	0,09	0,5
77051	187	0,19	0,3
77052	742	0,74	0,6
77053	248	0,25	0,5
77056	315	0,32	0,4
77062	611	0,61	0,4
77070	28	0,03	0,2
77071	746	0,75	1,3
77075	410	0,41	0,4
77076	296	0,30	0,3
77077	180	0,18	0,5
77079	9	0,01	0,2
77083	117	0,12	0,7

Sample ID	Au30	Au g/t	Ag
77084	24	0,02	0,4
77101	145	0,15	0,5
77102	766	0,77	0,7
77103	625	0,63	1,2
77104	379	0,38	0,3
77121	1187	1,19	0,7
77128	774	0,77	2,5
77132	76	0,08	0,2
77135	65	0,07	0,4
77136	134	0,13	0,4
77137	82	0,08	0,4
77139	260	0,26	0,5
77142	112	0,11	0,5
77146	96	0,10	0,6
77147	1112	1,11	1,5
77148	91	0,09	0,4
77152	32	0,03	0,4
77153	47	0,05	0,4
77154	62	0,06	0,4
77155	84	0,08	0,4
77156	76	0,08	0,2
77158	109	0,11	0,6
77160	167	0,17	0,3
77161	46	0,05	0,3
77162	63	0,06	0,5
77163	45	0,05	0,3
77165	235	0,24	0,4
77167	34	0,03	0,2
77168	61	0,06	0,6
77169	33	0,03	0,3
77170	47	0,05	0,2
77171	25	0,03	0,2
77172	584	0,58	0,3
77173	1514	1,51	0,6
77174	57	0,06	0,6
77175	206	0,21	0,4
77177	154	0,15	0,2
77178	226	0,23	0,5
77179	496	0,50	0,4
77181	124	0,12	0,5
77182	412	0,41	0,2
77183	311	0,31	0,2
77184	1116	1,12	0,2
77185	294	0,29	0,4
77187	115	0,12	0,2
77188	46	0,05	0,2
77189	80	0,08	0,5

Tab. C.1 : Au (ppb) and Ag (ppm) results obtained by Chimitec,Bondar Clegg

Sample ID	Au30	Au g/t	Ag
77193	1380	1,38	0,5
77194	294	0,29	0,3
77196	1404	1,40	0,2
77200	139	0,14	0,3
77203	948	0,95	1,1
77206	418	0,42	0,3
77207	173	0,17	0,2
77211	220	0,22	0,2
77212	124	0,12	0,6
77213	82	0,08	0,3
77217	210	0,21	0,4
77218	458	0,46	0,3
77219	150	0,15	0,6
77220	34	0,03	0,2
77223	78	0,08	0,2
77224	59	0,06	0,4
77226	94	0,09	0,6
77227	41	0,04	0,5
77229	151	0,15	0,3
77230	46	0,05	0,3
77232	62	0,06	0,3
77234	65	0,07	0,4
77239	94	0,09	0,6
77241	93	0,09	0,3
77242	42	0,04	0,4
77243	35	0,04	0,2
77244	20	0,02	0,3
77245	18	0,02	0,3
77248	176	0,18	0,4
77249	126	0,13	0,3
77250	84	0,08	0,2
77251	217	0,22	0,9
77252	304	0,30	0,5
77253	227	0,23	0,3
77254	577	0,58	0,5
77255	183	0,18	0,3
77256	211	0,21	0,3
77257	98	0,10	0,3
77258	79	0,08	0,5
77262	182	0,18	0,4
77271	41	0,04	0,3
77273	122	0,12	0,4
77277	34	0,03	0,2
77284	157	0,16	0,2
77286	96	0,10	0,2
77291	154	0,15	0,4
77296	20	0,02	0,2

Sample ID	Au30	Au g/t	Ag
77297	60	0,06	0,2
77298	42	0,04	0,3
77299	166	0,17	0,2
77305	113	0,11	0,4
77314	65	0,07	0,5
77320	85	0,09	0,2
77321	253	0,25	0,6
77322	323	0,32	0,5
77323	104	0,10	0,4
77327	71	0,07	0,3
77329	207	0,21	0,5
77337	22	0,02	0,3
77340	24	0,02	0,4
77345	10	0,01	0,2
77347	303	0,30	0,9
77349	92	0,09	0,7
77350	84	0,08	0,8
77351	125	0,13	0,7
77352	108	0,11	0,8
77353	19	0,02	0,3
77354	73	0,07	1,2
77355	154	0,15	0,3
77358	125	0,13	0,4
77359	477	0,48	0,5
77360	249	0,25	0,6
77363	335	0,34	0,5
77367	138	0,14	0,2
77368	245	0,25	0,2
77369	88	0,09	0,3
77372	145	0,15	0,2
77373	31	0,03	0,2
77376	48	0,05	0,4
77377	40	0,04	0,2
77380	57	0,06	0,2
77416	120	0,12	0,3
77420	142	0,14	0,2
77425	167	0,17	0,4
77426	399	0,40	0,4
77427	149	0,15	0,6
77431	298	0,30	1,2
77432	740	0,74	2,4
77433	461	0,46	1,7
77434	598	0,60	1,5
77435	213	0,21	0,2
77442	179	0,18	0,7
77443	57	0,06	0,5
77447	360	0,36	0,9

Sample ID	Au30	Au g/t	Ag
77448	815	0,82	0,9
77449	275	0,28	0,5
77450	725	0,73	0,3
77451	202	0,20	0,3
77464	100	0,10	0,2
77475	948	0,95	0,4
77476	1935	1,94	0,3
77479	1285	1,29	0,3
77487	1146	1,15	0,2
77494	553	0,55	0,6
77513	142	0,14	0,4
77517	73	0,07	0,3
77519	37	0,04	0,7
77520	72	0,07	2,1
77521	19	0,02	0,4
77524	154	0,15	0,4
77526	44	0,04	0,8
77533	306	0,31	0,4
77536	124	0,12	0,4
77537	197	0,20	0,3
77538	97	0,10	0,2
77544	164	0,16	0,7
77545	78	0,08	0,5
77546	99	0,10	0,4
77553	98	0,10	0,4
77555	355	0,36	1,1
77567	191	0,19	0,2
77574	278	0,28	0,2
77596	1574	1,57	0,2
77602	149	0,15	0,2
77603	112	0,11	0,3
77611	93	0,09	0,9
77612	281	0,28	0,8
77613	186	0,19	1,9
77614	117	0,12	0,8
77615	214	0,21	0,5
77616	155	0,16	0,4
77618	472	0,47	0,6
77620	832	0,83	1,1
77631	360	0,36	1,2
77632	288	0,29	0,8
77635	160	0,16	0,4
77637	204	0,20	0,3
77638	83	0,08	0,3
77640	140	0,14	0,3
77642	174	0,17	1
77643	262	0,26	1,4

Sample ID	Au30	Au g/t	Ag
77644	115	0,12	1,2
77645	1128	1,13	2,1
77647	784	0,78	1,7
77648	1638	1,64	1,4
77649	853	0,85	2,7
77650	582	0,58	3,1
77651	1038	1,04	1
77652	161	0,16	0,9
77660	208	0,21	0,4
77670	311	0,31	0,4
77671	175	0,18	0,2
77675	81	0,08	0,7
77676	391	0,39	1,2
77677	171	0,17	0,7
77678	63	0,06	0,4
77679	46	0,05	0,5
77680	72	0,07	0,5
77681	42	0,04	0,3
77682	21	0,02	0,2
77686	695	0,70	0,3
77693	53	0,05	0,2
77697	73	0,07	0,3
77701	1158	1,16	0,4
77704	137	0,14	0,5
77706	397	0,40	0,4
77707	663	0,66	1,2
77709	634	0,63	1,9
77710	473	0,47	0,8
77711	240	0,24	0,5
77712	606	0,61	2,3
77715	476	0,48	1,1
77716	185	0,19	1,3
77717	204	0,20	0,5
77718	38	0,04	0,3
77721	145	0,15	0,6
77722	83	0,08	0,8
77723	46	0,05	0,4
77727	114	0,11	0,7
77729	186	0,19	0,6
77730	1041	1,04	0,8
77731	669	0,67	0,8
77732	545	0,55	2,9
77733	683	0,68	1,3
77736	331	0,33	1
77737	364	0,36	0,9
77738	95	0,10	0,5
77740	94	0,09	0,5

Sample ID	Au30	Au g/t	Ag
77741	340	0,34	0,8
77742	24	0,02	0,3
77743	1365	1,37	0,9
77744	46	0,05	0,4
77745	38	0,04	0,7
77746	232	0,23	0,5
77747	502	0,50	0,9
77748	45	0,05	0,3
77749	55	0,06	0,2
77752	86	0,09	0,4
77753	47	0,05	0,2
77754	707	0,71	0,5
77755	323	0,32	0,7
77756	342	0,34	0,7
77757	300	0,30	0,9
77758	281	0,28	0,5
77759	654	0,65	1
77760	92	0,09	0,3
77762	146	0,15	0,3
77763	324	0,32	0,4
77764	817	0,82	0,9
77765	184	0,18	0,4
77766	1741	1,74	0,8
77767	1682	1,68	1,1
77769	99	0,10	0,2
77770	306	0,31	0,3
77771	1243	1,24	2,1
77772	1083	1,08	1,8
77773	351	0,35	0,6
77775	28	0,03	0,3
77779	52	0,05	0,7
77780	33	0,03	0,3
77783	79	0,08	1,2
77784	58	0,06	0,7
77785	68	0,07	0,4
77786	49	0,05	0,4
77787	124	0,12	0,2
77788	149	0,15	0,3
77790	169	0,17	0,3
77791	46	0,05	0,2
77793	67	0,07	0,3
77795	114	0,11	0,2
77796	170	0,17	0,3
77802	327	0,33	0,5
77805	170	0,17	0,4
77806	342	0,34	0,4
77808	216	0,22	0,5

Sample ID	Au30	Au g/t	Ag
77809	720	0,72	0,9
77810	84	0,08	0,5
77812	151	0,15	0,7
77813	201	0,20	1
77814	266	0,27	0,7
77815	58	0,06	0,5
77816	59	0,06	0,4
77817	175	0,18	0,5
77818	155	0,16	0,7
77819	93	0,09	0,8
77820	336	0,34	1,4
77821	154	0,15	0,6
77822	182	0,18	0,3
77823	458	0,46	1
77825	576	0,58	3
77826	407	0,41	1,6
77829	576	0,58	0,3
77832	981	0,98	1,2
77833	1001	1,00	1,4
77834	1228	1,23	0,5
77838	151	0,15	0,3
77839	324	0,32	0,3
77840	1097	1,10	0,6
77846	12	0,01	0,4
77849	208	0,21	0,3
77852	208	0,21	0,5
77855	76	0,08	0,6
77856	128	0,13	0,6
77857	1257	1,26	3,3
77858	1644	1,64	2,4
77859	1317	1,32	2,6
77860	1244	1,24	1,6
77862	1089	1,09	2
77864	944	0,94	2,9
77865	666	0,67	2,8
77867	266	0,27	0,2
77869	386	0,39	0,5
77871	74	0,07	0,3
77882	155	0,16	0,2
77886	584	0,58	1
77888	29	0,03	0,2
77889	1805	1,81	3,4
77890	105	0,11	0,4
77893	492	0,49	2,5
77894	840	0,84	2,3
77895	1331	1,33	2
77898	86	0,09	0,8

Sample ID	Au30	Au g/t	Ag
77902	506	0,51	1,6
77904	93	0,09	0,3
77907	53	0,05	0,3
77911	69	0,07	0,4
77913	88	0,09	0,3
77914	73	0,07	0,2
77917	269	0,27	0,9
77925	279	0,28	0,4
77927	150	0,15	0,7
77930	1602	1,60	2,1
77932	265	0,27	0,6
77935	140	0,14	0,3
77941	68	0,07	0,3
77945	144	0,14	0,9
77946	125	0,13	0,6
77948	349	0,35	0,3
77953	368	0,37	0,6
77954	421	0,42	0,2
77956	518	0,52	0,2
77962	116	0,12	0,3
77963	127	0,13	0,5
77972	1432	1,43	1,2
77973	178	0,18	0,4
77974	231	0,23	0,3
77975	186	0,19	0,5
77976	182	0,18	0,4
77977	177	0,18	0,2
77981	164	0,16	0,4
77982	48	0,05	0,3
77984	240	0,24	0,9
77985	205	0,21	0,9
77994	413	0,41	0,3
77998	710	0,71	0,6
77999	216	0,22	0,4
80001	68	0,07	0,5
80002	259	0,26	0,5
80003	58	0,06	0,3
80004	61	0,06	0,3
80005	209	0,21	0,4
80006	98	0,10	0,3
80009	41	0,04	0,2
80010	178	0,18	0,4
80013	424	0,42	1,5
80014	165	0,17	0,8
80015	175	0,18	0,5
80017	168	0,17	1
80019	89	0,09	0,2

Sample ID	Au30	Au g/t	Ag
80021	77	0,08	0,3
80022	229	0,23	0,4
80024	50	0,05	0,2
80025	48	0,05	0,2
80026	134	0,13	0,3
80027	117	0,12	0,3
80028	235	0,24	0,7
80029	545	0,55	1,8
80031	145	0,15	0,4
80033	393	0,39	0,8
80035	241	0,24	0,3
80036	84	0,08	0,2
80041	56	0,06	1,3
80042	6	0,01	0,2
80045	37	0,04	0,2
80046	58	0,06	0,2
80053	49	0,05	0,6
80055	82	0,08	0,3
80056	174	0,17	0,9
80057	56	0,06	1,2
80065	102	0,10	0,9
80066	539	0,54	2
80067	146	0,15	0,8
80068	428	0,43	1,5
80069	110	0,11	1,7
80070	274	0,27	1,2
80073	534	0,53	1,1
80074	488	0,49	1,4
80075	561	0,56	0,8
80076	413	0,41	0,8
80080	113	0,11	0,5
80089	200	0,20	0,4
80090	144	0,14	0,7
80092	182	0,18	0,3
80093	335	0,34	2,2
80094	30	0,03	1
80096	357	0,36	1,5
80099	323	0,32	0,4
80109	375	0,38	1
80111	1029	1,03	1,4
80113	73	0,07	0,2
80114	153	0,15	0,4
80119	54	0,05	0,3
80120	236	0,24	0,5
80123	712	0,71	1
80124	230	0,23	0,4
80165	70	0,07	0,2

Sample ID	Au30	Au g/t	Ag
80167	36	0,04	0,2
80169	265	0,27	0,3
80180	365	0,37	0,4
80182	80	0,08	0,4
80183	37	0,04	0,3
80195	269	0,27	0,3
80199	782	0,78	0,3
80200	850	0,85	0,4
80203	102	0,10	0,3
80206	353	0,35	0,3
80209	281	0,28	0,2
80221	373	0,37	0,4
80222	270	0,27	0,6
80224	1017	1,02	0,4
80239	45	0,05	0,2
80246	220	0,22	0,3
80250	157	0,16	0,3
80255	227	0,23	0,2
80256	152	0,15	0,2
80261	78	0,08	0,3
80278	238	0,24	0,2
80284	1546	1,55	0,2
80290	159	0,16	0,3
80297	135	0,14	1,4
80298	458	0,46	0,4
80299	435	0,44	0,3
80307	219	0,22	0,4
80315	102	0,10	0,2
80319	160	0,16	0,3
80321	288	0,29	0,4
80322	768	0,77	0,8
80325	704	0,70	0,2
80331	386	0,39	0,5
80332	78	0,08	0,3
80333	260	0,26	0,4
80338	359	0,36	0,4
80339	301	0,30	0,5
80342	997	1,00	1
80343	46	0,05	0,2
80346	1253	1,25	0,6
80357	156	0,16	0,3
80362	103	0,10	0,5
80366	80	0,08	0,4
80367	177	0,18	0,4
80369	89	0,09	1
80370	131	0,13	0,5
80371	159	0,16	0,8

Sample ID	Au30	Au g/t	Ag
80372	55	0,06	0,3
80373	39	0,04	0,3
80376	7	0,01	0,2
80377	14	0,01	0,2
80378	8	0,01	0,2
80379	13	0,01	0,4
80380	24	0,02	0,3
80385	8	0,01	0,2
80388	12	0,01	0,5
80391	6	0,01	0,3
80392	12	0,01	0,3
80393	22	0,02	0,2
80395	10	0,01	0,2
80396	8	0,01	0,3
80397	12	0,01	0,3
80399	26	0,03	0,3
80400	34	0,03	0,3
80401	10	0,01	0,4
80404	16	0,02	0,3
80405	9	0,01	0,2
80407	9	0,01	0,3
80408	13	0,01	0,4
80409	12	0,01	0,3
80412	28	0,03	0,4
80414	25	0,03	0,3
80415	43	0,04	0,3
80416	39	0,04	0,3
80419	22	0,02	0,2
80421	19	0,02	0,3
80423	17	0,02	0,3
80425	26	0,03	0,8
80426	13	0,01	0,2
80435	29	0,03	0,2
80436	51	0,05	0,3
80437	138	0,14	0,8
80440	832	0,83	1,5
80458	28	0,03	0,2
80464	596	0,60	1,7
80466	149	0,15	0,5
80470	109	0,11	0,3
80476	136	0,14	0,4
80486	43	0,04	0,2
80508	60	0,06	0,5
80512	290	0,29	1,5
80513	163	0,16	1,4
80526	135	0,14	0,4
80530	76	0,08	0,2

Sample ID	Au30	Au g/t	Ag
80542	31	0,03	0,2
80556	275	0,28	2,1
80558	52	0,05	0,4
80559	38	0,04	0,3
80560	102	0,10	0,5
80561	38	0,04	0,2
80562	52	0,05	0,3
80565	74	0,07	0,5
80566	45	0,05	0,5
80567	73	0,07	0,7
80568	93	0,09	0,9
80569	101	0,10	1,4
80570	130	0,13	0,7
80582	157	0,16	0,4
80584	84	0,08	0,4
80585	280	0,28	2,1
80588	169	0,17	0,5
80590	225	0,23	0,2
80593	77	0,08	0,4
80594	1001	1,00	2,4
80595	735	0,74	3,2
80596	1177	1,18	3,4
80597	125	0,13	0,6
80609	109	0,11	0,3
80611	276	0,28	0,4
80612	107	0,11	0,2
80616	35	0,04	0,4
80617	35	0,04	0,2
80673	87	0,09	0,7
80674	418	0,42	1,4
80682	1881	1,88	3,1
80683	776	0,78	0,9
80684	555	0,56	0,7
80685	1065	1,07	0,9
80686	1298	1,30	2,1
80687	89	0,09	0,2
80688	312	0,31	0,7
80689	234	0,23	0,3
80692	144	0,14	0,6
80694	87	0,09	0,3
80695	78	0,08	0,3
80697	114	0,11	0,3
80698	507	0,51	0,4
80699	245	0,25	0,3
80706	593	0,59	0,3
80707	1575	1,58	0,3
80709	233	0,23	0,3

Sample ID	Au30	Au g/t	Ag
80710	160	0,16	0,4
80712	83	0,08	0,3
80714	92	0,09	0,3
80715	176	0,18	0,2
80716	148	0,15	0,3
80717	41	0,04	0,3
80718	1839	1,84	0,4
80720	177	0,18	0,5
80721	933	0,93	0,5
80722	337	0,34	0,6
80724	474	0,47	0,5
80725	174	0,17	0,7
80726	118	0,12	0,4
80727	709	0,71	0,4
80728	44	0,04	0,2
80731	318	0,32	0,4
80732	281	0,28	0,6
80733	453	0,45	0,8
80737	24	0,02	0,2
80738	7	0,01	0,3
80740	41	0,04	0,2
80741	33	0,03	0,4
80742	26	0,03	0,4
80743	20	0,02	0,4
80744	62	0,06	1,2
80745	36	0,04	0,7
80747	27	0,03	0,3
80748	59	0,06	0,9
80750	62	0,06	1,1
80751	90	0,09	1,5
80752	7	0,01	0,3
80754	11	0,01	0,3
80756	19	0,02	0,4
80767	18	0,02	0,2
80768	9	0,01	0,2
80770	18	0,02	0,3
80771	28	0,03	0,3
80777	5	0,01	0,2
80779	109	0,11	0,6
80783	128	0,13	0,5
80785	7	0,01	0,3
80787	22	0,02	0,2
80788	74	0,07	0,2
80789	74	0,07	0,2
80790	50	0,05	0,2
80793	1248	1,25	1,1
80794	333	0,33	1

Sample ID	Au30	Au g/t	Ag
80796	1849	1,85	0,4
80797	1433	1,43	0,4
80799	254	0,25	0,3
80800	110	0,11	0,2
80805	562	0,56	0,5
80806	1008	1,01	0,9
80807	162	0,16	0,7
80808	458	0,46	1,5
80809	65	0,07	0,6
80811	277	0,28	0,6
80812	94	0,09	0,5
80813	353	0,35	0,7
80816	115	0,12	0,6
80817	197	0,20	0,5
80818	51	0,05	0,2
80820	108	0,11	0,4
80822	26	0,03	0,3
80826	40	0,04	0,3
80827	45	0,05	0,3
80828	34	0,03	1,3
80829	206	0,21	2,5
80830	99	0,10	0,5
80831	41	0,04	0,3
80832	55	0,06	0,5
80833	72	0,07	0,4
80834	131	0,13	0,3
80836	53	0,05	0,7
80839	34	0,03	0,2
80840	43	0,04	0,3
80842	478	0,48	0,4
80843	89	0,09	0,8
80844	64	0,06	0,2
80847	160	0,16	0,3
80848	311	0,31	0,4
80849	132	0,13	1
80850	43	0,04	0,3

Sample ID	Au30	Au g/t	Ag
80853	39	0,04	0,4
80857	41	0,04	0,2
80860	414	0,41	0,5
80863	95	0,10	0,5
80864	254	0,25	0,6
80865	387	0,39	1,1
80867	247	0,25	0,7
80872	58	0,06	0,2
80873	283	0,28	0,9
80876	34	0,03	0,2
80900	36	0,04	0,4
80901	1298	1,22	0,4
80902	186	0,19	0,4
80903	163	0,16	0,2
80905	496	0,50	1,1
80906	518	0,52	0,6
80909	527	0,51	0,3
80917	188	0,19	0,9
80918	92	0,09	0,3
80919	480	0,48	1,4
80920	556	0,56	2
80924	124	0,12	0,5
80925	161	0,16	0,4
80927	119	0,12	0,7
80929	257	0,26	1
80930	124	0,12	0,6
80934	46	0,05	0,3
80956	132	0,13	0,3
80958	74	0,07	0,3
80961	112	0,11	0,2
80963	224	0,22	1,1
80965	138	0,14	0,5
80966	233	0,23	0,8
80967	76	0,08	0,4
80969	88	0,09	0,5
929514	284	0,28	0,8

APPENDIX D

Na_2O, K_2O AND SiO_2 RESULTS FROM ICPAS ANALYSIS OF CORE SAMPLES PERFORMED BY CHIMITEC, BONDAR CLEGG LTD. FOR MAUDE LAKE EXPLORATION

D.1 Preparation of Samples by Chimitec, Bondar Clegg LTD.

- The full sample is ground to a –10 sized mesh
- 250 grams of the –10 mesh powder is extracted
- The 250 grams is then pulverised to a 95% -150 sized mesh
- Resulting powder is then analysed by ICPAS for all wanted elements except for Au

FIELD OBSERVATIONS	ROCK CLASSIFICATION	Na2O	K2O	Na2O+K2O	SiO2
FEL bx,BoMu,1-3%Py	Felsic	3,44	1,93	5,37	66,84
FEL bx,SrBoSi,2-3%Py(Sp)	Felsic	1,13	2,5	3,63	68,05
FEL frag,(fol)	Felsic	6,28	1,44	7,72	67,32
FEL tuf	Felsic	6,83	0,36	7,19	64,42
FEL tuf fol,SrBo,2-3%Py	Felsic	1,29	4,17	5,46	64,67
FEL tuf fol+,Sr+,2-3%PySp	Felsic	0,49	3,92	4,41	69,84
FEL tuf lap bloc, Bo+	Felsic	4,41	1,73	6,14	65,74
FEL tuf lap,fol	Felsic	5,67	1,04	6,71	66,58
FEL tuf mas	Felsic	3,56	2,17	5,73	62,45
FEL tuf Qz	Felsic	4,81	1,24	6,05	63,87
FEL tuf Qz,fol	Felsic	4,94	1,22	6,16	66,47
FEL tuf Qz,Sr+±Si,2%Py	Felsic	0,93	4,6	5,53	68,02
FEL tuf,2%Py(Cp)	Felsic	5,59	0,9	6,49	68,52
FEL tuf,fol	Felsic	3,93	0,97	4,90	69,5
FEL tuf,fol	Felsic	4,24	2,3	6,54	64,76
FEL tuf,fol,Bo	Felsic	4,72	1,07	5,79	62,41
FEL tuf,Sr,1-3%Py	Felsic	1,06	3,77	4,83	67,9
FEL tuf,Sr+Sil?,3-5%Py	Felsic	1,37	2,9	4,27	66
FEL VOL? dyke?,(fol)	Felsic	5,53	0,72	6,25	64,28
FEL/INT bx,BoSr(nod AcCcPy),	Felsic	1,25	2,68	3,93	67,66
FEL/INT tuf	Felsic	2,69	1,56	4,25	61,94
FEL/INT tuf	Felsic	3,64	3,35	6,99	63,23
FEL/INT tuf	Felsic	5,16	0,82	5,98	68,19
FEL/INT tuf lap,Cl	Felsic	3,58	1,23	4,81	60,19
GAB	Gabbro	1,76	0,09	1,85	47,37
GAB	Gabbro	1,59	0,07	1,66	46,15
GAB	Gabbro	1,45	0,16	1,61	46,6
GAB mag	Gabbro	1,7	0,07	1,77	48,8
GAB,fol+,ClCc	Gabbro	0,24	0,1	0,34	47,37
INT frag	Intermediate	1,81	1,56	3,37	58,56
INT frag,fol,BoAc	Intermediate	3,12	1,1	4,22	61,49
INT frag,fol,BoAc	Intermediate	3,11	1,23	4,34	62,11
INT frag,fol,BoAc	Intermediate	2,96	1,05	4,01	61,97
INT frag?,fol,BoAc	Intermediate	3,08	1,01	4,09	59,18
INT frag?,fol,BoAc	Intermediate	4,12	1,96	6,08	64,07
INT frag?,fol,BoAc	Intermediate	4,4	0,44	4,84	64,42
INT tuf blo	Intermediate	5,41	0,36	5,77	56,66
INT tuf lap,±Cc	Intermediate	3,92	0,46	4,38	60,39
INT tuf lap,fol	Intermediate	3,6	1,55	5,15	61,48
INT tuf lap,fol	Intermediate	3,76	1,47	5,23	61,42
INT tuf lap,fol	Intermediate	5,96	0,4	6,36	60,56
INT tuf mas?	Intermediate	4,25	0,17	4,42	55,99
INT tuf? Qz	Intermediate	4,81	0,08	4,89	52,16

Tab. D.1:Result obtained by Chimitec, Bondar Clegg and field observation by Maude Lake Exploration

FIELD OBSERVATIONS	ROCK CLASSIFICATION	Na2O	K2O	Na2O+K2O	SiO2
RHY Qz mas,SrBo,1-2%Py	Rhyolite	1,6	3,68	5,28	69,65
RHY Qz mas,tr.PySp?	Rhyolite	4,49	1,69	6,18	70,29
RHY Qz zeb,SrSi,2-4%Py	Rhyolite	0,57	4,59	5,16	70,58
RHY Qz,(Bo),1%Py	Rhyolite	1,92	2,24	4,16	68,66
RHY Qz,(Bo)'tr.Py	Rhyolite	2,23	1,63	3,86	68,7
RHY Qz,(fol),Sr,2-3%Py	Rhyolite	0,19	4,43	4,62	67,43
RHY Qz,(Sr),tr.Py	Rhyolite	0,9	4,01	4,91	71,26
RHY Qz,±fol,Bo(Sr)Si?,1-3%Py	Rhyolite	1,06	3,3	4,36	69,59
RHY Qz,±fol,Sr(BoCl),3-4%PyC	Rhyolite	1,55	4,68	6,23	61,88
RHY Qz,Bo(Sr),2%Py	Rhyolite	0,78	3,27	4,05	70,72
RHY Qz,Bo(Sr)Si,3-5%Py	Rhyolite	0,75	3,83	4,58	70,46
RHY Qz,Bo+Sr,1-2%Py	Rhyolite	0,73	3,25	3,98	70,28
RHY Qz,Bo+Sr,1-2%Py	Rhyolite	1,64	2,31	3,95	69,35
RHY Qz,fol,(SrBo),tr.Py	Rhyolite	0,75	3,65	4,40	68,62
RHY Qz,fol,BoSi?,1-3%Py	Rhyolite	0,8	3,97	4,77	67,95
RHY Qz,fol,Sr(Bo),3-4%Py	Rhyolite	0,86	4,22	5,08	67,09
RHY Qz,fol,Sr+(BoClGr),5%PyS	Rhyolite	1,31	3,57	4,88	68,05
RHY Qz,fol,Sr+,3%Py	Rhyolite	0,28	4,53	4,81	67,7
RHY Qz,fol,Sr+Cl,3-4%Py	Rhyolite	0,51	3,92	4,43	72,13
RHY Qz,fol,SrBo,1-3%Py	Rhyolite	0,99	3,71	4,70	69,95
RHY Qz,fol,SrCl±Si,2-5%Py	Rhyolite	1,38	3,68	5,06	71,05
RHY Qz,fol++,2-3%Py(Cp)	Rhyolite	0,61	4,2	4,81	70,33
RHY Qz,Sr	Rhyolite	0,87	3,97	4,84	70,97
RHY Qz,Sr	Rhyolite	0,8	4,61	5,41	70,41
RHY Qz,Sr,1%Py	Rhyolite	0,6	4,41	5,01	69,09
RHY Qz,Sr,1%Py	Rhyolite	0,39	4,24	4,63	69,43
RHY Qz,Sr,1%Py	Rhyolite	0,92	3,97	4,89	70,05
RHY Qz,Sr,1-3%PyPo	Rhyolite	0,43	4,47	4,90	69,5
RHY Qz,Sr,2%Py	Rhyolite	0,29	4,67	4,96	68,91
RHY Qz,Sr,tr.Py	Rhyolite	1,11	4,28	5,39	71,08
RHY Qz,Sr+,1%Py	Rhyolite	0,75	4,45	5,20	68,39
RHY Qz,Sr+Cl?,tr.Py	Rhyolite	0,63	3,81	4,44	70,76
RHY Qz,Sr+Cl?,tr.Py	Rhyolite	0,57	4,01	4,58	69,94
RHY Qz,Sr+Gr,0.5%Py	Rhyolite	0,98	3,88	4,86	69,18
RHY Qz,SrBo,2-3%Py	Rhyolite	0,99	3,19	4,18	70,86
RHY Qz+,BoSr,2-3%Py	Rhyolite	1,52	2,96	4,48	68,75
RHY Qz+,SiBo,3%Py	Rhyolite	1,81	2,34	4,15	71,69
RHY Qz+Fp mas	Rhyolite	2,44	1,99	4,43	70,71
RHY QzFp	Rhyolite	5,7	1,19	6,89	69,59
VOL INT (DAC?),He	Intermediate	5,16	1,25	6,41	66,25
VOL INT ±mas,BoAc	Intermediate	2,1	2,14	4,24	60,54
VOL INT ±rub,(Bo),1%PyPo	Intermediate	1,83	1,06	2,89	56
VOL INT bx/rub,AcBo	Intermediate	1,59	1,63	3,22	56,7

Tab. D.1 (con't): Result obtained by Chimitec, Bondar Clegg and field observation by Maude Lake Exploration

FIELD OBSERVATIONS	ROCK CLASSIFICATION	Na2O	K2O	Na2O+K2O	SiO2
MAF sill	Mafic	1,99	0,2	2,19	45,03
MAF VOL	Mafic	3,28	0,99	4,27	52,61
MAF VOL mas	Mafic	3,32	1,01	4,33	52,84
MAF VOL mas	Mafic	2,21	0,19	2,40	45,28
MAF VOL,Si?	Mafic	2,9	0,79	3,69	54,46
MAF/INT tuf,fol	Mafic	2,62	0,73	3,35	49,87
RHY aph	Rhyolite	0,72	2,57	3,29	75,01
RHY aph mas	Rhyolite	1,45	2,91	4,36	73,92
RHY aph mas	Rhyolite	1,76	2,08	3,84	72,57
RHY aph mas	Rhyolite	1,25	2,87	4,12	75,76
RHY aph mas	Rhyolite	1,14	3,67	4,81	71,61
RHY aph mas,(Bo),1-3%Py	Rhyolite	2,22	1,51	3,73	68,94
RHY aph mas,(Sr),3-4%Py	Rhyolite	1,29	3,54	4,83	72,98
RHY aph mas,(Sr),3-5%Py	Rhyolite	1,7	1,73	3,43	72,59
RHY aph mas,(Sr),tr.Py	Rhyolite	1,42	2,23	3,65	70,79
RHY aph mas,1-3%Py	Rhyolite	0,53	4,15	4,68	68,64
RHY aph mas,2-3%Py	Rhyolite	1,48	3,38	4,86	70,29
RHY aph mas,SiBo,3-4%Py	Rhyolite	4,59	1,76	6,35	68,89
RHY aph mas,Sr,0,5%Py	Rhyolite	0,75	3,87	4,62	68,43
RHY aph mas,Sr,2-3%Py	Rhyolite	0,81	3,7	4,51	69,4
RHY aph mas,Sr±Bo,1-2%Py	Rhyolite	2,08	2,69	4,77	70,91
RHY aph mas,stgrs AcPy	Rhyolite	1,87	1,87	3,74	70,01
RHY aph,(Ffol),Sr,3-4%Py	Rhyolite	0,65	3,45	4,10	72,03
RHY aph,(fol),(Bo),2%Py	Rhyolite	1,9	3,13	5,03	70,86
RHY aph,(fol),Sr(Cl),3-5%Py	Rhyolite	1,36	4	5,36	68,8
RHY aph,(Sr),2-3%Py	Rhyolite	0,48	4,26	4,74	68,7
RHY aph,±fol,Sr(Bo),3-5%Py	Rhyolite	0,47	3,82	4,29	70,84
RHY aph,1-2%Py	Rhyolite	4,39	2,06	6,45	68,43
RHY aph,fol,Sr+,2-4%Py	Rhyolite	1,1	3,58	4,68	69,39
RHY aph,fol,Sr+Cl,1-3%Py	Rhyolite	0,67	3,74	4,41	70,48
RHY aph,fol,SrBoGr,5%Py	Rhyolite	0,58	3,55	4,13	66,14
RHY aph,fra vns PyAc	Rhyolite	1,65	2,46	4,11	72,45
RHY aph,fra,Sr,2-3%PyPo	Rhyolite	1,74	2,23	3,97	75,29
RHY aph,Sr,3%Py	Rhyolite	1,62	2,64	4,26	67,63
RHY aph,Sr,tr.Py	Rhyolite	1,54	3,08	4,62	69,49
RHY aph,Sr+,1%Py	Rhyolite	0,99	3,82	4,81	70,67
RHY Fp	Rhyolite	4,27	1,27	5,54	67,05
RHY mas,(Bo),1-2%Py	Rhyolite	1,11	4,02	5,13	69,54
RHY Qz bx	Rhyolite	0,67	3,78	4,45	69,77
RHY Qz frag,Sr+,2-3%Py	Rhyolite	0,45	3,81	4,26	67,43
RHY Qz mas	Rhyolite	4,45	1,9	6,35	68,58
RHY Qz mas,±Bo(Sr),tr.Py	Rhyolite	3,89	2,07	5,96	67,86
RHY Qz mas,Bo	Rhyolite	2,13	2,22	4,35	68,75
RHY Qz mas,Sr+,2-3%Py	Rhyolite	1,13	3,18	4,31	68,51

Tab. D.1 (con't): Result obtained by Chimitec, Bondar Clegg and field observation by Maude Lake Exploration

FIELD OBSERVATIONS	ROCK CLASSIFICATION	Na2O	K2O	Na2O+K2O	SiO2
VOL INT frag,fol,SrHe	Intermediate	3,44	2,21	5,65	65,85
VOL INT frag,fol,SrHe	Intermediate	3,44	2,12	5,56	64,65
VOL INT mas	Intermediate	2,23	1,73	3,96	63,93
VOL INT mas	Intermediate	1,7	1,3	3,00	61,76
VOL INT mas,Bo+Si?,0.5%Py	Intermediate	1,92	1,36	3,28	66,12
VOL INT nod Ac, Bo+2-3%Py	Intermediate	2,34	1,36	3,70	61,27
VOL INT rub AcBo(Si?)	Intermediate	1,04	1,83	2,87	61,82
VOL INT rub, BoAc	Intermediate	2,27	1,7	3,97	60,63
VOL INT rub,AcBo	Intermediate	1,37	2,07	3,44	60,14
VOL INT rub,AcBo	Intermediate	2,61	1,58	4,19	63,96
VOL INT rub,Bo+Ac	Intermediate	2,22	1,34	3,56	61,64
VOL INT rub,Bo+Si,tr.Py	Intermediate	3,19	1,24	4,43	64,69
VOL INT rub,Bo±Si,tr.Py	Intermediate	1,71	1,54	3,25	56,27
VOL INT rub,BoAc	Intermediate	1,88	1,33	3,21	59,51
VOL INT rub,BoAc	Intermediate	1,69	1,02	2,71	51,76
VOL INT rub,BoAc	Intermediate	1,31	1,49	2,80	57,84
VOL INT rub,BoAc	Intermediate	1,79	1,64	3,43	61,99
VOL INT rub,BoAc	Intermediate	3,89	1,01	4,90	63,92
VOL INT rub,BoAc	Intermediate	2,85	1,17	4,02	61,94
VOL INT rub,BoAc(SiSr)	Intermediate	1,19	1,58	2,77	66,06
VOL INT rub,BoAc,stgrsPyPoC	Intermediate	1,04	1,82	2,86	62,93
VOL INT rub,BoAc±Si	Intermediate	0,66	1,65	2,31	61,9
VOL INT rub,BoAcSi	Intermediate	0,65	1,05	1,70	59,4
VOL INT rub,BoAcSi	Intermediate	0,93	3,26	4,19	61,14
VOL INT rub,BoAcSi,2-3%Py	Intermediate	0,72	2,39	3,11	59,39
VOL INT rub,BoRb?	Intermediate	0,74	1,42	2,16	55,32
VOL INT rub,BoSiAc,3-4%Py	Intermediate	3,2	2,12	5,32	58,07
VOL INT rub,fol,BoAc,0.5%MtP	Intermediate	2,18	1,22	3,40	60,1
VOL INT rub,SrSi	Intermediate	1,61	2,53	4,14	66,36
VOL INT rub/bx,BoAcSr	Intermediate	0,94	3,05	3,99	64,33
VOL INT, Bo+AcRb?	Intermediate	1,08	1,2	2,28	67,43
VOL INT,cis/bx,±He	Intermediate	4,66	2,23	6,89	64,12
VOL INT,patchy,(fol)	Intermediate	3,18	0,91	4,09	59,32
VOL MAF	Mafic	1,84	0,44	2,28	46,34
VOL MAF	Mafic	1,47	0,46	1,93	45,23
VOL MAF	Mafic	1,83	0,25	2,08	43,44
VOL MAF	Mafic	1,5	0,07	1,57	47,36
VOL MAF cou	Mafic	1,86	0,41	2,27	48,61
VOL MAF mas	Mafic	1,36	-0,05	1,31	44,4
VOL MAF mas	Mafic	4,06	0,52	4,58	49,56

Tab. D.1 (con't): Result obtained by Chimitec, Bondar Clegg and field observation by Maude Lake Exploration

FIELD OBSERVATIONS	ROCK CLASSIFICATION	Na2O	K2O	Na2O+K2O	SiO2
VOL maf mas,2-3%Py	Mafic	1,85	1,03	2,88	59,19
VOL MAF mas,Bo,<1%Py	Mafic	2,07	1,69	3,76	58,45
VOL MAF mas,fol	Mafic	0,06	2,19	2,25	52,45
VOL MAF mas,fol	Mafic	0,67	2,02	2,69	49,06
VOL MAF mas/GAB	Mafic	1,54	0,06	1,60	46,94
VOL MAF?,(Sr)	Mafic	5,52	0,88	6,40	65,97

Tab. D.1 (con't): Result obtained by Chimitec, Bondar Clegg and field observation by Maude Lake Exploration

REFERENCES

Barrett, T.J., W.H. Maclean and S.C. Tennant. 2001. «Volcanic sequence and alteration at the Parys Mountain volcanic-hosted massive sulfide deposit, Wales, United Kingdom; applications of immobile element lithogeochemistry». *Economic Geology and the Bulletin of the Society of Economic Geologists*, vol. 96, no 5, p.1279-1305.

Chown, E.H., Real Daigneault, Wolf Mueller et J. Mortensen. 1992. «Tectonic evolution of the Northern Volcanic Zone, Abitibi belt, Quebec». *Canadian Journal of Earth Sciences*, vol. 29, p. 2211 – 2225.

Daigneault, Réal, W. Mueller and E.H. Chown. 2003 (in press). «Abitibi greenstone belt plate tectonics: the diachronous history of arc development, accretion and collision». *Developments in Precambrian Geology; Tempos of events in Precambrian time.* P. Eriksson, W. Alterman, D. Nelson, W. Mueller, O. Catuneanu and K. Strand eds..

Dawson, K.M., 1996. «Skarns Aurifères». In *Géologie des types de gîtes minéraux du Canada*, Canadian Geological Survey, Géologie du Canada, no 8, p529-543. Reviewed by O.R. Eckstrand, W.D. Sinclair and R.I. Thorpe.

Dilles, J.H. and M.T. Einaudi. 1992. «Wall-rock alteration and hydrothermal flow paths about the Ann-Mason porphyry copper deposit: a 6-km vertical reconstruction». *Economic Geology*, vol. 87, p.1963-2001.

Dussault, C. 1990. «Géologie de la région de Vezza-Le Tardif». Ministère de l'Énergie et des Ressources du Québec, MB 90 – 43.

Friesen, R.G., G.A. Pierce and R.M. Weeks. 1982. «Geology of the Geco base metal deposit». In *Precambrian Sulphide Deposits: Geological Association of Canada.* Special Paper no 25, p. 343-363. R.W. Hutchinson, C.P. Spence and J.M. Franklin eds..

Gaboury, Damien and Réal Daignealt. 1999. «Evolution from sea floor-related to sulphide-rich quartz vein-type gold mineralisation during deep submarine volcanic construction: The Geant Dormant gold mine, archean Abitibi belt, Canada». *Econonic Geology,* vol.94, p.3-22.

Gagnon, Y. 1981. «Lithogéochimie de la partie orientale du complexe rhyolitique de la mine Hunter, Abitibi-Ouest». Ministère de l'Énergie et des Ressources du Québec, DPV-826.

Galley, A.G., 1993. «Characteristics of semi-conformable alteration zones associated with volcanic massive sulphide districts». *Journal of Geochemical Exploration*, vol. 48, p. 175-200.

Galley, A.G., I.R Jonasson and D.H. Watkinson. 2000. «Magnetite-rich calc-silicate alteration in relation to synvolcanic intrusion at the Ansil volcanogenic massive sulfide deposit,Rouyn-Noranda, Quebec, Canada». *Mineralium Deposita*, vol. 35, p. 619-637.

Gibson, H.L. and D.J. Kerr. 1993. «Giant volcanic-associated massive sulphide deposits; with an emphasis on Archean deposits». In *Giant Ore Deposits: Society of Economic Geologists* Special Publication no 2, p.319-348. B.H. Whiting, C.J. Hodgson and R. Mason eds..

Gustason, L.B. and J.P. Hunt. 1975. «The Porphyry Copper Deposit at El Salvador, Chile». *Economic Geology* vol. 70, p. 857-912.

Gustason, L.B. and J.G. Quiroga. 1995. «Patterns of Mineralization and Alteration below the Porphyry Copper Orebody at El Salvador, Chile». *Economic Geology*, vol. 90, p. 2-16.

Hannington, M.A., I.M. Kjarsgaard, A.G. Galley and B. Taylor. 2003. «Mineral-chemical studies of metamorphosed hydrothermal alteration in the Kristineberg volcanogenic massive sulfide district, Sweden». *Mineralium Deposita*, vol. 38, no 4, p. 423-442.

Hemley, J.J., J.W. Montoya, J.W. Marinenko and R.W. Luce. 1980. «Equilibria in the system Al_2O3-SiO_2-H_2O and some general implications for alteration /mineralization processes». *Economic Geology*, vol. 75, p. 210-228.

Hocq, M. 1983. «Région de la rivière Gale». In Rapports d'étape des travaux en cours à la division du Précambrien. Ministère de l'Énergie et des Ressources du Québec, ET 82-01, p. 207 – 250.

Knoph, A.. 1929. «The Mother Lode system of California, United States». Geological Survey, Professional Paper 157, 88 p.

Lang, J.R., C.R. Stanely, J.F.H. Thompson and K.P.E. Dunne. 1995. «Na-K-Ca magmatic-hydrothermal alterstion in alkalic porphyry Cu-Au deposits, British Columbia». In *Magmas, Fluids, and Ore Deposits: Mineralogical Association of Canada, Short Course,* vol. 23, p. 339-366. J.F.E. Thompson ed..

Lauzière, K., E. H. Chown and K. N. M. Sharma. 1989. «Rapport intérimaire du projet Caopatina, secteur du lac Remick», Ministère de l'Énergie et des Ressources du Québec, MB 89-60.

Le Bas, M.J., R.W. Le Maitre, A. Streckeisen, and B. Zanettin. 1985. «A Chemical Classification of Volcanic Rocks based on the total Alkali-Silica Diagram». *Journal of Petrology*, vol. 27, no 3, p. 745 – 750.

Lemiere, B., J. Delfour, B. Moine, M. Piboule, A. Ploquin, P. Isnard and M. Tegyey. 1986. «Hydrothermal alteration and the formation of aluminous haloes around sulfide deposits: A model for alterites at Chizeuil, Morvan, France». *Mineralium Deposita*, vol. 21, p. 147-155.

Ludden, J., D. M. Francis and G. Allard. 1984. «The geochemistry and evolution of the volcanic rocks of the Chibougamau region of the Abitibi metavolcanic belt». In *Chibougamau, stratigraphy and mineralization, Canadian Institute of Mining and Metallurgy*, Special vol. 34, p. 20 – 34. J. Guha and E. H. Chown eds..

MacDonald, G.A. and T. Katsura. 1964. «Chemical composition of Hawaiian lavas». *Journal of Petrology*, vol. 5, p. 82 - 133.

MacRae, N.D. 1974. «Sulfuization of Basalt Under Metamorphic Conditions to Produce Cordierite-Bearing Rocks». *Canadian Journal of Earth Sciences*, vol. 11, p. 246-253.

Mueller, Wolf., E. H. Chown, K. N. M. Sharma, L. Tait and M. Rocheleau. 1989. «Paleogeographic and paleotectonic evolution of a basement-controlled Archean Supracrustal sequence, Chibougamau-Caopatina, Quebec». *Journal of Geology*, vol. 97, p. 399 – 420.

Paterson, S. R., O. Tobisch., and R.H. Vernon. 1989. «Criteria for establishing the relative timeng of pluton emplacement and regional deformation». *Geology*, vol. 17, p. 475-476.

Picard, C. and M. Piboule. 1986. «Pétrologie des roches volcaniques du sillon de roches vertes archéennes de Matagami-Chibougamau à l'ouest de Chapais (Abitibi est, Québec) : Le groupe basale de Roy». *Canadian Journal of Earth Sciences*, vol. 23 p. 561 – 578.

Piché, Mathieu, J. Guha, J. Sullivan, G. Bouchard and Réal Daigneault. 1990. «Les gisements volcanogènes du camp minier de Matagami: structuures, stratigraphie et implications métallogéniques». In *The Northwestern Quebec Polymetallic Belt : a summary of 60 years of mining exploration, Canadian Institute of Mining and Metallurgy*, Special vol. 43, p. 327–337. M. Rive, P. Verpaelst, Y. Gagnon, J.-M. Lulin, G. Riverin, and A. Simard eds..

Pilote, P. 1989. «Géologie de la région de Casa-Berardi, Dieppe, Collet et Laberge». Ministère de l'Énergie et des Ressources du Québec, MB 89-43.

Potvin, R. 1991. «Étude Volcanologique du centre volcanique felsique de lac des Vents, Région de Chibougamau». M.Sc. thesis, Université du Québec à Chicoutimi, Chicoutimi.

Poulsen, K.H., 1996, «Gîtes d'or primaires». In *Géologie des types de gîtes minéraux du Canada.* Canadian Geological Survey, Géologie du Canada, no 8, p. 355-361. Reviewed by O.R. Eckstrand, W.D. Sinclair and R.I. Thorpe.

Poulsen, K.H. and Hannington, M.D.,1996, «Gîtes de sulfures massifs aurifères associés à des roches volcaniques». In *Géologie des types de gîtes minéraux du Canada*, Canadian Geological Survey, Géologie du Canada, no 8, p. 202-217. Reviewed by O.R. Eckstrand, W.D. Sinclair and R.I. Thorpe.

Robert, F., 1996, «Filons de quartz-carbonates aurifères», In *Géologie des types de gîtes minéraux du Canada*, Canadian Geological Survey, Géologie du Canada, no 8, p. 387-405. Reviewed by O.R. Eckstrand, W.D. Sinclair and R.I. Thorpe.

Riverin, G. and C.J. Hodgson. 1980. «Wall-rock alteration at the Millenbach Cu-Zn mine, Noranda, Quebec». *Economic Geology*, vol. 75, p. 424-444.

Wyman, D.A., R. Kerrich and B.J. Fryer. 1986. «Gold mineralisation overprinting iron formation at the Agnico-Eagle Deposit, Quebec, Canada : Mineralogical, Microstructural and Geochemical Evidence». In *Proceedings of Gold '86, an International Symposium on the Geology of Gold*, p. 108-123. A.J. MacDonald ed..